Sheffield Hallam University

Application of FTIR imaging and spectroscopy to solid dosage formulations.

MUTHUDOSS, Prakash.

Available from the Sheffield Hallam University Research Archive (SHURA) at:

http://shura.shu.ac.uk/20107/

A Sheffield Hallam University thesis

Application of FTIR Imaging and Spectroscopy to Solid Dosage Formulations

Prakash Muthudoss

A thesis submitted in partial fulfilment of the requirements of
Sheffield Hallam University
for the degree of Doctor of Philosophy

April 2011

Collaborating Organisation: AstraZeneca, Macclesfield,
United Kingdom

ABSTRACT

The preparation of solid dispersions, in this study felodipine/polyvinyl pyrrolidone solid dispersion, is a multifaceted phenomenon. In order to understand the formation of solid dispersions two different mixed solvent system, three different temperatures and different drug loadings were selected and monitored in real time using Attenuated Total Reflectance- Fourier Transform Infrared Spectroscopy. 50 µl of the prepared solution was placed onto a pre-heated ATR crystal. The effect of PVP/API ratio, molecular interactions and effect of temperature (30°C, 40°C and 50°C) on the rate of film formation (solid dispersions) was evaluated. The changes in the peak positions, peak intensities and peak width as a function of time was monitored. The data were then analysed using peak height measurements, statistical and chemometric data analytical tools. It was shown that the nature of the solvent, the working temperature, presence of polymer and low drug loading was found to influence the rate of evaporation of solvent, molecular interactions and quality of the final product. Moreover, using thermogravimetric techniques it was complemented that the residual solvent within the systems was within the studied limits.

The spatial arrangement or distribution of components within solid dispersion was found to influence the physical stability, phase behaviour, dissolution and bioavailability. Mid infrared spectroscopic imaging has been shown to be useful and has provided unique insights in to various fields. However, it has very limited applications in analysing the pharmaceutical materials. This work aims to evaluate various image processing tools in extracting process related information. Three model systems with varying chemical composition were selected. The chemical images from the regions of interest were collected using a Varian 620 FTIR Imaging instrument equipped with 64 x 64 MCT-Focal Plane Array (FPA) detector. Firstly we showed the impact of optical artefacts on the quality of the acquired image. The data was then pre-processed to remove baseline effects, pathlength variations and image processed to extract distribution maps. Agreement between the data generated using peak height measurements, compare correlation, principal component analysis and multivariate curve resolution was obtained only with the simple systems, the advantage with the latter being that the supervised and unsupervised chemometric approaches do not require any prior information about the sample and does not suffer from any physical or chemical interferences. The success of MCR-ALS over compare correlation and PCA methods is that it does not require any pure materials library and provides chemical information respectively. Moreover, implementation and data extraction is easy using MCR-ALS. It was then showed that once the optical artefacts are separated and chemically significant information is extracted, the benefits of infrared imaging was multitude.

The optimised procedures were then applied to other samples to expand the applications of mid infrared imaging. There is no established paper to date describing the application of FTIR imaging to study the solvent induced phase separation in solid dispersions. One of the aims of this work is to study the impact of two different solvents on the phase behaviour of felodipine/polyvinyl pyrrolidone solid dispersions cast from different binary solvent systems. The temperature induced phase separation and degradation have been studied using differential scanning calorimetry, scanning electron microscopy, thermogravimetric etc, however we have shown the application of FTIR imaging in assessing the temperature induced degradation complemented and supported by *in situ* ATR-FTIR spectroscopy and thermogravimetric analysis.

ACKNOWLEDGEMENTS

Contents

v

CHAPTER 1.
BACKGROUND AND INTRODUCTION

1.1 Pharmaceutical Substances

A pharmaceutical substance or active pharmaceutical ingredient (API) or drug is a compound that is intended to furnish pharmacological activity or other direct effect in the diagnosis, cure, mitigation, treatment or prevention of a disease or to affect the structure of any function of the human body.[1] However, these pharmaceutical substances do not include any intermediates used in the synthesis. Drug development is a tedious, expensive and a time-consuming process and the time frame for drug development from screening to market launch on average requires 10-12 years.[1,2] Various stages from discovery to marketing are, drug discovery, drug development, clinical trials, manufacturing procedures, marketing approval.[1]

Drugs are hardly ever administered as pure chemical substances, instead formulated in combination with one or more non-medicinal agents or excipients.[3] These formulations are termed dosage forms. An active ingredient can be formulated into a variety of dosage forms. The dosage forms are classified based upon the routes of administration like Oral, Rectal, Topical, Parenteral, Nasal, Eye, Ear, etc. The preferred route for administering drugs is through mouth or commonly termed as oral route of administration. Solid oral dosage forms are more stable, easy to produce and more or less accurately delivered than the other oral dosage forms like suspensions, emulsions, syrup etc. However, formulating a successful dosage form requires consideration of physical, chemical and biological characteristics of ingredients and excipients used in fabricating the product.[3,4]

1.2 Aqueous solubility, dissolution rate and bioavailability

When the dosage form is administered, the aqueous soluble drugs are dissolved or solubilised either in the stomach or small intestine through the action of gastro-intestinal (GI) fluids (dissolution) and transported to the blood or systemic circulation.[5] The amount of drug required to reach the systemic circulation determines the physiological action and is termed as bioavailability.[5,6]

New drug molecules with poor aqueous solubility have risen sharply[7] and compounds having solubility as low as less than 1 µg/ml are reported.[6] Due to poor aqueous solubility, the available GI volume will not be able to dissolve the required dose of drug directly affecting the bioavailability. Dissolution may be the rate limiting step for such

1

hydrophobic drugs.[8] The problem of delivering poorly water soluble active pharmaceutical ingredients (APIs, or "drugs") is one that is increasingly taxing the pharmaceutical scientists. The first and foremost focus during drug development is enhancing the bioavailability of hydrophobic drugs.[9-11]

The relationship between solubility and dissolution is well understood using the modified Noyes-Whitney equation which is

$$\frac{dM}{dt} = \frac{AD(C_s - C_t)}{h} \tag{1}$$

where dM/dt is the dissolution rate; A is the specific surface area; D is the diffusion co-efficient; h is the diffusion layer thickness, C_s is the saturation solubility and C_t is the drug concentration at time t.

The diffusion coefficient and diffusion layer thickness are physiological parameters which are often difficult to be manipulated.[5] However, improving the solubility through formulation approaches is the most attractive option.[7,10] Tailoring the surface area and manipulation of saturation solubility are some of the available approaches to improve aqueous solubility. The available surface area for dissolution can be increased by reducing the particle size (e.g. milling, micronisation).[5,7,12] The saturation solubility can be altered by chemically modifying the pharmaceutical substances (e.g. salts) or changing the physical state of the drug in the formulation (e.g. metastable polymorphs, amorphous form).[7,13]

1.3 Amorphous systems and Solid Dispersions

A crystalline substance melts at a certain temperature which is the melting temperature (T_m) and rapid cooling of this melt yields supercooled liquid. Further cooling produces glassy material: the temperature at which this transition occurs is termed as the glass transition temperature.[14,15] The property of materials at T_m, below and above T_g vary significantly.

The amorphous phases or forms of pharmaceutical active substances have received greater attention.[15] This is due to the fact that amorphous forms contain higher free energy which helps to attain higher dissolution rate and hence better bioavailability.[16-18] The solubility advantage of factors approximately >1000 for amorphous pharmaceuticals over crystalline forms has been predicted.[16] The incorporation of polymeric stabilisers to the amorphous form and presenting the drug as a molecular dispersion, also called solid dispersion, offers a multitude of functional advantages.

2

With solid dispersions, there are improvements in bioavailability because there is reduction in particle size, improved wettability, higher porosity and change in drug crystallinity.[7,10,19-21] Moreover, aforementioned improvements are the parameters concerning the surface area and saturation solubility with the Noyes-Whitney solubility relationship.[5]

Solid dispersion refers to solid state mixtures, prepared through the dispersion, typically by solvent evaporation or melting (fusion) or melting-solvent methods, of one or more active ingredients in an inert carrier matrix.[13,20,22] It also refers to a product formed by converting a fluid-carrier combination to the solid state.[13,21,23]

When the technique was first introduced it was believed that the drug was in a microcrystalline state in the drug/polymer mixture with the formation of eutectic systems[24] and was later termed as "solid dispersion".[20] Conversely, it was suggested that some of the drug particles might be molecularly dispersed (solid solution) or drug being present as small particles embedded (solid suspension) in the polymeric matrix.[25,26] Nevertheless, the fundamental principle remains the same, that is, the drug particles are released as fine particles upon exposure to aqueous media when the carrier component of the solid dispersion dissolves.

As already mentioned, the amorphous forms have higher solubility than the crystalline counter-parts. To quantify the benefits, the thermodynamic or thermal properties have been used to compare the predicted and experimental solubility. Hancock and Parks[16] using a simple thermodynamic approach (based on the free energy difference between two physical forms) reported a procedure for the estimation of solubility advantage. However, the predicted and experimental solubility was in close agreement only with crystalline materials. Pikal and co-workers[17,18] proposed a modified procedure for the estimation of amorphous solubility, yet the procedure was successful only for amorphous systems that were slowly crystallising from the aqueous media. For rapid crystallising materials there are more limitations. Nevertheless, the number of marketed products developed using the solid dispersion approach is very limited[10,13] whilst there have been many publications concluding increased dissolution rates. This could be attributed to the lack of basic understanding of these systems at the molecular level.[27]

1.4 Solid Dispersion and Potential Characteristics

1.4.1 Choice of manufacturing process

Various approaches used in the generation of solid dispersions are the melt or fusion method,[10] the solvent method,[13] melting-solvent method,[20] etc. If the carrier selected has a lower glass transition temperature (T_g), as with PVP and felodipine the preferred choice is the solvent method. The drug and the polymer are mixed in a common solvent upon removal of the solvent, solid dispersions are obtained.[5,10] Since the solvent evaporation occurs at ambient or room temperature, this method is suitable for processing thermolabile compounds.[6,7] Practical or industrial applications of pilot scale solvent evaporation method are spray drying and freeze drying. However, finding a common solvent is not easy; toxicity or physical instabilities of residual solvents and high manufacturing cost are some of the limitations of the solvent method.[28] The choice of preparation method (Spray drying or melting) influenced morphology or particle size of triamterene-D-mannitol solid dispersions and the dissolution rate.[29]

1.4.2 Solvent selection

In the solvent method, the solubility of drug and the polymer in the solvent is a prerequisite to obtain stable solid dispersions. The physical state of the prepared dispersions is influenced by the drug-to-solvent and/or carrier–to-solvent ratio, solvent-solid interactions, temperature of drying, evaporation rate and the nature of the solvent.[10,30] Solvent nature, Gutmann's acceptor-donor number and density are some of the factors that are important while selecting the solvents. Spectroscopic studies have shown that solvents can alter molecular interactions of 1,4 dihydropyridine,[31] swelling behaviour of hydrogels,[32] change in the conformation,[33] alter the denaturation of urea[34,35] etc. These effects are characterised by solvent induced frequency shifts[31] (SIFS) in carbonyl moieties and other groups involved in the intermolecular interactions. In contrary, self-association and solvent-solvent interactions can decrease the maximum solubility of the drug.[36]

1.4.3 Importance of Molecular interactions

Various interactions known to-date[37] are H-bonding, ion-dipole, dipole-dipole, complexation and Vander Waal's interactions or combinations of the aforementioned interactions.[38] Likewise electrostatic interactions between the drug and the polymer are reported.[39] The physico-chemical properties of the drugs are altered due to the presence of strong heteromolecular interactions like hydrogen bonds.[11] In addition, these interactions have a pronounced effect on the molecular state of the drug.[40] Applications

4

include improvement of the solubility of hydrophobic drugs, enhanced dissolution rates, increased drug release rate, improved stability, enhanced bioavailability, altered therapeutic activity and reduced side effects.[37] Interestingly, Timmins et al.,[38] showed that drug-polymer interactions could reduce crystallinity even if the products are physically mixed.[38]

1.4.4 Understanding dissolution behaviour or drug release

Compared to the crystalline form, the amorphous systems require no additional energy to dissolve in the gastro-intestinal enzymes or fluids. Additionally, the advantage of solid dispersions over amorphous forms in enhancing the release of drug and dissolution rate of the drug is enormous.[41-43] Water soluble polymers together with biological factors like bile acids and fatty acids solubilise the dissolved drug and hence facilitate the dissolution rate.

1.5   Implications of knowing these characteristics

Several experiments have been conducted in the past few years to understand the stability of amorphous pharmaceutical formulations. These can be illustrated by considering the solution state stability and solid state stability separately. The solid state stability concerns with the manufacturing and storage aspects; while the solution state stability mainly concerns with drug release and dissolution rate in the stomach or small intestine.

To understand the recrystallization process or solid-state stability of solid dispersions, evaluation of kinetic and thermodynamic factors is quite important.[30,44] From a kinetic point of view, molecular mobility is a key factor that is frequently reported detrimental when assessing the stability of amorphous forms. In a thermodynamic perspective, solid-solid or drug-polymer miscibility is a prerequisite to retard the amorphous-amorphous phase separation and hence improve the physical stability of solid dispersions. The recrystallization process in the solution state always starts by a nucleation event followed by crystal growth.[5]

To overcome these undesirable events, various formulation strategies were developed. Addition of polymers reduces the molecular mobility either by increasing the viscosity of the mixture (antiplasticization effect) or through specific drug-polymer molecular interactions.[27,45,46] Manipulating the drug-polymer interactions not only facilitates thermodynamic solid-solid miscibility or drug dissolution rate but does provide the opportunity in designing optimally stabilized amorphous systems.[47] Taylor et al.,[48]

investigated physical stability of model hydrophobic drug-PVP solid dispersions upon exposure to high relative humidities. It was shown that model drugs with NH moieties underwent moisture-induced drug-polymer immiscibility while model drugs with COOH moieties were miscible. The physical stability was influenced by solid-solid or drug-polymer miscibility. It was showed that the hydrophobic-drug polymer systems which were partially miscible were more prone to phase separation and subsequent recrystallization than systems which showed complete miscibility.[48-50]

From the biopharmaceutical point of view, the selected polymer should solubilize the drug, molecularly interact and reduce the nucleation rate. Additionally, the kinetics of drug release from the solid dispersion depends on the dissolution mechanism like wetting or dispersability and an extensive knowledge of this would help in formulating better process conditions.[13,47] For dissolution enhancement, Telang et al., prepared ternary dispersions of indomethacin (IMC) by incorporating the surfactant meglumine (MU) in the polymer polyvinyl pyrrolidone (PVP) in an attempt to prevent crystallization from the supersaturated solutions. The prepared ternary dispersion showed improved physical stability and enhanced dissolution rate.[51]

Moreover, Vanden Mooter et al.,[52] showed that sprayed dried itraconazole/eudragit E100 solid dispersions were superior in product performance to the melted products and concluded that the influence of drying kinetics on phase behaviour or solid-solid miscibility has to be understood. Patel et al., formulated solid dispersions of two poorly soluble anti-cancer drugs (CurcurbitacinB and CurcurbitacinI) using PEO-b-PCL diblock polymer.[53] At low levels of PCL there was increased solubility; however increasing the content decreased the dissolution rate due to retardation of drug release from the polymer matrix. That is, the degree and nature of molecular interaction can affect the dissolution and bioavailability.[42,54,39,53,55] Moreover, the addition of surfactants could increase the nucleation rate and hence decrease the solution stability.[5]

Poor prediction still persists in understanding the importance of these individual characteristics. The challenges concerning the basic understanding could be due to poor predictability of the properties of the resultant material, influence of manufacturing conditions or factors governing stability considerations. Major difficulties for this knowledge gap have most certainly been the limitation of characterisation techniques to study the solid-state and the solution-state stability and the interplaying factors on a molecular level. Understanding the potential characteristics involved in the formulation

of solid dispersions will be a good starting point to design an effective characterisation protocol as shown in Figure 1.1.

A wide range of analytical methods have been used to study the prepared solid dispersions with the aim to understand the structure of solid dispersions, the crystallization kinetics, drug-polymer-excipient interactions, molecular mobility and thermodynamics of the molecular state.[47] The advantages of using infrared (bulk spectroscopy and spectroscopic imaging) and complementary techniques to improve the understanding of the distribution of each component within the polymer matrix, the dynamics of solid dispersion formation and the physical stability of solid dispersions will be discussed in the following chapters.

1.6   Aims and Objectives

The objective of this project was to investigate the applicability of mid-infrared spectroscopy and spectroscopic imaging techniques to characterise the drying kinetics, molecular interactions, phase separation, phase transition and homogeneity or heterogeneity in distribution. In this context, the aim of this research was to develop methodologies and experimental toolbox involving mid infrared spectroscopy to effectively characterise the solid state stability of solid dispersions.

Fourier Transform Infrared Imaging (FTIR-Chemical Imaging) allows us a new dimension to probe the distribution of the components on the micron scale. However, it has also raised particular challenges in extracting useful information from the chemical images. In this direction, particular attention will be paid to the evaluation and optimisation of experimental design and of procedures to provide statistical and chemometric data analysis schemes.

In order to achieve our motivation model drug (felodipine), model polymer (polyvinylpyrrolidone, PVP) and various solvents (acetone, methanol and dichloromethane) were included in the study. These model systems were selected because extensive work has been carried out among different groups across the globe to prepare, characterise and study the stability of felodipine/PVP solid dispersions. Moreover, these model systems are widely used in the pharmaceutical industry.

Since there is no exploration to date in describing the formation of solid dispersions, one of the main objectives of this research is the application of vibrational spectroscopy to understand the dynamics involved in solid dispersion formation. The effect of temperature, solvent, polymer and drug loading will be studied in detail. Furthermore,

the residual solvents present within these systems were studied by applying thermogravimetric measurements. Once the formation of solid dispersions and image processing tools are established, the influence of solvents on phase behaviour, moisture induced phase transition and temperature induced chemical decomposition/degradation of the selected systems will be studied in depth.
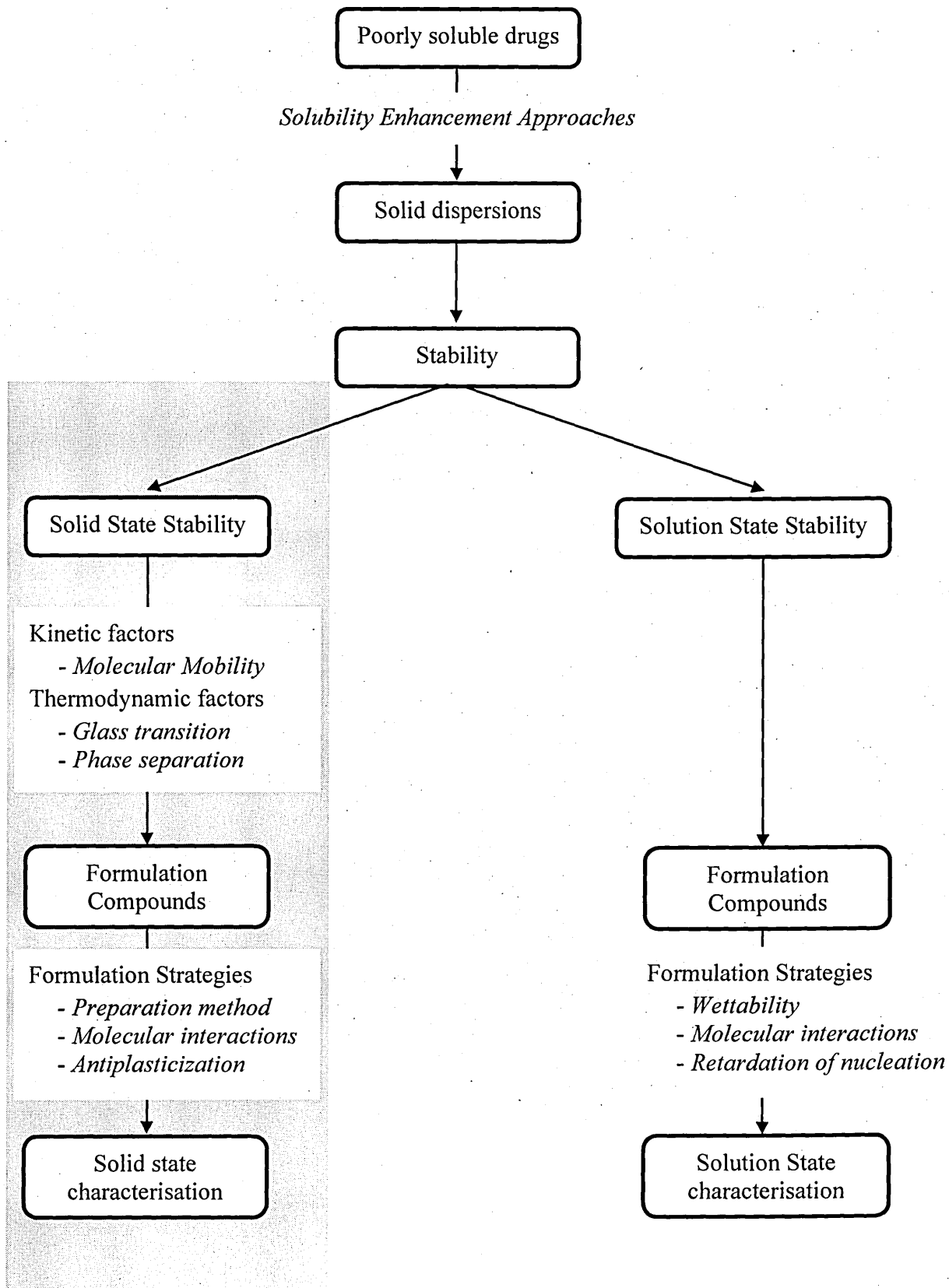
Figure 1.1. Understanding the potential characteristics involved in the formulation of solid dispersions as a starting point to design an effective characterisation protocol.

9

CHAPTER 2.
FELODIPINE/POLYVINYLPYRROLIDONE SOLID DISPERSIONS

2.1   Model Polymer-Polyvinylpyrrolidone (PVP)

Polyvinylpyrrolidone (PVP) is made from the monomer N-vinyl pyrrolidone.[56] PVP has hydrophilic and hydrophobic groups which makes it soluble in water and various other solvents.[57,58] The relative molecular mass of PVP ranges from 2500 to 1 million and PVP of lower relative molecular mass are used in pharmaceutical industries.[56] PVP grades are distinguished by their K-value, a measure of specific viscosity and this correlates with the molecular weight.[56]
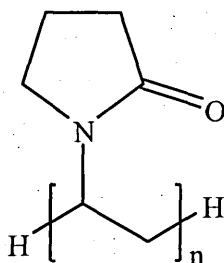
Chemical Structure of Polyvinylpyrrolidone (PVP)[56,59,60].

PVP forms a molecular adduct solubilising the insoluble substances;[7] thus PVP is one of the common carriers used in preparing solid dispersions.[6,61] Due to the steric hindrance, the lone pair of electrons on nitrogen atom doesn't involve in the intermolecular interactions, while the involvement of the C=O group is favoured.[62] Precisely, PVP stabilises the solid dispersions through intermolecular interactions with proton donating drugs,[22,62] ion-dipole interactions with proton accepting drugs[63] and the antiplasticing effect with neutral drugs.[30]

In addition, PVP polymers are used as crystal growth inhibitors and/or rheological additives in soft gelatine capsules, oral liquids and suspensions, parenteral formulations, topical gels creams, lotions and ophthalmic preparations.

2.2   Model Drug-Felodipine

Felodipine is a dihydropyridine derivative that is chemically described as ethyl methyl-4-(2, 3-dichlorophenyl)-1, 4-dihydro-2,6- dimethyl-3, 5-pyridine-dicarboxylate,[64,65] a calcium channel blocker, widely used in the treatment of angina pectoris and hypertension.[66-68] It acts by relaxing the vascular smooth muscle. In addition, felodipine when administered dilates the coronary and peripheral arteries.

Felodipine shows polymorphism[69] and chirality[68] unlike other 1, 4 dihydro pyridine derivatives. The different crystal forms and the properties are given in the Table 2.1.

10

Partial decomposition is found in the annealed and molten form but not in the commercially available products.[68]
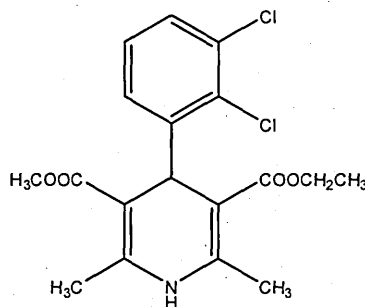
Chemical structure of Felodipine[68-70]

Felodipine is very poorly soluble in water and the aqueous solubility at ambient temperature is determined to be 0.5 mg/l.[69] Srcic et al.,[31] studied the molecular interactions of 1,4 dihydro pyridine (DHP) derivatives like nifedipine, nitrendipine, nimodipine and amlodipine in different organic solvents. For uncharged molecules there was good correlation between the acceptor-donor number and the carbonyl stretching vibrations of the derivatives. The DHP's act as H-bond donors in solvents with low acceptor number (AN) whereas they are strong H-bond acceptors in solvents with high AN. However, in protic solvents like ethanol/methanol, the DHP's can act as H-bond donors and acceptors.

These properties affect the dissolution rate of felodipine, if it is formulated as a conventional dosage form.[65] Several approaches to increase the dissolution rate of felodipine have been undertaken.[71-74] The formation of a glassy phase by producing amorphous felodipine is one such method.[65] Amorphous felodipine is prepared either by cooling the melt at room temperatures or by quenching under liquid nitrogen and has a glass transition temperature (Tg) of 43 °C. Velaga et al.,[75] obtained felodipine form II reproducibly by co-crystallising with isonicotinamide. The results were confirmed through the appearance of the NH stretching peak at 3336 cm^{-1} and carbonyl peaks at 1698 and 1683 cm^{-1}.

Table 2.1. Data of (±)- and (+)- Felodipine crystal forms[68]

Description	(±)- Felodipine			(+)- Felodipine	
	Mod. I	*Mod. II*	*S_{Ac}*	*En Mod. I*	*En. Mod II*
Preparation	Methanol or ethanol	n-hexane /methanol (10:1)	Suspension of mod. I in acetone	Crystallization from solvents	Crystallization by slow evaporation of solvent
Melting point (°C)	141-146	131-135	~70	141-145	132-134
Thermodynamic Stability	Stable	Unstable	Unstable	Stable	Unstable

Chamarthy and Pinal[12] milled felodipine crystals to induce crystal disorder. A high degree of crystal disorder can introduce amorphous character; however, milling felodipine material induced crystal defects but not amorphous character. Lindfors and co-workers[76] showed that even the amorphous felodipine nanoparticles were sensitive to very small amounts of crystalline material in seeding experiments. However, the prepared metastable states can revert to the more thermodynamically stable crystalline polymorph. Hancock and co-workers[15] showed that amorphous compounds above and just below their T_g experience molecular mobility which is one of the factors responsible for the physical instability. However, utilization of different polymers to inhibit the crystallization[39] and improve the release kinetics have been proposed.[47] When high T_g polymeric materials are added to the crystalline drugs, the T_g of the resulting amorphous solid dispersions is increased thereby reducing the molecular mobility of the high energy states consequently inhibiting the crystallization.

2.3   Felodipine/PVP Solid Dispersions

Hwang et al.,[77] studied the influence of preparation method (rotary evaporation or conventional solvent method and supercritical fluid anti-solvent precipitation) on the physicochemical characteristics of felodipine/hydroxylpropylmethylcellulose (HPMC) solid dispersions. The mean particle size of felodipine was 200-250 nm with supercritical fluid anti-solvent precipitation but was found to be irregular with voids when prepared using conventional solvent method. These properties did influence the dissolution rate to a marked extent and the authors concluded that the supercritical fluid anti-solvent precipitation method of preparation was far superior to the conventional methods. An alternative method to solvent evaporation and melting was the microwave irradiation wherein the model drug felodipine along with the polymer was placed in a beaker in the microwave chamberl.[74] The microwave energy was used as a source of heat to transform the crystalline material to amorphous, instead of the conventional melting method.[74,78] Many studies have been focussed upon the novel methods for preparing the amorphous forms; however, physical instability has been the major hurdle for solid dispersion techniques to reach the market.

Bhugra et al.,[79,80] showed that a simple correlation does not exist between the molecular mobility and crystallization tendency. Zografi and co-workers[81] in a series of studies has shown that even at low levels of polymeric materials the crystallization was inhibited. Neither molecular weight nor T_g of polymer had influence on the crystallization inhibition. Using spectroscopic studies these improvements were related to the

intermolecular interaction between the drug and the polymer. In another study, Aso and Yoshioka[82] showed that molecular interactions were responsible for the nifedipine and phenobarbital-PVP amorphous solid dispersion having reduced molecular mobility and hence its physical stability. In felodipine, the polar groups C=O, Cl and NH are involved in the intermolecular interactions. With lipophilic excipients both C=O and NH interact while with hydrophilic excipients only the NH group is involved[48]. Moreover, researchers[41,54] studied the effect of particle morphology, physical state of the drug, particle size distribution and the drug polymer interactions on the felodipine dissolution mechanism.

The intermolecular interaction between the drug and the polymer differentiates the physicochemical properties of the pure drug molecules. Karavas et al.,[11] and Bikiaris et al.,[22] studied the potential effects of H-bonding interactions on solubility, dissolution profile and contact angle. It was established that the interactions reduce the particle size and enhance the solubility of felodipine thereby improving the dissolution rate. The contact angle measurements suggested that the hydrophilicity of the polymer did not significantly influence the dissolution rate. Moreover, at low drug concentrations (10% w/w) the release of felodipine from PVP was diffusion controlled and at high drug concentrations the release was dissolution controlled.[22,73,83]

Vasanthavada et al.,[84] showed that intermolecular interactions favour the solid solubility of drug in the polymer. The solid solubility was found to influence the physical stabilisation, that is, of the two models studied, drugs indoprofen interacts with PVP while griseofulvin does not. The interacting system was physically stable but Gris-PVP was phase separated.

Ktistis et al.,[85] showed that although there is strong interaction of felodipine with PVP, these systems are only partially miscible. Interestingly, this interaction is sufficient to reduce the particle size to the nanoscale which was found to influence the dissolution rate but this reduction is dependent upon drug-polymer ratio.

Sigalas and Teberekidis[86] showed based on quantum mechanical modelling and computational studies, that felodipine forms stronger hydrogen bonds with PVP than polyethylene glycol (PEG).

Kestur et al.,[87] studied the effect of molecular weight and viscosity on the crystallisation kinetics of felodipine/PVP solid dispersions. Intermolecular interaction between the drug and the polymer (PVP) was not dependant on the molecular weight or different

14

grades of the polymer. The results indicate that molecular weight and viscosity have limited effects on the molecular mobility and thence the recrystallization of amorphous solid dispersions. Moreover the inhibition of crystal growth rate is due to reduced molecular mobility and hence it is a kinetic rather than thermodynamic one, through the formation of drug-polymer interactions.

Marsac et al.,[88] studied the effect of temperature and moisture on the miscibility of felodipine/PVP amorphous solid dispersion's and amorphous felodipine. The NH stretching peak in crystalline felodipine is centred at 3372 cm^{-1} while in the amorphous felodipine due to drug-drug interactions the peak is centred at 3341 cm^{-1} and in solid dispersion's this peak is centred at 3290 cm^{-1}. All compositions of felodipine/PVP are miscible at room temperature as suggested by the presence of drug/polymer interactions, the value of T_g and modelling studies.[88,89] When the amorphous polymer was heated from 5 °C to 160 °C the NH peak centred at 3337 cm^{-1} shifted to 3350 cm^{-1}, which is indicative of a weakening of the intermolecular interactions. This shift was found to occur close to the T_g of the studied system. However, these effects were reversible. When felodipine/PVP ASD's was exposed to high relative humidity (atmospheric moisture or liquid water) >75% there was irreversible disruption of drug/polymer interactions and there was amorphous-amorphous phase separation. In contrast, long exposures induced crystallisation. This study shows that drug/polymer combinations are susceptible to moisture induced immiscibility.

Rumondor et al.,[48] studied the influence of different degrees of moisture (54%, 75%, 84% and 94%) and compared the phase behaviour of four model systems consisting of nifedipine, droperidol, ketoprofen, indomethacin and pimozide. Drug-polymer interactions provide information on the intimacy of mixing and hence the solid-solid miscibility. Any disruption of these interactions at the expense of drug-drug interactions is indicative of amorphous-amorphous phase separation. The results of this study indicated that the crystallisation could happen either directly from the miscible dispersions or through amorphous-amorphous phase separation. The latter route was found to impose faster crystallisation as the polymer inhibitory effect is reduced. Moreover, the NH moieties were sensitive to moisture induced immiscibility while model systems with COOH moieties were less susceptible. The other factors that were found as co-influences were strength of drug water interactions and total moisture absorbed by the system.

Rumondor et al.,[90] studied the impact of moisture and polymer type (PVP and HPMCAS) on the physical stability of felodipine/PVP amorphous solid dispersion's. In the absence of moisture both the polymers were crystallisation inhibitors. When the RH>75% HPMCAS was a better polymer than PVP in inhibiting the crystallisation. However the system firstly undergoes amorphous-amorphous phase separation followed by crystallisation.

Rumondor et al.,[91] studied the influence of different degrees of moisture (13% to 80%) of felodipine solid dispersions prepared from PVP and HPMCAS. The researchers showed that for <64% moisture PVP was a better polymer but for >64% HPMCAS was better because there was moisture-induced drug-polymer phase separation.

Ivanisevic[49] studied the physical stability of twelve model amorphous solid dispersion's (consisting two polymers PVP, PAA and four drugs felodipine, ketoprofen, nifedipine and indomethacin) for the period of nine to twenty-two months. The systems initially determined to be miscible were amorphous (as determined by XRD) for the entire length of the study. The initially phase separated systems crystallised within one or two months while amorphous systems (in the absence of polymers) crystallised within days. The conclusion of the study was that good physically stable dispersions were obtained with good drug polymer miscibility.

Eerdenbrugh, Baird and Taylor[92,93] investigated 51 model compounds and evaluated their crystallisation tendency. These compounds were prepared using melting and rapid solvent evaporation methods. The crystallisation tendency of the model compounds from the melt was based upon molecular weight, structure and orientation of the molecules. These physicochemical properties were also descriptors of the model compounds glass forming ability (GFA) and in producing stable amorphous/glass (glass stability, GS) compounds. The results indicated clear differences in the crystallisation behaviour. Based upon the crystallisation tendency, a "crystallisation classification system" was developed and the compounds were described as being class I (rapid crystallizers or crystallization immediately after spin coating), class II (intermediate crystallizers or crystallization within 7 days of storage) or class III (slow crystallizers or no signs of crystallization even after 7 days of storage). Moreover, the results suggested that class I compounds were not ideal condidates to be adapted for the solid dispersion technology.[93]

With the aforementioned understanding about the pure amorphous compounds, Eerdenbrugh and Taylor[46] investigated the ability of 7 chemically diverse polymers to

inhibit the crystallisation of class I and class II model drugs from amorphous solid dispersions. The results of this investigation showed that acidic polymers were better crystallisation inhibitors for neutral and basic model compounds. Hence there is no superior polymer universally better than the others but a rationale for good selection can be based on the drug-polymer chemistry.

Konno et al.,[72] demonstrated the importance of solid state and solution state stability by preparing felodipine amorphous solid dispersions (ASD's) with different polymers (PVP, HPMC and HPMCAS). This study was carried out to understand the inhibition of recrystallization of the amorphous form from the supersaturated dissolution medium. Of the studied polymers, HPMCAS was not only found to produce higher amounts of supersaturated solution but was superior at inhibiting the crystal growth rates compared to PVP or HPMC. This study shows the importance of reconsidering the suitability of polymers to show good solid and solution state stability.

Taylor et al.,[94] studied the dissolution behaviour of felodipine and indomethacin (IMC) solid dispersions prepared from three different polymers (PVP, HPMC and HPMCAS) at 25 °C and 37 °C. These two drugs were selected because they both had similar glass transition temperatures. The results of dissolution profile shows that supersatured solutions were formed for both the compounds upon dissolution at 25 °C but at 37 °C only IMC produced supersaturated solutions but not felodipine. These results implicate the complexity of dissolution behaviour (T_g is not the key factor).

Since much structural information and basic understanding is available in the literature about the felodipine/polyvinylpyrrolidone systems, this particular system will be carried further to survey the range of potential physical characterisation methods and data analytical approaches.

CHAPTER 3
RESEARCH DESIGN AND METHODS

3.1 Preparation of Solid Dispersions

Various preparation methods for solid dispersions have been reported. Of the available approaches, preparation of solid dispersions involving solvents is most common[6,7,10] The first step in the solvent method is to mix the drug and the polymer in a common solvent. The second step involves the removal of solvent(s) which results in the formation of a solid dispersion. The other strategies are the use of binary solvent mixtures (BSM's) which can be solvent-solvent (both drug and the polymer are soluble) or solvent-nonsolvent (drug is soluble in both the solvents but polymer is insoluble in one of the solvent) mixtures. In this research, solvent casting and spray coating were the two pilot scale solvent methods used for the preparation of solid dispersions.

3.2 Characterization of Solid Dispersions

A wide range of analytical methods (shown in Table 3.1) are used to investigate the properties of the resulting amorphous solid state materials as a result of employing the solid dispersion technique; with the aim to understand the mechanism, crystallization kinetics, drug-polymer interactions, molecular mobility and thermodynamics of the molecular state.[47] The most frequently employed techniques to characterize solid dispersions are Fourier Transform-Infrared Spectroscopy, powder X-Ray diffraction, Differential Scanning Calorimetry, Scanning Electron Microscopy and Dissolution techniques. However, to tailor the research, various other techniques are combined, such as Transmission Electron Microscopy, Nuclear Magnetic Resonance, Thermally Stimulated Current, etc.[21,95] Of the aforementioned techniques, FT-IR has been successfully applied to study the molecular structure, polymorphism, degree of crystallinity and molecular interactions in the solid dispersion systems.[11,21,71] FT-IR will be applied to understand the real time film formation, to investigate drug-polymer interactions, spatial distribution, stability of solid dispersions employed in this research.

3.3 Fourier Transform Infrared Spectroscopy

3.3.1 Introduction

Infrared radiation is an electromagnetic radiation which is beyond the visible region of the spectrum or radiation not visible to the human eye.[96] IR spectra provide information on the vibrational and rotational changes within the molecules under study and this technique is also called vibrational spectroscopy.[97] The infrared radiation is divided into

three regions; near infrared ($12800 - 4000$ cm^{-1}), mid infrared ($4000 - 400$ cm^{-1}) and far infrared regions ($400 - 20$ cm^{-1}).[98]

Table 3.1 Analytical techniques applied in the characterisation of solid dispersions[6,7]

Characterization	Examples
Molecular interactions **Physical form**	*Fourier Transform- Infrared Spectroscopy* *Nuclear Magnetic Resonance spectroscopy* *UV-Vis spectroscopy* *Raman spectroscopy*
Thermodynamics	*Thermogravimetric Analysis* *Differential Scanning Calorimetry* *Modulated DSC*
Physical form	*Single crystal XRD* *Powdered XRD studies* *X- Ray scattering (small and wide angle)*
Morphology	*Scanning Electron Microscopy* *Transmission Electron Microscopy* *Hot Stage Polarising Microscopy*
Distribution **Morphology and** **Molecular interactions**	*Fourier Transform- Infrared Imaging systems* *Confocal and Global Raman Imaging* *Nuclear Magnetic Resonance Imaging*
Release kinetics	*Dissolution* *Microviscometry*

3.3.2 Principle

Infrared spectroscopy is based on the fact that the molecular system should absorb electromagnetic radiation.[97] For this to happen, one of the molecular vibrations should have the same frequency as the incident beam of light.[96] The other specific feature is that, there should be a change in net dipole moment of the molecule during its vibration.[99]

3.3.3 Theory and Molecular Vibrations

In the context of vibrational spectroscopy, it is common to use, the wavenumber ($\bar{v}$ in cm^{-1}); which is the number of waves per cm. It is given as;

$$\bar{v} = \frac{1}{\lambda} = \frac{v}{C} \qquad (1)$$

where,

v is the frequency in hertz,

19

C is the velocity of light (3 x 10^8 m/s),

$\bar{v}$ is the wavenumber in cm^{-1}

λ is the wavelength in cm.

The advantage of using wavenumber is that, it is linear with the frequency or energy.[58,][59] The relationship between frequency, energy and wavelength is given by Planck's equation which is;

$$E = hv = \frac{hC}{\lambda}$$ (2)

where,

    E is the energy,

    h is the Planck's constant (6.625 x 10^{-34} m^2 kg s^{-1} or J s),

    v is the frequency,

    C is the velocity of light

If some energy is transferred from electromagnetic radiation by absorption, the amplitude of vibrations is increased. In the simplistic harmonic model, the transitions can only occur between the adjacent levels, that is, v_0 to v_1, v_1 to v_2 and the energy associated with these levels are the same.[100] If the energy of the radiation matching this difference is absorbed then the molecules are promoted from ground vibrational state to higher vibrational state which is given as;

$$\Delta E = E_{v1} - E_{v0}$$ (3)

Moreover,

$$\Delta E = hv \ or \ v = \frac{\Delta E}{h}$$ (4)

Substituting 3 in 4,

$$v = \frac{E_{v1} - E_{v0}}{h}$$ (5)

However, the frequency of vibration is related to the mass and the force constant and follows Hooke's law which is;

$$v = \frac{1}{2\pi}\sqrt{\frac{k}{\mu}}$$ (6)

where,

    v is the vibrational frequency,

    k is the classical force constant,

μ is the reduced mass of the two atoms $\left(\frac{m_1.m_2}{m_1+m_2}\right)$

The simplistic harmonic model is best suited for diatomic molecules and for molecules that do not dissociate. For polyatomic and dissociating molecules a good approximation would be to consider the bond behaving as an anharmonic oscillator.[101] If there are N numbers of atoms in the molecule, there will be $3N$ degrees of freedom.[97] The number of vibrations[99] is described based on a three fold set of co-ordinate axes known as normal modes of vibration. Subtracting the translational and rotational motions of the molecule we get $3N$-6 normal modes of vibration for non-linear molecule and $3N$-5 for linear molecule.[97] These vibrations can involve either stretching (change in bond length) or bending (change in bond angle). There are two types of stretching; symmetrical and antisymmetrical stretching and four types of bending vibrations which are rocking, scissoring, wagging and twisting.

3.3.4 Infrared Spectrum

An infrared spectrum is the plot of absorbance vs. wavenumber. A model infrared spectrum of felodipine is shown in Figure 3.1
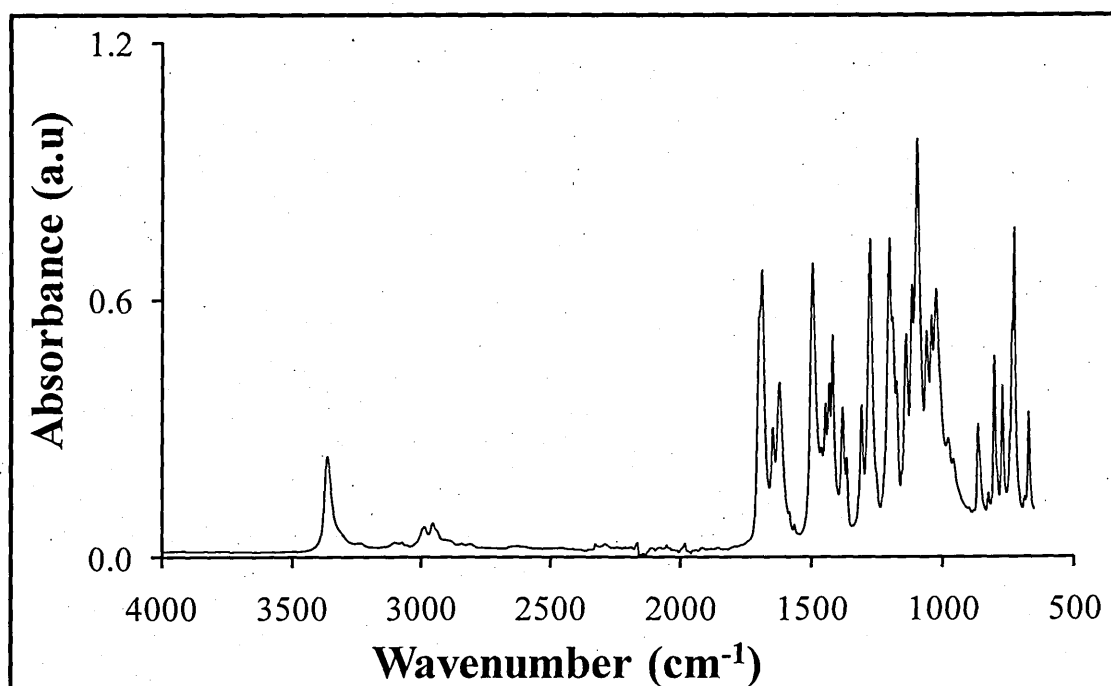
Figure 3.1. Model representation of infrared spectrum of felodipine

3.3.5 Instrumentation

The significant development of FT-IR spectrometers began with the introduction of the Michelson interferometer (Figure 3.2) and, requires the Fourier transform mathematical procedure to convert the interference pattern to spectra generated by the interferometer.[102] These developments outweighed the application of dispersive and

21

grating IR spectrometers. FT-IR spectrometers employ Globar or Nernst sources in the mid-IR region and widely used detectors being DTGS (Deuterated Tri-Glycine Sulfate) in an alkyl halide window resistant to temperature changes and for more sensitive work the MCT (Mercury-Cadmium-Telluride) is used, however, it has to be cooled with liquid nitrogen.[96]

The radiation from the infrared source is directed on to a semi-reflecting beam-splitter made of germanium or iron-oxide coated onto a IR transparent material such as potassium bromide or caesium iodide.[96] The beam splitter reflects approximately half the radiation to the moving and half to the fixed mirror.[102] The beams then return to the beam splitter where they interfere and are partially reflected or transmitted again. The beam returning to the source is of rare interest while the beam travelling perpendicular to the input beam is measured.[102] The two beams then recombine to produce an interference pattern, specific wavelengths within this beam will be constructive (in-phase) or destructive (out of phase) interfered depending on the path difference. At the zero path difference, all wavelengths will be in-phase. This result in the interferogram which is converted to a single beam spectrum by means of a Fourier transform mathematical function.

3.3.6   Advantages of FT-IR over traditional instruments

- Jacquinot or throughput advantage:[98,102] FT-IR doesn't employ any slits and the resolution is defined by the path length of the moving mirror.
- Felgett or multiplex advantage:[98,102] the detector observes all the frequencies concurrently, and the time taken is considerably reduced and the signal to noise ratio is increased.
- Connes advantage:[98,102] the accuracy of the Wavenumber measured is enhanced due to the internal He-Ne reference lasers which not only monitor the movement of the mirrors, but also calibrates the wavelength.

The interferometer modulates the IR frequency differently thereby stray light impact is reduced.[98]

Infrared Detector

Beam

Fixed Mirror

Sample

Moving mirror
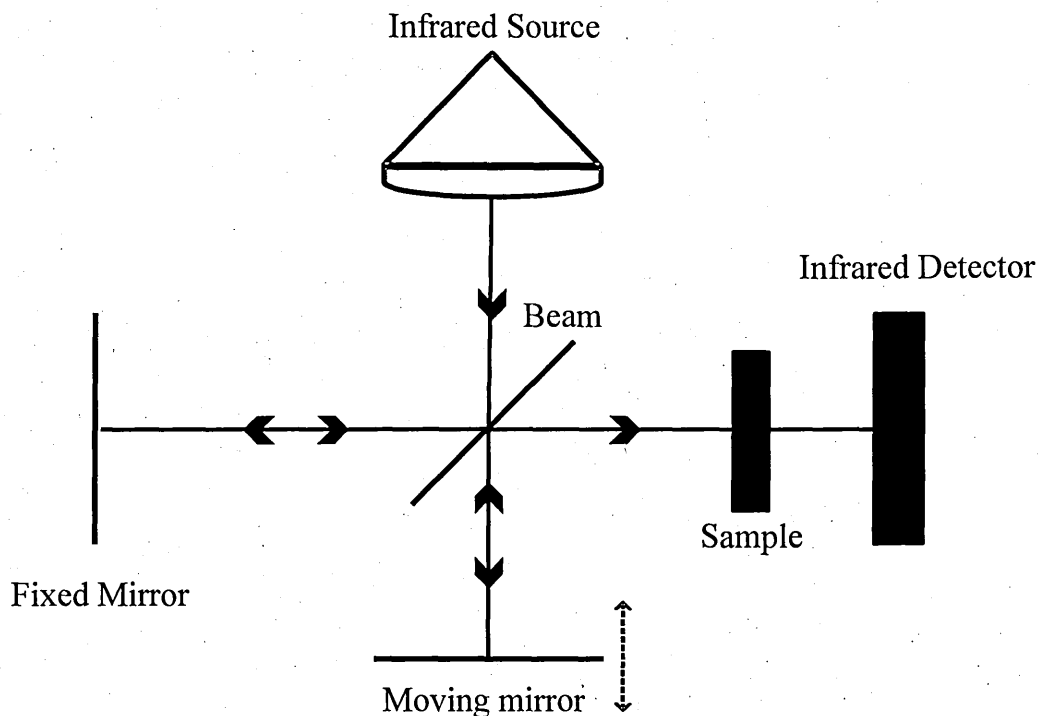
Figure 3.2. Michelson Interferometer with FT-IR components

3.3.7 Attenuated Total Reflectance-Fourier Transform Infrared Spectroscopy

Attenuated Total Reflectance is a total internal reflection sampling technique and is widely used for measuring IR spectra[103] and the schematic representation is shown in Figure 3.3. In ATR, the sample has to be placed in close optical contact with the ATR crystal.[96] The ATR crystal, also called the denser medium, is made from a high refractive material like Zinc Selenide (refractive index is 2.54), Diamond (refractive index is 2.4), Germanium, Silicon or Thallium-Iodide,[103] etc. Of the available ATR crystals, diamond is widely used because it is thermally stable. The sample also called the rarer medium has a low refractive index compared to the ATR crystal. Although, there is total internal reflection at the surface, a small amount of the radiation does penetrate a short distance into the sample.[97] The penetration is the evanescent wave and the absorption of this energy at a particular wavenumber leads to the surface specific spectrum this can relate to a surface equal to 2-10 μm.[103] The evanescent wave and its intensity or penetration depth decays exponentially with increasing distance from the interface. The penetration depth *(d$_p$)* of the evanescent wave at the interface could be calculated using the following equation, which is as follows;[97]

$$d_p = \frac{\lambda}{\sqrt{sin^2\theta - \left(\frac{n_2}{n_1}\right)^2}}$$

(7)

where;

d_p is the penetration depth in μm,

λ is the wavelength in μm,

θ is the angle of incidence,

n_1 and n_2 are the refractive indices of the crystal and sample respectively.

From the equation it is clear that depth of penetration increases with λ at constant θ, n_1 and n_2 while it decreases with increasing θ at constant λ, n_1 and n_2.[96] However, other factors affecting the ATR spectrum include,[97]

1. Angle of incidence which must be greater than the critical angle (θ_c) and given as $\theta_c = sin^{-1} (n_2/n_1)$.

2. Wavelength of the radiation and

3. Refractive indices of the sample and the crystal which governs the nature of interaction of the radiation at the interface.

$$d_P = \frac{\lambda_1}{2\pi n_1 \sqrt{\sin^2\theta_{inc} - \left(\frac{n_2}{n_1}\right)^2}}$$
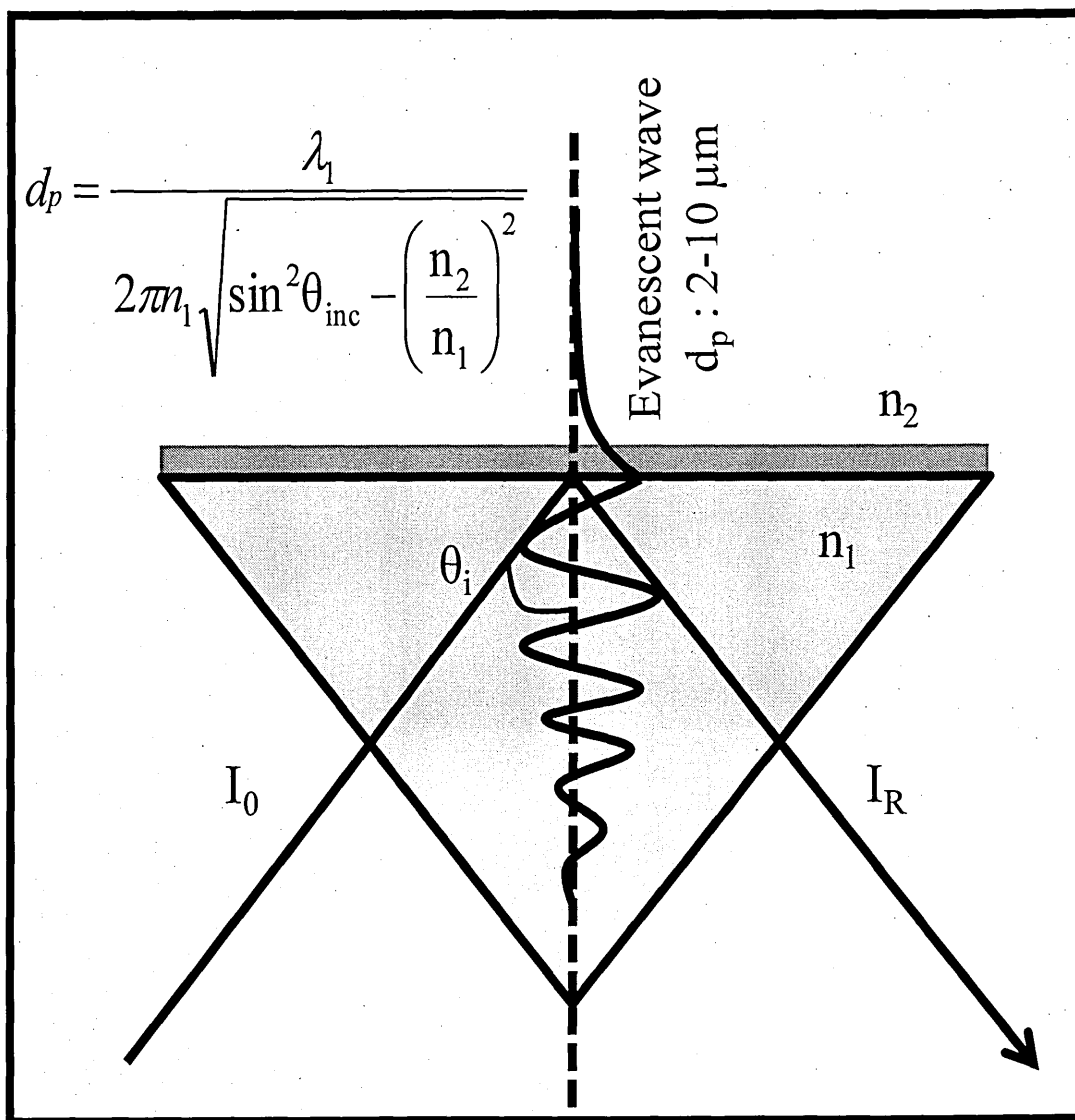
Figure 3.3. Schematic representation of attenuated total reflection

3.4 Spectroscopic Imaging

3.4.1 Introduction

Spectroscopic imaging is also known as chemical imaging or hyperspectral imaging. Infrared microspectroscopy using prism monochromator was made available during the 1940's[104], but the performances of these instruments were marginal.[105] The first true chemical imaging[104,105] was reported in the mid 1990's. With the imaging investigations, apart from the conventional spectroscopic benefits, the distribution and location of the individual components within the mixture can be established.[106,107] These advancements enhanced the chemical characterization of samples on a microscopic scale, its morphological form (typically polymorphs and hydrates).[106,108,109] Thousands of infrared spectra with near-diffraction limited spatial resolution and moderate spectral resolution can be acquired in minutes depending on the instrumentation type.[105] More recently applications have involved real time analysis of complex systems.[107]

The aforementioned vibrational spectroscopic imaging can be approached by single-point measurements or mapping or imaging. In the single-point measurements, firstly, the sample is visually inspected for desirable features using optical microscopy.[105] Then the spatial localization is accomplished by restricting the incident radiation at the sample plane.[108] This is achieved by placing an opaque mask with an aperture of controlled size.[108,110] Spectra are then acquired using single element detector. The microscopic stage is then moved to record spectra from other regions.[104] Precise positioning, accuracy and longer time of analysis make this approach undesirable.[108-110]

The application of infrared microscopy, when coupled to a dispersive instrument, is severely hampered by the low amount of energy passing through the aperture onto the sample from the grating. This can be overcome by the use of an interferometer where all wavelengths of light are measured simultaneously.[105,108,111,112] This technique involves sequential measurement of neighbouring points one at a time.[105,106,113] If these measurements are done in one direction (x-axis), it is termed as line mapping.[104,108,114,115] Moreover, it is possible to move and measure the spectra in both x, y directions. Although this resembles imaging measurements, since the spectra are not acquired using array detectors it is still a mapping technique.[105,108,110]

Imaging utilizes a focal plane array (FPA) detector, were the radiation from the sample plane is segmented at the detector plane[106,108] and is referred to as hyperspectral

imaging.[105,108,109] FPA detectors enable one to acquire thousands of spectra simultaneously and have become increasingly popular in the recent years.[104]

Spectroscopic or hyperspectral imaging can be accomplished by measuring the mid-infrared, near-infrared or the Raman spectrum.[104] In near infrared and Raman, the signal at a given wavelength is recorded at each pixel.[104,105] With the NIR chemical imaging, the light is passed to a monochromator or liquid crystal tunable filter (LCTF).[105] The radiation is then passed onto the sample and the signal from the sample is acquired by the array detector. The image from one wavelength is measured at all pixels simultaneously. The wavelength is then changed and the process is repeated until all the wavelengths are measured.

The monochromator is also located before the sample in Raman Imaging.[105] With Raman imaging, the signal to noise ratio is good, therefore longer integration times are required, also, collection times are longer as a typical Raman dispersion element will only collect data covering a 'spectral window' of around 600 cm^{-1} at a resolution of 2 cm^{-1}. In the NIR imaging, the signal to noise ratio is low but the images can be acquired rapidly. The spectral resolution in both the measurements is determined by the optics (band pass of the monochromator or the filter).

In mid-infrared imaging,[104,105,108,116] the array detectors are coupled to an interferometer. Interferogram from the different regions are acquired simultaneously, after which it is Fourier transformed to yield the desired hyperspectral data.

3.4.2   Infrared imaging background

Infrared imaging utilizes a focal plane array (FPA) detector and allows measurement of spatially resolved images[117,118] which carries spectral information.[105] Chemical imaging combines the benefits of digital imaging and the spectroscopy. The driving force behind this technology jump is the availability of multi-channel detectors[105] and the development of efficient chemometric tools.[108-110,117,119,120] The acquisition of chemical images using linear array of detector is called pushbroom approach whereas acquisition using 2-D array detectors is called quilting or mosaicing.[105]

3.4.3   Instrumentation

The marriage between the traditional techniques like microscopy, infrared spectroscopy, interferometry and focal plane array detectors (FPA) have led to the fast development of the Fourier transform infrared chemical imaging[105,108,110,117,121] (shown in Figure 3.4).

Infrared microscopes differ from optical microscopes in physical construction and source. Since glass doesn't transmit radiation of wavelength longer that 4.5 μm all

26

reflective Schwarzschild objective is used.[105] Radiation selection optics are designed for flexibility in switching between visible and infrared light. That is, the regions of interest can be selected using visible light source while data collection or scanning is carried out using infrared light. Moreover, to increase the spot size and spatial homogeneity/field of view (FOV) diverging lenses like lightly sanded KRS-5 are used.[105,108]

The infrared microscope is interfaced to a Michelson interferometer for the imaging studies and requires the Fourier transform mathematical procedure to convert the interference pattern (intensity path difference from the static and moving mirror) to spectra generated by the interferometer.[102] There are two scan modes available, continuous scan and step scan. If the moving mirror is scanned at a constant rate between data collection points it results in continuous scan process and often used for steady state measurements. When the moving mirror is stopped and dithered at fixed distances over the length of the data collection sweep, the collected data can be recombined to form an interferogram and this process is known as 'step-scan'.[105,108] Step scan mode will be a powerful tool for studying spectroscopic changes occurring on the nanosecond or microsecond time scale. The primary advantage of operating interferometer in continuous scan mode is reduced instrument cost (no additional hardware or software modifications required) and increased data collection efficiency (mirror stabilisation time is eliminated).[108]

The infrared microscopes and interferometer are then assembled to the multichannel or large format array detectors arranged in two dimensional grid patterns.[105,108] The earliest FPA detectors were made from indium antimonide (InSb) but were replaced quickly due to low spatial area focus (500 µm x 500 µm) and high cut off (1800 cm^{-1}). These were replaced with mid-IR mercury-cadmium-telluride (HgCdTe) focal plane array (MCT-FPA) detectors. The imaging FPA detectors operate in the photovoltaic (PV) mode rather than the conventional photoconductive mode MCT detectors. Consequently, the cut-off wavenumber for the PV-MCT is at about ~850 cm^{-1} and MCT detectors operate effectively at -20 °C, hence requires cryogenic cooling.[105]

The infrared sources used in the laboratory based instruments are incandescent (silicon carbide) Globar sources.[102,105] Other sources are synchrotron and free electron laser but the sample has to be moved from labs. The modulated radiation from the source is passed through the apertureless Schwarzschild optics which is then focussed on to the sample. The entire field of view (FOV) or region of interest in the sample is illuminated and is recorded by the large format MCT-FPA detectors. As mentioned previously, the FPA's are operated in the photovoltaic mode; hence the FPA response is triggered by

the interferometer. At each trigger, the pixel responses are read in snapshot mode.[105] That is, all the pixel responses are read simultaneously, processed and transferred to the data system to provide an interferogram. The interferogram is then Fourier transformed.

The chemical image can be viewed as a 3D block termed as hypercube comprising of two spatial (x, y) and one wavelength (z) dimension[104,110,122] (Figure 3.5). Each data point in the cube provides spectral information, and the process of acquiring the image is called as hyperspectral imaging. Single data point in the image is termed as the pixel (1D) which yields spectral information while the collection of pixels represents image plane or channel (2D) and carries information on spatial and distribution patterns within the selected system.[104,115,123]

A variety of sampling techniques have been utilised in spectroscopic imaging experiments like transmission or external reflection like reflection-absorption, specular reflectance or diffuse reflectance techniques and attenuated total reflection sampling modes are utilised. However, these choices depend upon nature and thickness of the sample.[105,108]
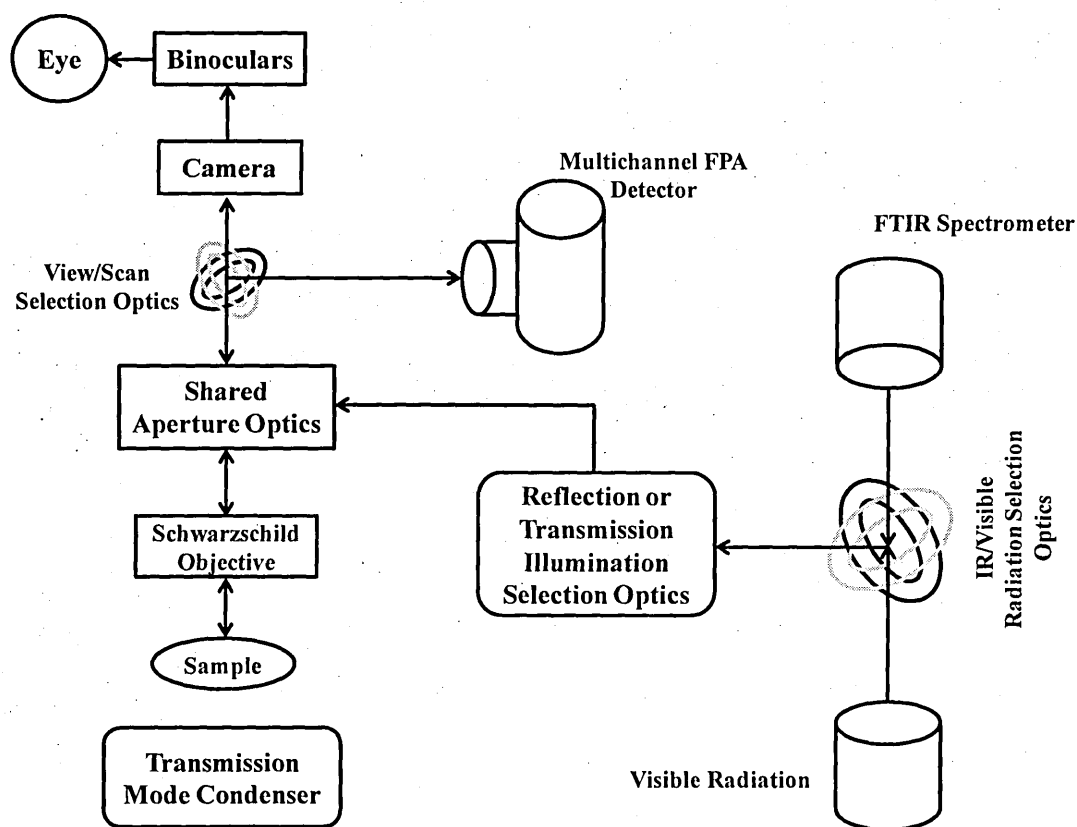
Figure 3.4. Schematic representation of FTIR chemical imaging

Table 3.2. Strategies to improve SNR to obtain high fidelity image cube[108,124-126]

Modifications	Strategies	Significances
Hardware modifications	Bandpass filters	restricts unwanted radiations
	Diffusers or diverging lenses	improves spatial homogeneity
	Cold-shield	rejects thermal background noises
Signal acquisition protocols	Time averaging data cubes	Signal integration (every pixel) at each interferometer position
	Frame or Image co-addition	Reading each pixel response several times and then co-addition
	Median filtration time averaging	Removes random or high intensity frame integrations.
Image transformation schemes	Gain averaging	Normalisation of interferogram intensities
	Apodization and Truncation	Applied to synthetically eliminate the high-frequency noises.
Post data refinement	Pseudo co-addition	Referencing single sample image to several BG images
	Data processing algorithms	Removes spectral and spatial artefacts

Note: Protocols improving SNR without affecting the temporal resolution is ideal.

Spectrum - One Dimensional Data

Spatial distribution of absorbance corresponding to a wavenumber - 2D data

Chemical image or hypercube - 3D data
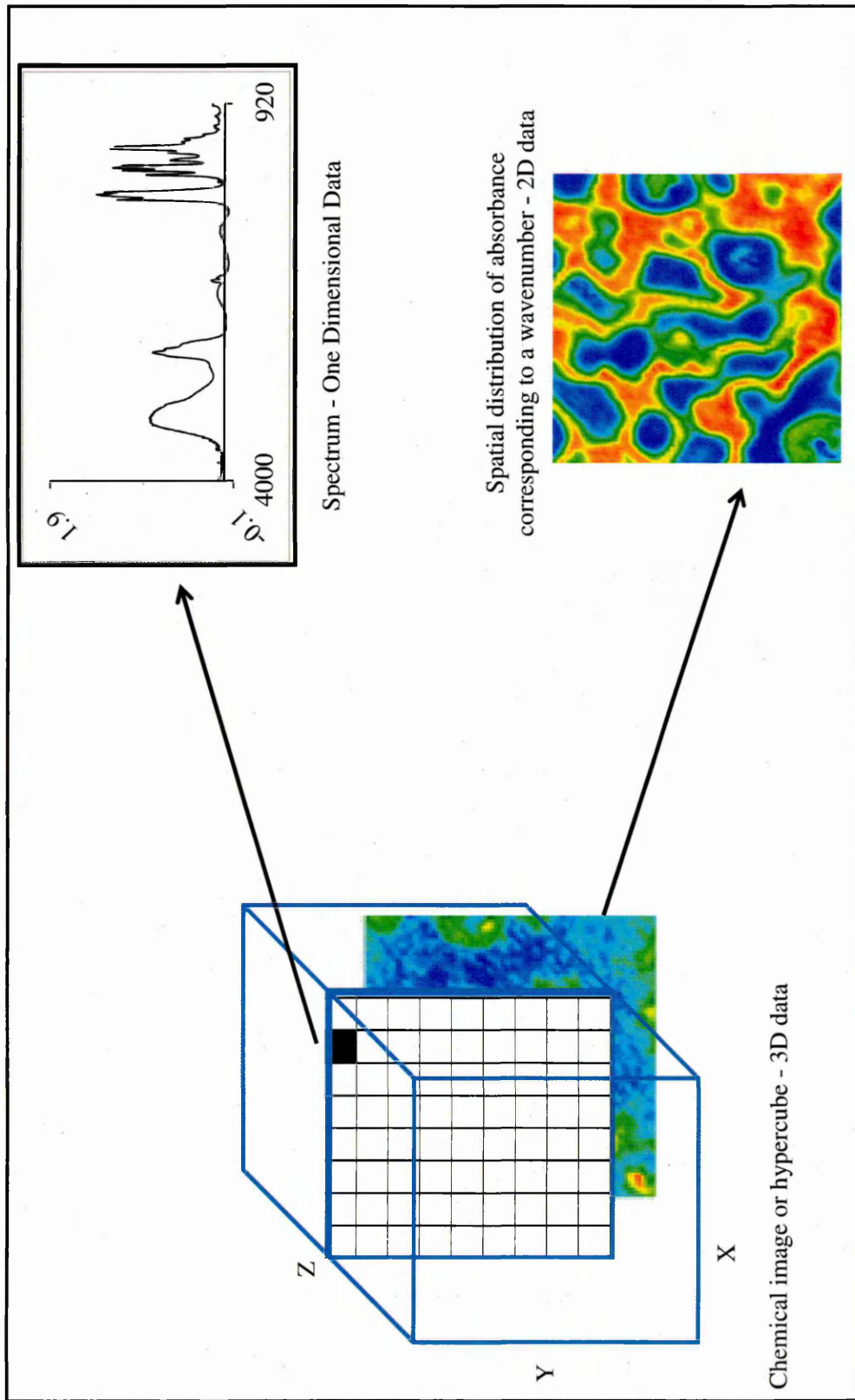
Figure 3.5. Schematic representation of a data cube generated during mid infrared chemical imaging experiment

30

3.4.4 Resolution

The performances of the FTIR imaging systems are limited by the identity of the sample, physical state of the sample or particle size of the sample.[108] However, these limitations are discussed as resolution limit (spatial, spectral and temporal). Although these systems do not have apertures for image collection, the detector elements are of finite size. That is, each pixel size resolution or spatial resolution is 5.5 μm.[105,102] Spectral resolution is governed by the distance that the moving mirror travels; longer distances provide a higher resolution, but there will be a time penalty at a fixed velocity. There will also be a S/N penalty at higher spectral resolution as the system is detector noise limited, therefore a compromise between acceptable acquisition time, S/N and spectral resolution has to be made.[108]

3.4.5 Signal to noise ratio (SNR)

To obtain spectra or image at high fidelity the signal to noise ratio is considered as the performance characteristics of the imaging system. The major efforts to improve the SNR can be divided into four categories which are hardware modifications, signal or data acquisition protocols, image transformation schemes and post data refinement protocols,[108] shown in Table 3.2.

3.5   Thermogravimetry-Mass Spectrometry or Evolved Gas Analysis

Thermoanalytical techniques are universal tools in which the changes in a physical property of a material are monitored continually as a function of temperature.[127] For example, with thermogravimetric analysis or differential thermal analysis, the changes in the sample weight or thermal events during programmed temperature treatment are recorded.[127,128] It is useful for measuring physical or thermal properties, composition and stability of the materials.[128-130] However, often the obtained results lack chemical and analytical information.[127,128,130,131]

For complete characterisation of a compound, simultaneous techniques that can provide complementary information will be useful.[127] Thus, coupling thermal analysis like TGA with mass spectrometry or infrared spectroscopy allows evolved gases to be analysed and identified; supplementing the required information.[130] Of the available choices, coupling mass spectrometry with TGA is preferred because of the advantages like high specificity, sensitivity, fast response, low detection limit, multiple ion and isotope detection abilities.[130] Evolved Gas Analysis (EGA) is a technique in which the nature and/or amount of volatile products released by the substance which can be residual

solvents, degradation products, moisture, etc. are studied.[129,132] Samples under investigation can be subjected to isothermal or ramping temperature treatments.

The thermogravimetric measurements require thermobalance or precision balance (made of material depending upon experimental temperature range, sample quantity, etc.) operating with a temperature programmed furnace.[127] Mass spectrometers compose of ion source, mass filter and ion detector.[128-130] The TG instrument works at atmospheric pressure (typically 10^3 mbar) while mass spectrometer works under high vacuum (typically 10^{-5} mbar).[129] Therefore an interface for reducing pressure is required to couple thermobalance to the mass spectrometer which depends upon instrumentation and applications.[128,132] A schematic diagram of such an instrument is shown in Figure 3.6.

During the measurement, a sample weighing few milligrams is placed in a refractory crucible which is subjected to isothermal or ramping temperature program. Also the weight is recorded in the instrument by means of a sensitive balance.[130] The measurements can be performed from 25 °C to 1000 °C (or higher) in the presence of air or nitrogen. The quality of the data is influenced by the sample size, carrier gas, sample holder or heating rate.[133]
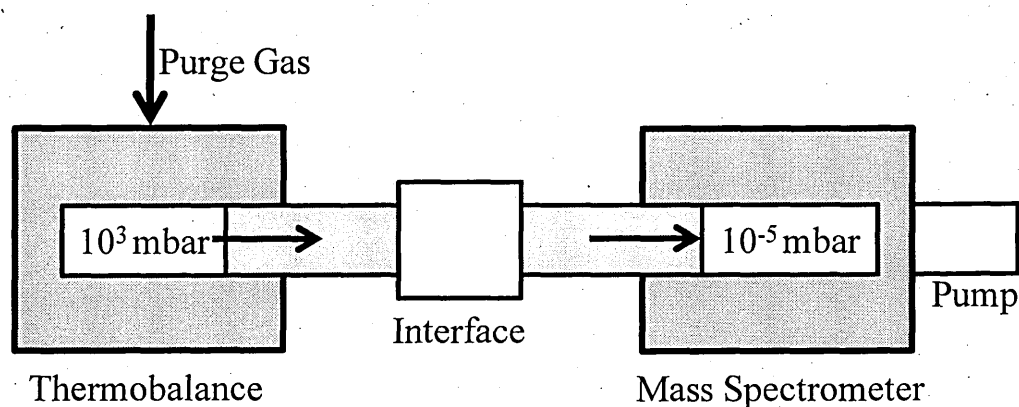
Figure 3.6. Schematic representation of TG-MS instrument

Moreover, these hyphenated techniques can also be combined to enable the differential thermal analysis (DTA) function.[127] DTA may be defined as a technique for recording the difference in temperature between a sample and a reference material against either time or temperature program.[130] DTA measurements are useful in studying decomposition, dehydration, glass transition, melting etc. DTA results are useful in the better understanding of results from spectroscopic and thermogravimetric studies.
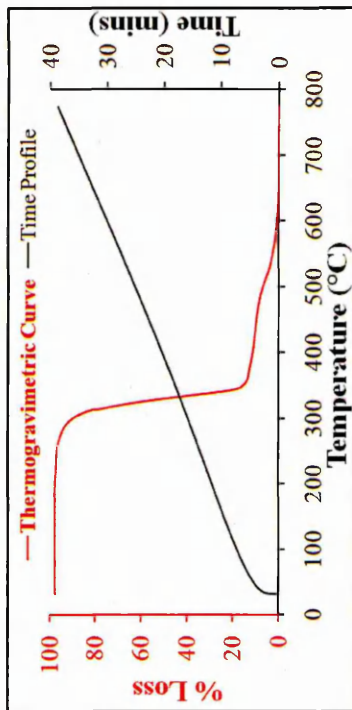
Figure 3.7. Model representation of TGA curves

Figure 3.8. Model representation of DTG curves

Figure 3.9. Model representation of DTA curve
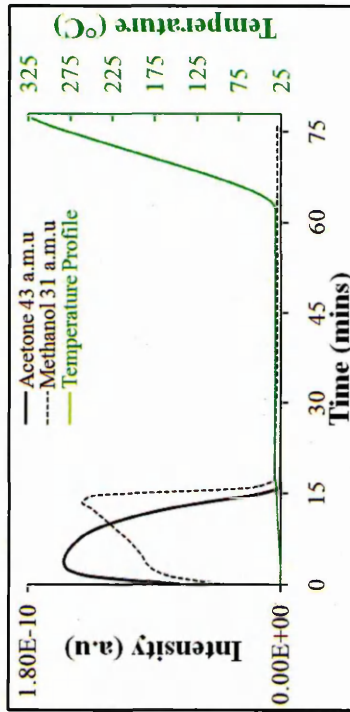
Figure 3.10. Model representation of ion chromatogram, m/z = 43 and 31 representing acetone and methanol, respectively from TG-MS

33

The output of such measurements is a thermogram or TG curve (Figure 3.7), derivative thermogram or DTG curve (Figure 3.8), differential thermal analysis curve or DTA curve (Figure 3.9), mass spectra or ion chromatogram (Figure 3.10). The thermogram shows the weight loss of the sample as it is heated which could be due to evaporation or degradation. Derivative thermogram is a mathematical manipulation to determine any subtle differences in the TG weight loss curve. The DTA curve shows the plot of temperature difference between sample material and reference material (mW/mg) against temperature (in °C). The exothermic events could be due to melting, T_g or degradation. The mass spectra or ion chromatogram is the plot of ion current against time (minutes) or temperature (°C). These are model representation and will be discussed in detail in the results and discussion section in the following Chapters.

3.6   Data Processing Tools

3.6.1   Univariate analysis

A univariate technique uses only one variation within the dataset to categorise the sample under investigation. When the sample contains few components with non-overlapping bands then the peak height or peak area measurements can be used to identify the components.[113] The method is fast, simple to understand and easy to calculate. However, it is well suited for uncomplicated samples and binary mixtures only. The method does suffer in distinguishing complex mixture samples; sample purity is also an important factor, which restricts its usage. The other drawbacks with the univariate techniques are that optical linearities are encountered.

3.6.2   Multivariate analysis

With complex systems there is high probability of overlapping bands making the identification more complicated.[113] To overcome this multivariate data analysis is done.

a.   Compare Correlation

Correlation mapping or compare correlation is a class of statistical pattern recognition approaches where the samples under investigation are classified according to a specific physical or chemical property.[134] The property of interest used to describe each sample within the dataset is called a pattern. A set of samples whose property is defined and known are called a training set or reference samples. Moreover, when the samples are classified based on a property or pattern it is termed recognition.[135] The most common assumption made is that the data set has Gaussian like distribution and then the data are classified by their mean and covariance.

The aforementioned classification systems are better expressed as correlation coefficient values which measures similarity or dissimilarity between the sample and the training dataset. The correlation coefficient values or simply correlation scale ranges between 0 and 1, with 1 being perfect correlation between two data or spectra. In order to differentiate these numerical values, each region is assigned different colours like blue, green and red and each colour represent correlation. These values are basically qualitative parameters used to better understand the homogeneity in distribution or phase separation,[136] etc. A correlation value between 0.99 and 0.80 (assigned red) indicates that the regions in the sample belong to the reference product to which it is compared; correlation value less that 0.5 indicates absence of similarity (assigned blue). The intermediate values would require cautious interpretation.

b. Principal Component Analysis

With complex systems there is high probability of overlapping bands due to the presence of multiple components within each pixel, making the identification more complicated.[113] To overcome this multivariate data analysis is done. One of the frequently applied tools is the Principal Component Analysis (PCA).

Principal Component Analysis (PCA) is widely used to reduce the dimensionality of the data that would contain large amount of information. Moreover, it is mainly applied to unravel the overlapping spectroscopic features and helps to identify a number of pure components present in the sample.[113] There are many ways to identify and one such method is to generate eigenvalues which are scalars. This is done iteratively and principal components are identified, however, assumption is that the signal collected is linearly related to concentration.

The maximum variance is explained by the first principal component (PC) and the second PC is constructed orthogonal to the first PC which explains the residual variance and so on[104] with additional PC's. Thus, PCA decomposes the complex data into sections of signal and noise,[113] moreover, the first few PC's explain the maximum variance or eigenvalues. The PC eigenvalues decrease with number of components and level off when the complete signal is calculated. The signal/noise can be increased by removing the noise from the data. The result of the analysis is discussed in terms of scores and loadings.[104] Loadings are the number of components that have detectable signal while the scores are related to the concentration of the components.[113]

PCA sometimes can provide inconclusive or overestimated results. Hence, working knowledge on how many components present in the sample is pre-requisite. Cross-

validation schemes like box-plot, F-test of the variance or the predicted residual error of the sum of squares are being widely used conjunctively to aid the better understanding the results.

c. Multivariate Curve Resolution-Alternating Least Squares

Multivariate Curve Resolution (MCR) is a chemometric multivariate approach and is a class of bilinear self-modelling curve resolution methods.[137,138] MCR is useful in analyzing large data matrices. Moreover, it does not require any prior knowledge about the sample, spectral corrections or manipulations but rather utilizes the raw data files. A detailed description can be found elsewhere.[137,138]

The main objective of MCR is to mathematically decompose the large amount of spectral data from the multi-component mixtures to pure spectra or pure intensities of the individual components. The MCR works by initially applying principal factor analysis (PFA) in order to recognise the pattern involved in the studied data. In this step, the PFA looks for major trends and categorises the data based on the varying factors. In the following step, alternating least squares (ALS) is applied to convert the mathematical results to more meaningful analytical data. A range of constraints can be applied to extract further information.[139]

Since the raw spectral data files contain noise associated with the measurements,[140] the predicted model can produce solutions (called principal factors) that fit mathematically, but do not carry any physical or chemical meaning and this uncertainty is called rotational or intensity ambiguities.[138,141-144] Hence, choosing the optimal number of factors is an issue so prior working knowledge about the sample is helpful. Additionally, application of exploratory data analysis is vital. Studies have shown that when the system is rank-deficient or homogenous, conventional MCR is unable to distinguish or extract all of the components. New approaches are being adapted to handle these uncertainties.[136,142,144]

The advantages and disadvantages of univariate, compare correlation, principal component analysis and multivariate curve resolution are shown in Table 3.3.

3.7 Statistical Analysis

In order to better interpret any experimental data, statistical significance testing is applied. Many statistical procedures are available to perform this. However, analysis of variance (ANOVA) is the procedure of choice. ANOVA is an example of a parametric statistical test. It is a very useful measure to compare similarity or differences among or

36

within means from different groups. All analysis is done at a 95% confidence level, as it is a common practice in pharmaceutical analysis.

Two way analysis of variance allows is carried out to understand the influence of temperature (30 °C, 40 °C, 50 °C) and sample (for example, binary solvent mixture, 100% drug, 100% polymer, various drug loaded solid dispersions) on the evaporation rate of solvents and formation rate of solid dispersions. ANOVA results are interpreted by taking into consideration of the F-values, F_{crit}-values and P-values. The ANOVA F-value is a ratio of the variance of the between group means divided by the variance of the within group means. A P-value is a measure of how much evidence we have in obtaining the result. If F-values are larger than the F_{crit}-values ($F > F_{crit}$) and if P-value is less than 0.05 (that is 5% significance testing) then any changes interpreted are significant (numerates are indicated in green), if $F < F_{crit}$; $P > 0.005$ then the results are insignificant and numerates are indicated in red. Unfortunately, ANOVA does not show were the difference lies.

Least Significant Difference (LSD) tables can be constructed from ANOVA results to further explore any significant changes between the measurements. LSD is a method used to make multiple comparisons between various treatments to ascertain where the difference lies. At the chosen level of significance, for each set of data a statistical value is calculated. The calculated value is then correlated with the results obtained from the experiments. If the difference between two temperature/sample means is greater than this calculated value then there is significant difference between the compared data and the values are coloured green, otherwise red.

Table 3.3. Comparison of various data analytical tools

	Univariate analysis	Compare Correlation	Principal Component Analysis	Multivariate Curve Resolution
Advantages	• Simplest Approach • Each pixel in image represents the intensity of the chosen wavenumber (cm^{-1})	• Easy and simple • Data classification according to similarity • Comparison is made at every pixel	• Purely descriptive or exploratory data analytical tool • Data reduction • Unsupervised approach	• Can be used as a predictive model • Direct comparison to pure spectrum • Provides pixel to pixel variations • Unsupervised approach

Disadvantages	• Unique peaks required
	• Misleading results from
	  - *Baseline shifts*
	  - *Overlapping bands*
	  - *Optical artefacts(cf. Chapter 5.4)*
		• Need pure materials library (supervised approach)
		• Reference and test materials have to be examined under same conditions
			• Since the outputs are variance, comparison of extracted spectrum to pure spectrum needs caution	• Rotational or intensity ambiguities (cf. Chapter 3.6.2)

CHAPTER 4.
THE APPLICATION OF VIBRATIONAL SPECTROSCOPY TO SOLID DISPERSIONS: KINETICS OF SOLVENT EVAPORATION AND DRYING

4.1 Introduction

In order to understand the structure of solid dispersions, crystallization kinetics, drug-polymer-excipient interactions, molecular mobility and thermodynamics of the molecular state a wide range of analytical methods have been used to characterise the prepared solid dispersions.[47] However, real time or *in situ* measurements are required to understand the dynamics of solvent evaporation and formation of solid dispersions. Real time measurements using a wide range of analytical instruments have proven indispensable in many fields. For example, FTIR spectroscopy,[145-161] Raman spectroscopy,[147,162-164] Near infrared spectroscopy, Nuclear Magnetic Resonance spectroscopy,[165] X-Ray Diffraction,[166,167] Surface Circular Dichroism, Neutron Scattering,[168] Small-Angle X-ray scattering[169] and Differential Scanning Calorimetry[162] have been used to understand the polymerisation, polymorphism, granulation process, topical drug delivery, dissolution, coatings and catalysis. Particular reasons for using IR are molecular specificity, signal strength, non-destructive nature and extreme sensitivity to subtle matrix and environment changes.[170] In particularly, the FTIR-Attenuated Total Reflectance mode has been the technique of choice in many fields like catalysis,[149,171] clay nano-composites,[150] polymerisation,[151,153,161] corrosion[158-160] and gelation.[153,157] In the pharmaceutical field FTIR-ATR (spectroscopy and imaging) *in situ* measurements are widely used to study the crystallisation,[172] polymorphism,[147] tablet compaction,[173] super critical carbon dioxide ($scCO_2$) polymer-drug formulation[40] and dissolution testing.[164]

The main objective of this work is the application of vibrational spectroscopy to understand the dynamics involved in solid dispersion formation. To the best of our knowledge this is the first time *in situ* FTIR-ATR has been applied to solid dispersions to address the following questions:

1. Can FTIR-ATR be applied to follow the rate of film or solid dispersion formation?
2. Does temperature have any effect on the nature of film formation?
3. Can spectroscopy be used to interpret molecular interactions (solvent-solvent, solvent-solid interactions and solid-solid interactions)?

4. Can spectroscopy be used to determine the final product characteristics based on temperature, solvent selection and drug loading?

To answer these questions, a model drug, felodipine and polymer, Polyvinyl pyrrolidone (PVP) were selected. Solvents (methanol, acetone and dichloromethane) were selected based on volatility, Gutmann's acceptor-donor numbers, density and refractive index as shown in Table 4.1.

In the preparation of solid dispersions one of the key components is the choice of solvent, because physical mixing of the drug and polymer would not yield solid dispersions. The drug and the polymer are mixed in a common solvent, and evaporation yields intimately mixed solid dispersions. Many other methods are available and details can be found elsewhere.[7,10,28] Solvent nature, Gutmann's acceptor-donor numbers and density are some of the factors that are the important while selecting the solvents. Spectroscopic studies have shown that solvents can alter molecular interactions of 1,4 dihydropyridine,[31] swelling behaviour of hydrogels,[32] change in the conformation of gramicidin[33] and alter the denaturation of urea.[34,35] These effects are characterised by the solvent induced frequency shifts[31] (SIFS) in carbonyl moieties and other groups involved in the intermolecular interactions.

Of the available analytical techniques, IR spectroscopy is widely used in investigating the drug-excipient interactions with the pharmaceutical formulations and hydrogen bonding in all states of matter.[37,174,175] The important characteristics studied are the appearance of new IR absorption bands, broadening of bands and changes in the peak intensities and position.[37,96,176]

4.2 Experimental part

4.2.1 Materials

Materials used are a model drug, felodipine (AstraZeneca, U.K) and the model polymer, polyvinylpyrrolidone (Plasdone K29/32, average molecular weight = 58,000), the latter being purchased from ISP. Acetone, dichloromethane and methanol (HPLC grades) were obtained from Sigma-Aldrich, Switzerland. Unless stated, the drug, the polymer and the solvents received were used as obtained.

Table 4.1. Properties of organic solvents

Solvents	AN	DN	Density	Bp (°C)	R.I	Surface Tension (mN/m at 20 °C)	Vapour Pressure (mmHg at 25 °C)	Polarizability (x 10^{-24} cm^3)	Dipole Moment (D)
Methanol	41.5	19	0.79	65	1.31	22.7	265.4	3.257	1.70
Acetone	12.5	17	0.78	56	1.35	25.2	348.4	6.334	2.88
DCM	20.4	1.0	1.32	39	1.40	26.5	448.0	6.490	1.60

Note: AN- Acceptor Number; DN- Donor Number; Bp - Boiling point, R.I - Refractive index

Table 4.2. Characteristic Infrared frequency

Components	Characteristic Bands		Penetration depth (d$_p$ in μm)	
			Pure Materials	*Mixtures*
Methanol	ν_{sym}(CH3)	2830[177]	0.71	0.34
Acetone	ν(C=O)	1711[176]	1.05	0.56
Dichloromethane	δ(CCl)	702[176]	2.19	1.35
Felodipine	ν(C-O)	1099[176]	1.20	0.87
PVP	ν_{sym}(CH2)	2880[57]	0.46	0.33

Note: The refractive index for felodipine and PVP in pure materials is considered to be 1.5. For mixtures, the refractive index (1.3) is calculated based on the weighted average of the starting material (R.I).

4.2.2 Sample preparation

Three different drug-carrier weight ratios (20:80, 50:50 and 80:20) for binary systems, 100% drug or 100% polymer and two different mixed solvent systems (acetone/methanol and DCM/acetone at 50:50, v/v) were used. 1 g of the solid was dissolved in 25 ml of the solvents to yield 4 wt% solutions. 50 μl of each solution was cast directly onto a pre-heated ATR crystal using a Gilson pipette. Studies were carried out at 30 °C, 40 °C and 50 °C. Each experiment was measured in 5 replicates to ensure reproducibility.

4.2.3 Experimental Parameters

FTIR spectra were collected using a variable temperature Graseby Specac single reflection diamond ATR attached to a Thermo Nicolet Nexus bench equipped with a Mercury-Cadmium-Telluride detector. The spectra were collected between 4000-650 cm^{-1} at a resolution of 4 cm^{-1} using 4 co-added scans. Since the formation of solid dispersions from mixed solvents proceeded at a rapid rate, the total experimental time was kept short and a time of 2 seconds was required for the 4 scans. The spectra were collected continuously (series) over a pre-determined period of 5 minutes. All the spectra during the kinetic study were collected in the Log (1/R) format. Background spectra of the blank ATR crystal were collected before each experiment. The ATR crystal was heated to a predetermined temperature and allowed to equilibrate. 50 μl of the prepared drug polymer solution is placed on to the ATR crystal. As soon as the solution is pippetted out onto the crystal, the initial data are dominated by the solvent spectra. As the solvents start to evaporate, drug and/or polymer bands appear in the evanescent wave and their spectrum is observed. The spectral changes are monitored and recorded.

4.2.4 Multivariate Curve Resolution

The purpose of using multivariate curve resolution (MCR) is to mathematically decompose the large amount and overlapping spectral data from the multi-component mixtures to pure spectra and pure intensities. The series runs were split into individual spectra which were then converted to a multifile using GRAMS. The compatible multifile was then loaded onto the MCR software version 3.19.04 (Courtesy: Dr. Thomas Hancewicz, Sr. Project Scientist, Unilever R&D, USA).[140,178,179] To achieve this, the following parameters were chosen to carry out the MCR procedure on the spectral data matrix:

1. Pure variable selection - Principal Factor Analysis

2. Transformation – Alternating Least Squares (ALS)

3. Constraints – Modified Alternating Least Squares (MALS-2D)

4. Maximum Iterations – 500 times

5. Data display – Rastering mode

6. Optimal number of factors – Prior knowledge about the sample

4.2.5 *Statistical Analysis*

In order to better interpret the kinetic data, statistical significance testing was applied. Many statistical procedures are available to perform this. However, analysis of variance (ANOVA) is the procedure of choice. ANOVA is an example of a parametric statistical test. It is a very useful measure to compare similarity or differences among or within means from different groups. Unfortunately, ANOVA does not show were the difference lies. Least Significant Difference (LSD) tables were then constructed from the ANOVA results to further explore any significant changes. LSD is a method to make multiple comparisons between the various treatments to ascertain where the difference lies. All the analysis was done at 95% confidence level.

4.3   Results

As a first step, typical infrared spectra for each of the pure components were obtained and are shown in Figure 4.1 A to E.

The main objective of the study is to monitor in real time the evaporation of solvents and formation of solids. Due to potential complexity of the system under investigation with overlapping infrared bands, before considering any measurements on drying solutions, it is required to select a single discriminating band for a component of interest in the mixture. The characteristic peaks selected are listed in Table 4.2. Moreover, the peak height measurements were chosen instead of the widely used peak area approach. Changes in intensity with time can be related to the relative concentration of the components within the 10 μm layer closest to the ATR crystal (depth of penetration, d_p = 2 to 10 μm). Typical spectral changes for felodipine/polyvinylpyrrolidone cast from acetone/methanol and dichloromethane/ acetone are shown in Figure 4.2 and Figure 4.3, respectively.
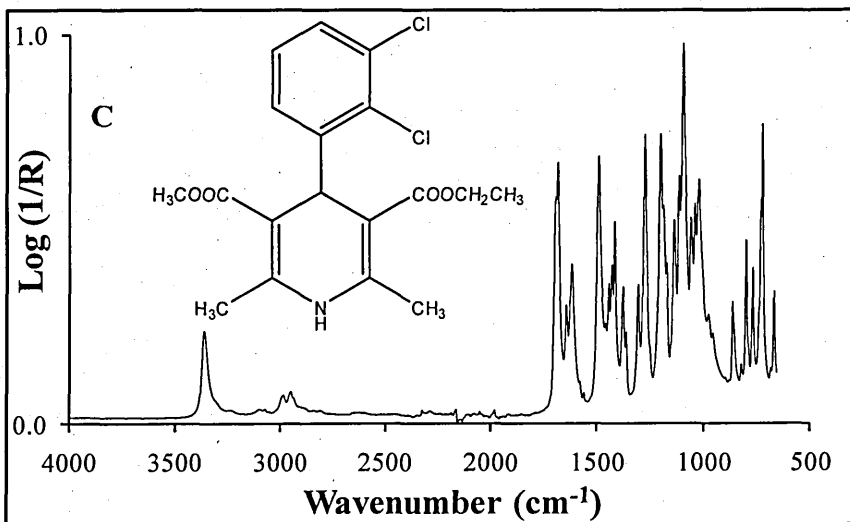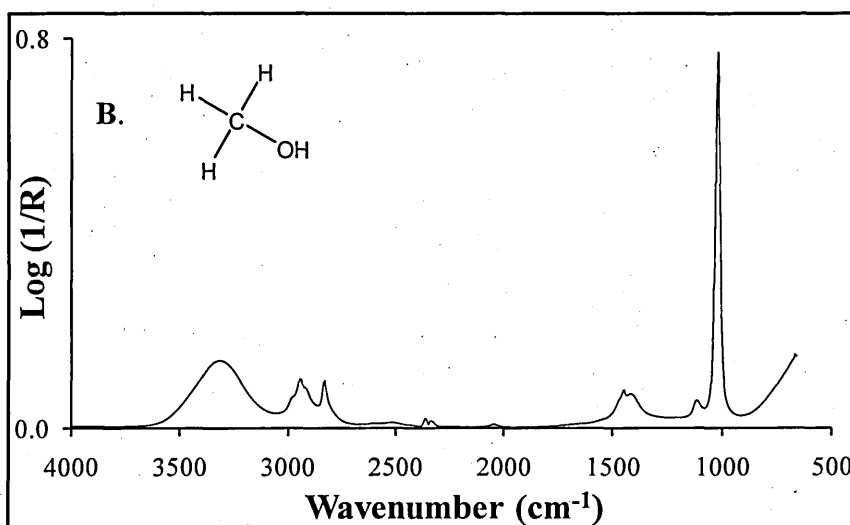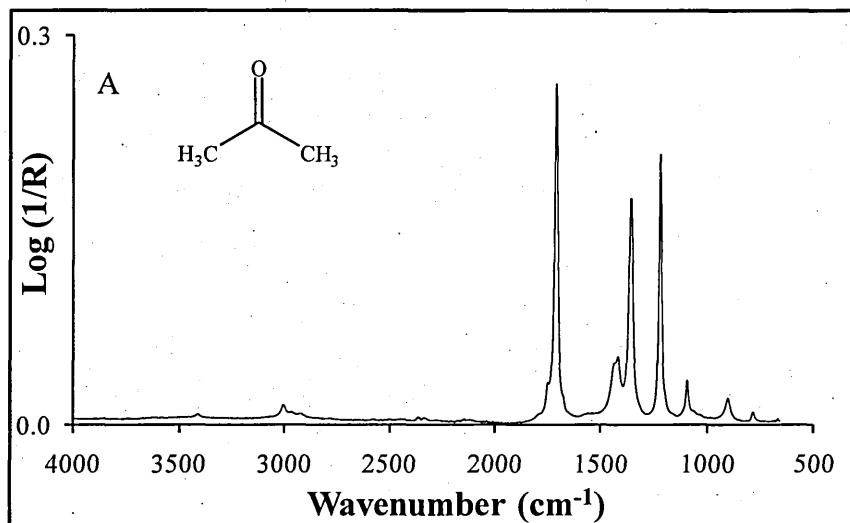
Figure 4.1. Structure & typical Spectra of Acetone (A), Methanol (B), Felodipine (C)
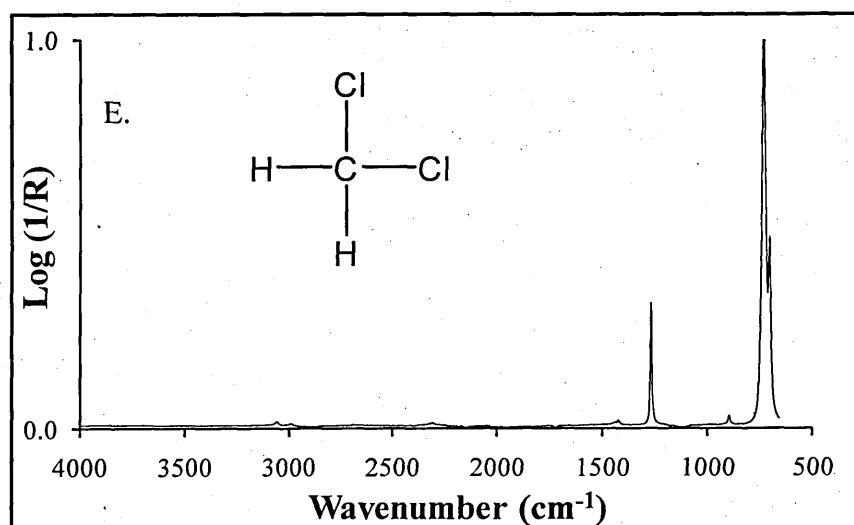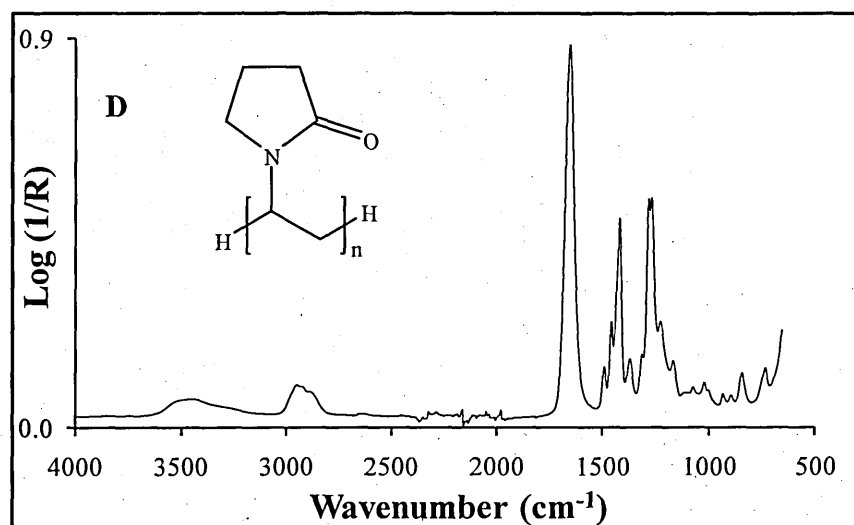
Figure 4.1. Structure and typical Spectra of PVP (D) and DCM (E)
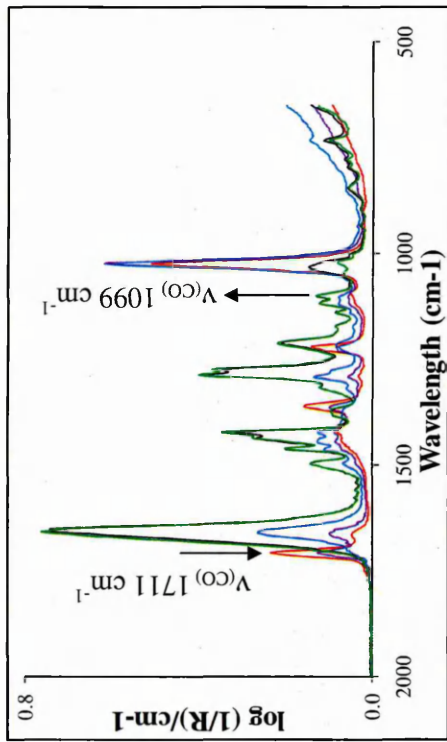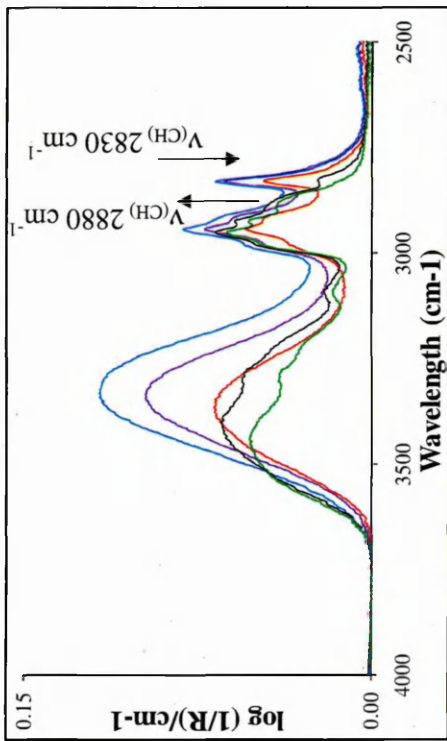
Figure 4.2 Spectral changes as a function of relative intensities-Fel/PVP solid dispersions cast from acetone/methanol mixture

—0.462 min   —0.693 min   —0.792 min   —1.056 min   —2.045 min
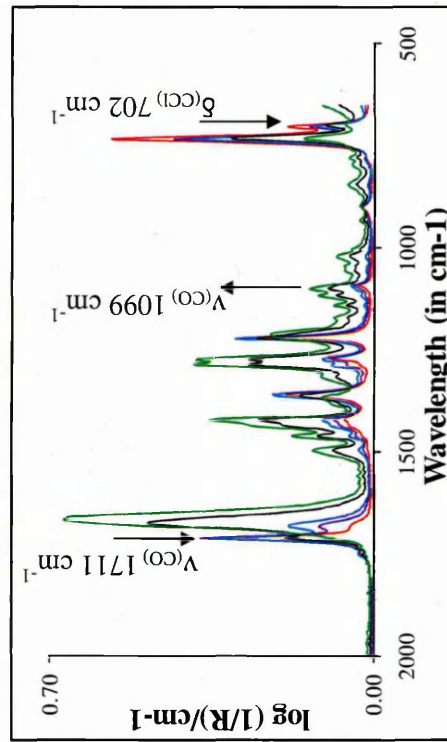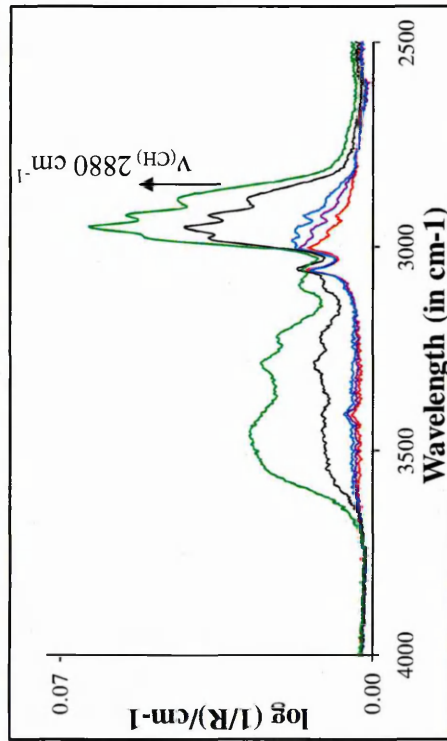
Figure 4.3 Spectral changes as a function of relative intensities-Fel/PVP solid dispersions cast from DCM/Acetone mixture

—0.198 min   —0.659 min   —0.692 min   —0.725 min   —2.011 min

46
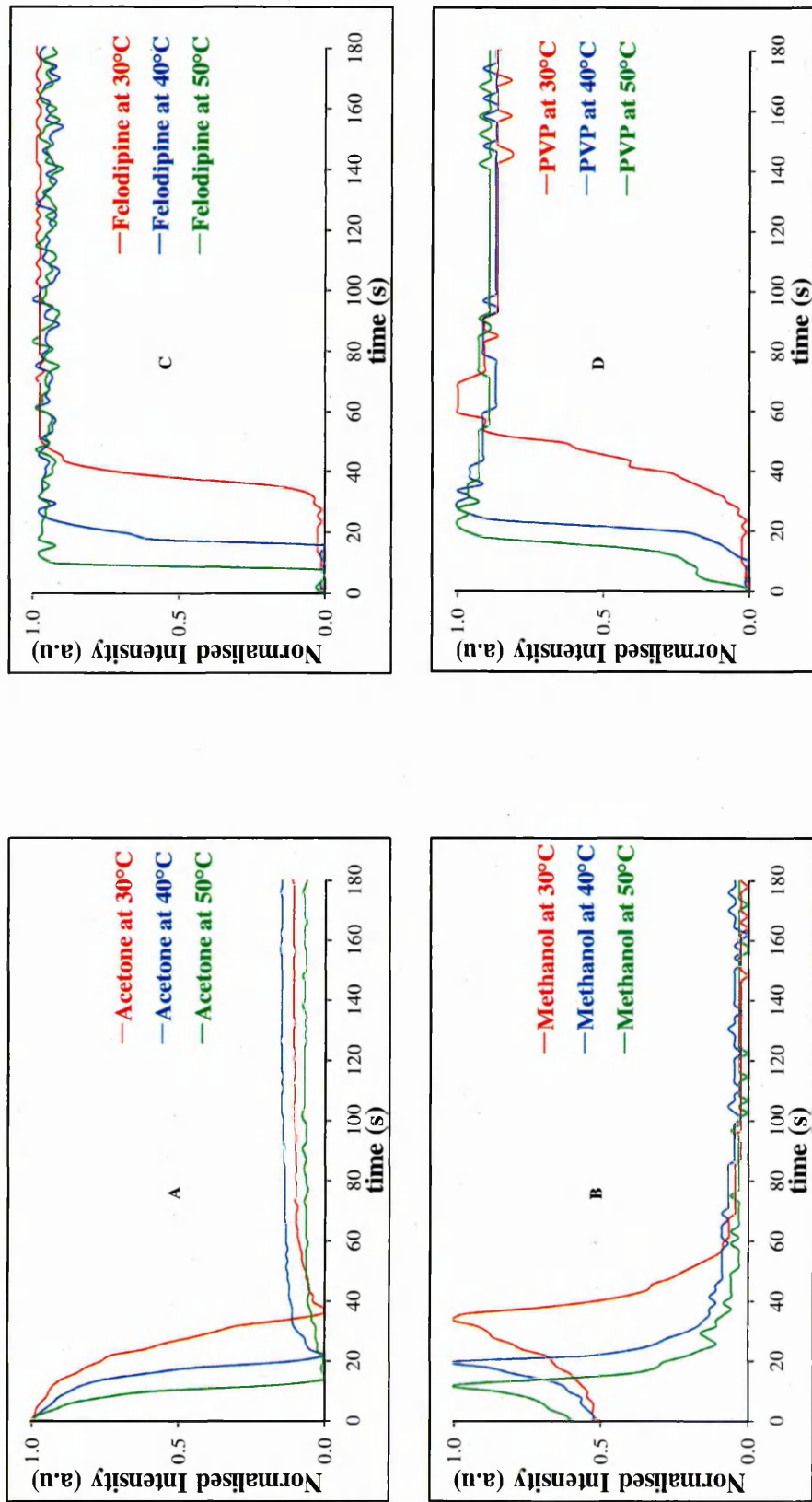
Figure 4.4. Kinetic profile of Acetone (A), Methanol (B), Felodipine (C) and PVP (D), Fel/PVP cast from Acetone/Methanol mixture
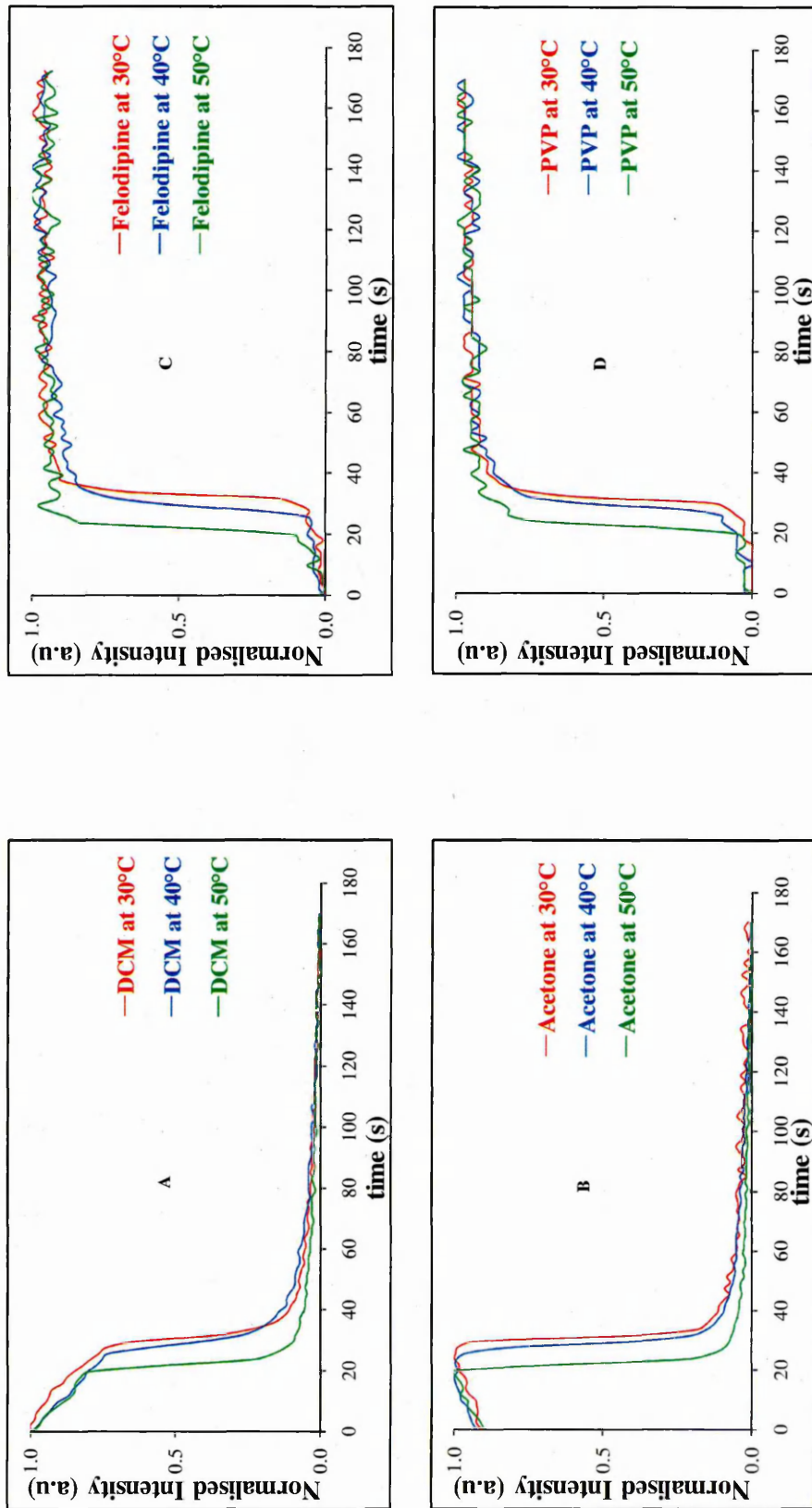
Figure 4.5. Kinetic profile of DCM (A),Acetone (B), Felodipine (C) and PVP (D), Fel/PVP cast from DCM/Acetone mixture

48

The kinetic or absorbance profiles for each of the components were then extracted from the data by plotting log (1/R) of a characteristic peak over time. The next step was to carry out a normalisation procedure. The normalisation procedure is as follows. For each profile, the data point with the lowest intensity was identified and this value subtracted from all data points within the data series. Then, the data point with the highest value was identified and all data points within the series were divided by this value, resulting in a profile that ranged between 0 and 1. Typical kinetic profiles after normalisation for the two different systems (felodipine/PVP cast from acetone/methanol and felodipine/PVP cast from DCM/acetone) are shown in Figure 4.4 and Figure 4.5, respectively.

The plots of intensity versus time appeared to be pseudo-sigmoidal in shape. The decrease in the intensity of the solvent peak is indicative of evaporation and the increase in the intensity of the drug/polymer peaks is indicative of solid dispersion formation. The relative volatility of the solvents used and the depth of the layer sampled by the evanescent wave are the key parameters during the evaporation process. Let us consider the acetone/methanol mixture. Since acetone is more volatile than methanol, it evaporates first causing an increase in the methanol proportion in the evanescent wave (or 10 μm sampling zone). Subsequently, methanol evaporates leaving the solid dispersion and this accounts for the maximum in methanol intensity in Figure 4.4B. However, in the DCM/Acetone mixture the rate of evaporation of DCM is somewhat faster (due to it being more volatile) than acetone causing an initial slight increase in the acetone proportion (Figure 4.5B).

4.3.1 *Extraction of kinetic information – Peak Height Measurements*

The kinetic profiles obtained as a result of solvent evaporation and solid formation studies are shown in Figure 4.4 and Figure 4.5. Firstly, it would be of interest to calculate the slope of the tangent and then derive the rate of the process. But this approach was not successful as slopes for each of the components was very similar and useful information was not readily obtained.

In order to fully utilise the kinetic information, the transition region in Figures 4.4 and Figure 4.5 was used to extract the time taken for solvent concentration to drop to 50% and 10% of its original value are termed t_{50} *and* t_{10}, respectively. Similarly the time taken for the solid concentration to rise to 50% and 90% of its final value are termed as t_{50} and t_{90}. Generally throughout this chapter the kinetics of solvent evaporation and

solid formation will be represented as t_{50}/t_{50} or t_{50} and t_{10}/t_{90} or t_{10} or t_{90}, respectively. A straight line of best fit was used in the transition region in order to better estimate the times corresponding to t_{10}, t_{50} and t_{90}, for example, between 30 (s) and 40 (s) on the solvent evaporation curve in Figure 4.6A. t_{10}, t_{50} and t_{90}, always fell in the transition region rather than on the other parts of the curves representing slower evaporation of solvent or formation of solids and therefore justifies this methodology.

Figure 4.8A, B, C and D shows values generated for t_{50}/t_{50} studies at various temperatures and different samples (binary solvent mixture, 100% pure drug, 100% pure polymer and various drug loaded solid dispersions). The error bars indicate reproducibility based on 5 replicates. The errors bars indicated here correspond to ± 1 standard deviation. From Figure 4.8. A-D, it can be seen that generally a rank order or interpreting interactions was not possible from these measurements. Values for t_{10} and t_{90} or t_{10}/t_{90} obtained in this way at the three different temperatures and for both solvent systems under investigation are shown in Figures 4.9 and 4.10 (A-D), respectively. Of the abovementioned approaches, the t_{10}/t_{90} values were found to be promising and the obtained results will be discussed in the following sections.

Acetone t_{10} measurements (in acetone/methanol mixtures) proved to be problematic, as can be seen from Figure 4.4A: here the peak intensity passes through a minimum, before gradually increasing at longer times. The cause of this artefact is the presence of overlapping features in the carbonyl region, with contributions from both drug and polymer. In order to attempt a better interpretation of the acetone evaporation, a Multivariate Curve Resolution approach was utilised.

4.3.2 Extraction of kinetic information – Multivariate Curve Resolution

A typical profile extracted from MCR is shown in Figure 4.7A. The MCR analysis extracts spectra-like factors that can be used to interpret which components are changing as a function of concentration and time. From the 20% Drug loaded felodipine/PVP solid dispersion data, four factors are derived, of which factors I and II reflect a chemical species that is being lost over time. These factors represent solvents. Factor III is growing at a rate comparable to the loss of factors I and II. These findings are analogous to the peak height measurements. The factor IV initially grows. However, this factor drops when the solvents disappear from the system. Figure 4.7B-E, shows the extracted 'pure component' factors from the MCR-ALS analysis which is compared to 'real' pure components. MCR factor I, II, III and IV show similarities to the pure spectrum of acetone, methanol, PVP and felodipine, respectively.

MCR analysis is particularly useful as compared to peak height measurements in the way that it extracts the factors which can be directly compared with real pure components. Moreover, studies have shown that the concentration profile extracted using MCR can be used to obtain quantitative information[137,140,178,180,181] and in our kinetic studies this was utilised to calculate the t_{10} acetone results from the kinetic intensity profiles. Moreover, the t_{10} MCR results of methanol, felodipine and PVP were compared for similarity with peak height results. The forms of the MCR kinetic profiles extracted matched the profiles from the peak height measurements, which gives us confidence in interpreting the t_{10} acetone results.

4.3.3 Statistical Analysis

However, significant differences in the results were obtained only with t_{10} methanol measurements. This is due to the fact that the multi-component mixtures give rise to overlapping features masking the characteristics of the other components within the mixture. As a result, statistical analysis has been carried out to better understand the kinetic results. Statistical analysis, most importantly, analysis of variance (ANOVA) and Least Significant Difference (LSD), has previously been widely applied in different fields of materials science and will be used in our studies at 95% confidence interval.

4.3.4 Thermogravimetry/Mass Spectrometry

TG-MS was applied to study trapped/residual solvent in felodipine/PVP (acetone or methanol or both) to complement the *in situ* FTIR experimental results. Samples used were blank or buoyancy correction files, binary solvent mixtures (BSM's, acetone/methanol), 100% drug and 100% polymer in acetone/methanol. The experiments were performed in triplicate. The initial temperature was set at 25 °C and the temperature was ramped to 30 °C over 14 minutes and maintained at this temperature for 46 minutes. After which, it was ramped to 320 °C at ≈ 20 °C/min and this temperature was reached within 16 minutes. The total analysis time was 76 minutes. Monitoring residual solvent was the prime objective hence evolved solvents over time were studied, mass/charge ratios (m/z) corresponding to acetone and methanol were selected. These m/z ratios were monitored over the analysis time and a profile was plotted. For methanol m/z = 31 (due to fragment $CH_3O^{\bullet}$) and for acetone m/z = 41 (due to fragment $CH_3CO^{\bullet}$) were used to measure the residual solvents. The solvent profiles from TG-MS (Figure 4.12) are similar to FTIR kinetic profile (Figure 4.4A and Figure 4.4B), that is, acetone evaporates first, followed by methanol, which is attributable to volatility and molecular interactions. The amount of residual solvents at two
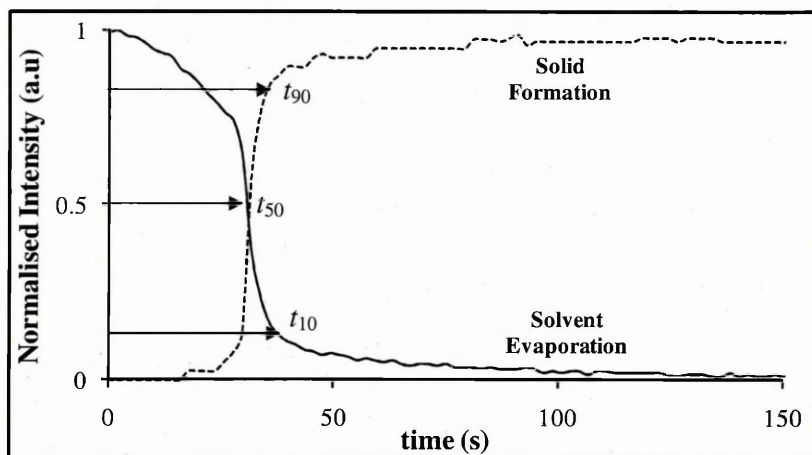
Figure 4.6 Typical transition region and t_{10} measurement
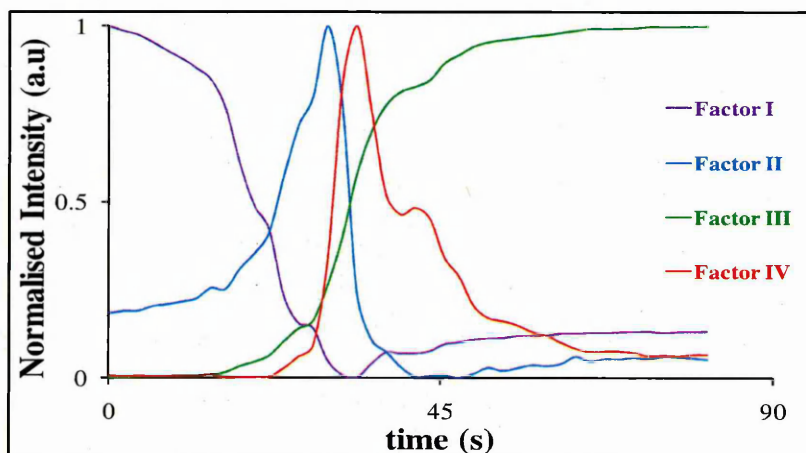
Figure 4.7A. Typical kinetic profile extracted from MCR
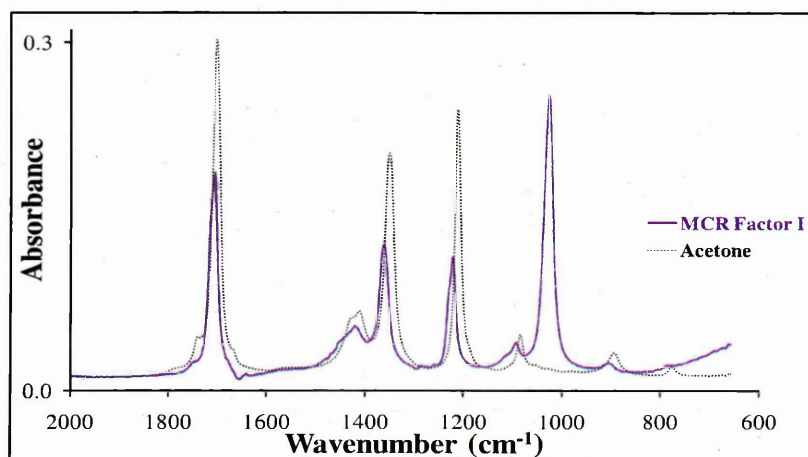
Figure 4.7B. Comparison of acetone spectrum from MCR and Peak Height
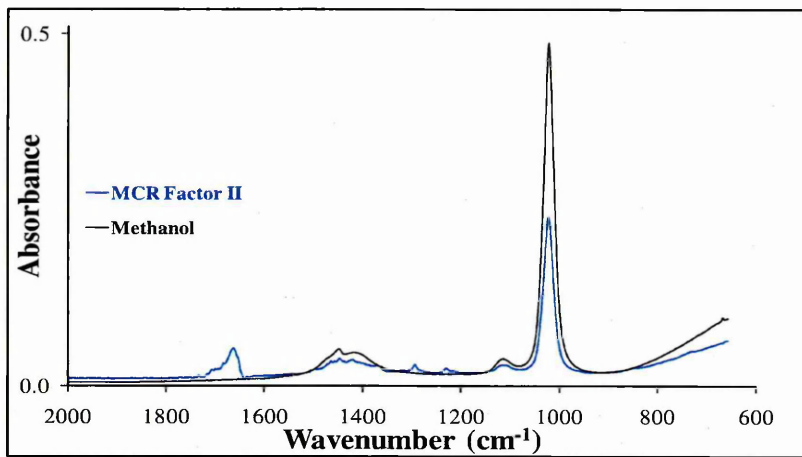
Figure 4.7C. Comparison of methanol spectrum from MCR and Peak Height
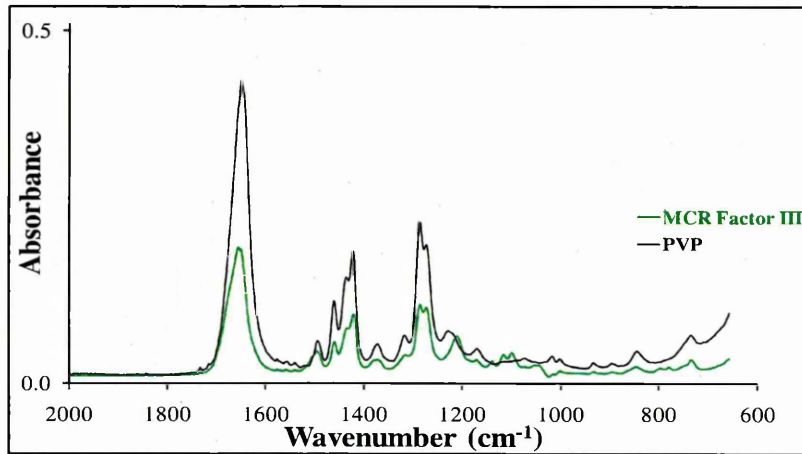
Figure 4.7D Comparison of PVP spectrum from MCR and Peak Height
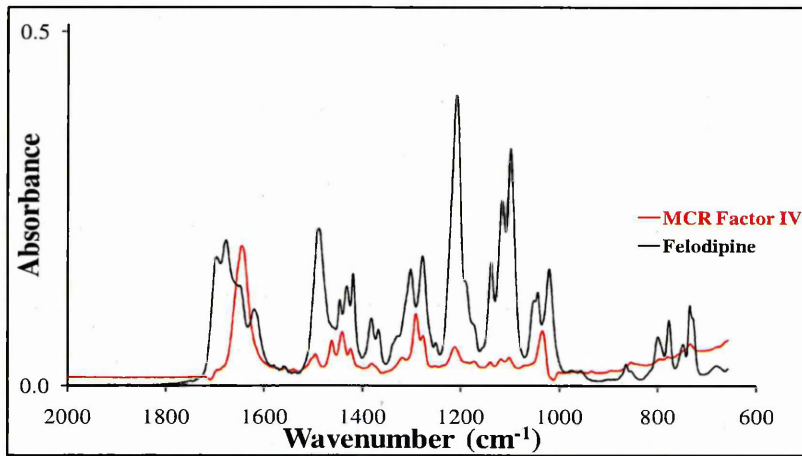
Figure 4.7E. Comparison of felodipine spectrum from MCR and Peak Height

53

temperatures, 27 °C and 30 °C were studied (Figure 4.12A, B and C) and the results of these measurements are discussed in the following sections.

4.4   Discussion

4.4.1   Surface tension and Wettability

From the data in Table 4.1, it can be seen that the surface tension for the components studied are very similar and as a result, the drop placed onto the ATR crystal completely covers the crystal, resulting in no issues with the wettability. That is, the solvents and the solids remained in close contact with the ATR crystal throughout the measurements.

4.4.2   Thickness of the Final Product

The final thickness was estimated to be ~7 μm based on the fixed volume (50 μl), a polymer density of 1.23 g/dm^3 and a final film area of 471 mm^2, meaning that the sample thickness was always greater than the depth of penetration. Optical measurements indicated a film thickness of ~6-7 μm.

4.4.3   The Applicability of Raoult's law and Henry's Law

The relationship between the vapour pressure and concentration is given by *Raoult's law*, which states that: "the vapour pressure of a solvent in the solution is equal to the vapour pressure of the pure solvent multiplied by its mole fraction in the solution".

At equilibrium, for a binary mixture (A and B) the law is expressed as

$$P_{total} = P_A M_A + P_B M_B \quad .... \quad (4.1)$$

where; P_{total} is the total vapour pressure of the binary mixtures; P_A and P_B are the partial vapour pressures of A and B respectively; M_A and M_B are mole fractions for A and B respectively.

This law holds good for mixtures where between intermolecular interactions (A...B) are similar to within molecular interactions (A...A and B...B).[182-184] These type of mixtures are called ideal solutions. That is, A...B intermolecular interactions = A...A and B...B interactions.

However when two different liquids are mixed, there are possibilities for increased or decreased interaction between liquids when compared to the pure solvent alone[183]. These mixtures deviating from the law can be grouped as follows,[182]

1. When the intermolecular interaction is reduced on mixing, the total vapour pressure of the mixture will be increased but this number does not exceed the maximum value of either pure solvent, a positive deviation. (**Condition:** A...B < A...A or B...B)

2. When the intermolecular interaction is increased on mixing, the total vapour pressure of the mixture will be decreased but not smaller than pure solvent values, a negative deviation. (**Condition:** A...B > A...A or B...B)

3. A mixture of two liquids showing positive deviation from *Raoult's law* with total vapour pressure value greater than maximum value of either pure solvent.

4. A mixture of two liquids showing negative deviation from *Raoult's law* a minimum value less than either individual value

In our studies, the binary solvent mixtures used are acetone/methanol and dichloromethane/acetone both deviate from Raoult's law. Since both the solvents show deviations from Raoult's law, the partial pressures can vary linearly with mole fraction; hence applicability of Henry's law can be appropriate. In order to apply Henry's law to any volatile solute-solvent or non-volatile solute-solvent combinations, vapour-liquid phase equilibrium or chemical potential measurements are required, respectively. Since determination of these properties were beyond the scope of this research concepts relating to Henry's law or Raoult's are discussed in theoretical perspective only. However, there is a strong relationship between intermolecular interactions and vapour pressure and will be utilized to predict any anomalous behaviour.

Acetone is a solvent for felodipine and a non-solvent for PVP, whereas methanol is a solvent for both. Methanol is a polar protic solvent or amphiprotic hydroxylic solvent,[31] that is, it can act as a proton donor (involving hydrogen from the hydroxyl group) and can be an electron pair donor (involving oxygen of hydroxyl group). Moreover, in protic solvents any solute that could form intramolecular H-bonding or self-association will be dissociated.[185,186] Acetone is a polar aprotic solvent or dipolar aprotic solvent,[31] that is, it acts as a proton acceptor and the carbonyl group is involved in this process. It interacts with methanol (MeOH) and can also interact with felodipine, but not with PVP.[187] In acetone/methanol BSM, methanol self-association could be inhibited through acetone H-bonding.

DCM is a solvent for felodipine and PVP, whereas acetone is a solvent for felodipine but non-solvent for PVP. Dichloromethane is a low polar but highly polarisable solvent (Table 4.1).[31] Due to the electronegativity of chlorine in DCM, it can interact with felodipine but with PVP to be explored.

4.4.4 Acetone/Methanol BSM : Molecular Interpretation of Raoult's Law

Since intermolecular (H-bonding) interactions of methanol-acetone are weaker than methanol-methanol (H-bonding) interactions, the binary mixture will have reduced vapour pressure and hence the methanol evaporation from BSM is increased.

Condition: *Methanol...Acetone < Methanol...Methanol (MeOH Evaporation Fast)*

Solids...Methanol> Methanol...Acetone (MeOH Evaporation Retarded)

Moreover methanol-acetone (H-bonding) interactions are greater than non-interacting acetone-acetone molecules; hence acetone evaporation from BSM or any interacting species will be retarded.

Condition: *Methanol...Acetone > Acetone...Acetone (Acetone Evaporation Slow)*

Solids...Acetone = Methanol...Acetone (No Effect)

4.4.5 DCM/Acetone BSM: Molecular Interpretation of Raoult's Law

Ketones are hydrogen-bond acceptors and are not usually hydrogen-bond donors, hence cannot hydrogen-bond to itself or "self-associate".

Hydrogen bonds exist in polar molecules where hydrogen is directly bonded to a strongly electronegative element such as F, O or N. In dichloromethane, hydrogen is bonded to the carbon atom, which is not considered to be a strongly electronegative element. Thus, we would not anticipate hydrogen bonding or self-association in this molecule. However, dipole-dipole interactions are reported for acetone...acetone and DCM...DCM molecules.[188]

When DCM is added to acetone, dipole interactions are induced between DCM and acetone. At low temperatures (in this study 30 °C), a greater proportion of DCM and acetone molecules are interacting. Hence, there is no distinction between DCM-acetone interactions and acetone-acetone interactions. Consequently, the rate of acetone evaporation from this BSM should not change. Since PVP is not soluble in acetone any solid-acetone interaction is attributed to acetone-felodipine intermolecular interactions.

Condition: *DCM...Acetone = Acetone...Acetone (No Change)*

Felodipine...Acetone > DCM...Acetone (Acetone Evaporation Retarded)

DCM-DCM interactions are weaker compared to DCM-acetone interactions; hence we anticipate that dichloromethane evaporation from this BSM should be retarded relative to the rate in pure sovent.

Condition: *DCM...Acetone > DCM...DCM (Evaporation is Retarded)*

Solids...DCM > DCM...Acetone (DCM Evaporation Retarded)

The scenario is quite different at higher temperatures (in this study 40 °C and 50 °C), the proportion of DCM and acetone molecules interacting are reduced. Hence, DCM-acetone interactions are weaker compared to acetone-acetone interactions; consequently the rate of acetone evaporation from this BSM should be increased. Felodipine-acetone interactions are stronger than DCM-acetone interactions; subsequently the rate of acetone evaporation from this BSM should be retarded.

Condition: *DCM...Acetone < Acetone...Acetone (Acetone Evaporation Fast)*

Felodipine...Acetone > DCM...Acetone (Acetone Evaporation Retarded)

At higher temperatures, DCM-acetone interactions are similar compared to DCM-DCM dipole interactions; hence the rate of dichloromethane evaporation from this BSM should not change. Solids-DCM interactions are stronger than DCM-acetone interactions; hence the rate of dichloromethane evaporation from this BSM should be retarded.

Condition: *DCM...Acetone = DCM...DCM (No Effect)*

Solids...DCM > DCM...Acetone (DCM Evaporation Retarded)

In order to verify these interpretations, pure solvents, binary solvent mixtures (acetone/methanol, DCM/acetone), 100% drug, 100% polymer and various drug loaded samples in binary solvent mixtures were studied. The results of these measurements for both the binary solvent mixtures are shown in Figure 4.9A-D. The experimental results are consistent with theoretical predictions and will be used to understand the formation of solid dispersion, molecular interactions, phase behaviour and final product characteristics.

4.4.6 t_{10} Measurements – Kinetics of solvent evaporation and film formation

With FTIR, it was possible to simultaneously monitor the rate of evaporation of the solvents and the formation of felodipine/PVP solid dispersions. Comparisons of t_{10} measurement results at three different temperatures for various samples are shown in Figure 4.10 and Figure 4.11. Error bars are the standard deviation from 5 repeated measurements and indicate reproducibility. The binary solvent mixtures (BSM) studied were acetone/methanol and dichloromethane/acetone.

a.   Binary Solvent Mixture

From Figure 4.10A it can readily be seen that temperature has a drastic impact on the rate of evaporation of methanol from the binary solvent mixture as expected. The rate of evaporation of methanol from the binary solvent mixtures is increased as the

temperature is raised. When the solids are incorporated the scenario is slightly different, that is, methanol evaporation rates at higher temperatures (50 °C) are different from those at 30 °C (Figure 4.10A). This is the trend irrespective of nature of solids. Interestingly, evaporation of methanol from a pure solvent mixture is thus different in the presence of solids. There is clear retardation when solids are incorporated. Statistical analysis using ANOVA (F and P values) shown in Table 4.3A confirms this observation, that is, temperature and sample composition have a significant effect on the methanol evaporation rates at a 95% confidence interval. In order to determine between temperatures and within sample variations, least significant difference (LSD) tests were carried out and the results are shown in Table 4.4A. LSD results showed that within sample variations are not probably significant at the 95% confidence level. That is, the retardation of methanol from 100% polymer or 100% drug or 20%, 50%, 80% drug loaded samples are not statistically significant.

Results from the t_{10} measurements of DCM/acetone binary solvent mixture, shown in Figure 4.11A, indicate that the DCM evaporation from the binary solvent mixture is retarded when the solids are incorporated except 50% drug loaded samples. This is more pronounced at 40 °C and 50 °C but no different at 30 °C. Moreover, the evaporation of DCM is slower in low drug loaded samples than the high drug loaded samples which indicate that the rate of evaporation of DCM from these systems is different. This is supported from the statistical results. ANOVA results (Table 4.3B) indicate that both temperature and samples are significantly different at the 95% confidence interval. The least significant differences indicate that the rate of evaporation of DCM at 40 °C and 50 °C are different to 30 °C but between them, the differences are probably statistically insignificant. DCM evaporation rate (Table 4.4B) is significantly retarded when the solids are incorporated. However, the evaporation of DCM from binary mixture and 50% drug loading (DL) samples are no different. As with peak height measurements, the retardation of DCM from high drug loaded (50%, 80% and 100%) samples are lower than the low drug loaded (0% and 20%) samples. However within high and low drug loadings there are no significant difference at the statistical level.

From Figure 4.10D, it is obvious that the temperature has a significant effect on the rate of evaporation of acetone in the presence of methanol. The evaporation of acetone from all the samples (including solids) is increased as the temperature is raised. Interestingly, the rate of evaporation of acetone from binary solvent mixture is not significantly
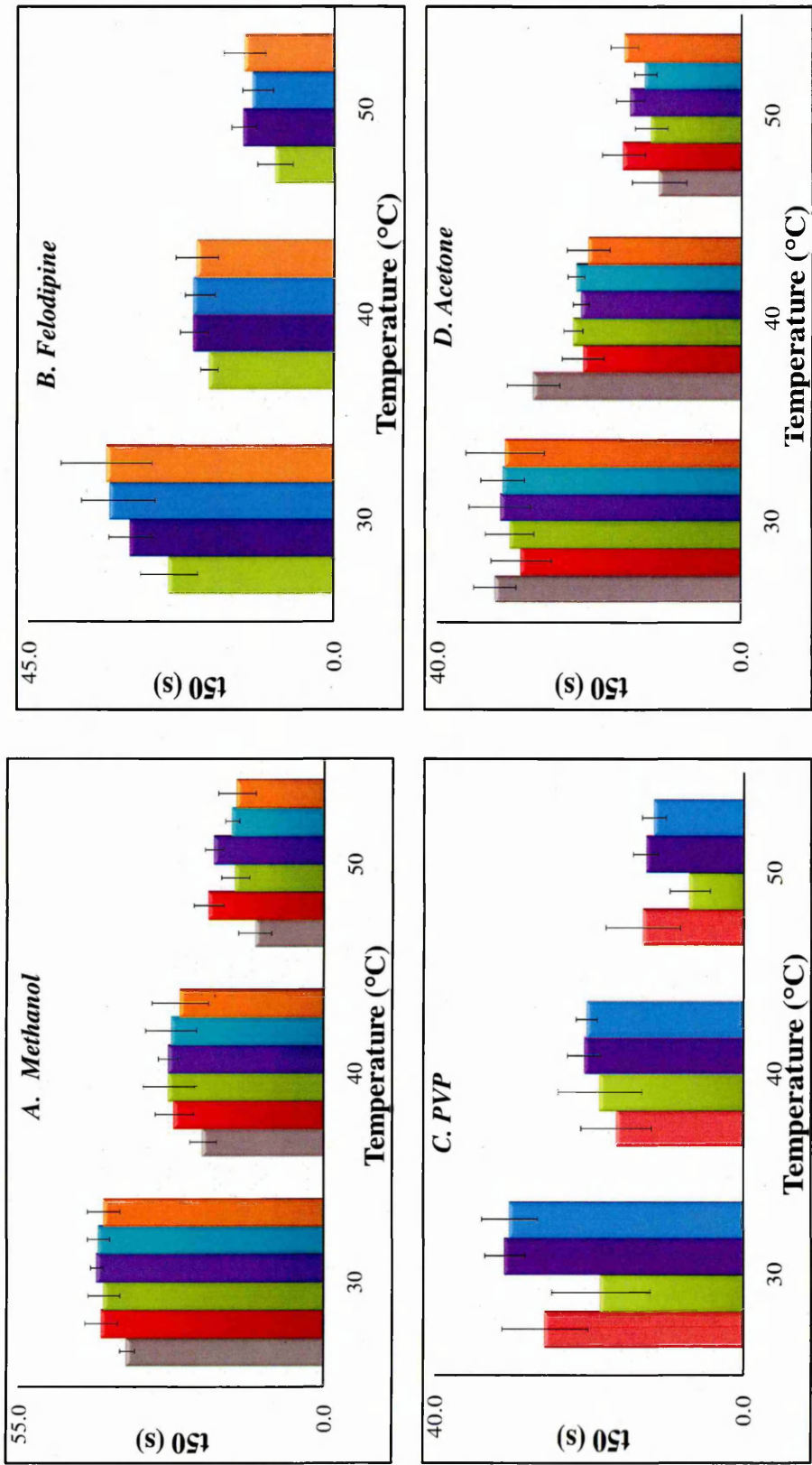
Figure 4.8 t_{50}/t_{50} acetone/methanol binary solvent mixtures (DL: Drug Loading)

59
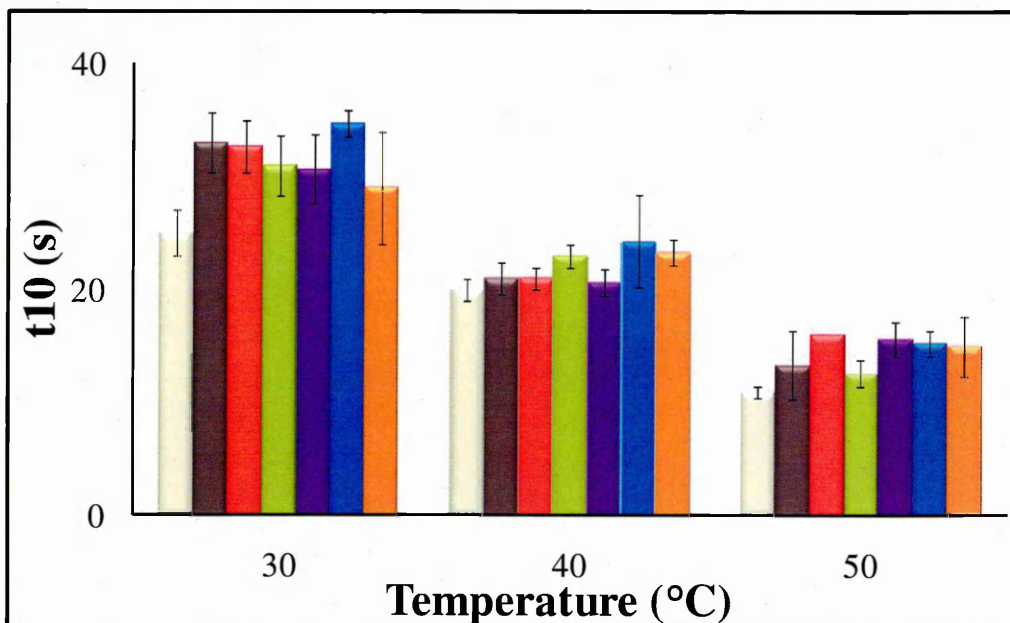
Figure 4.9A Comparison of t_{10} acetone results from pure and acetone/MeOH BSM

Acetone ▪ Acetone/MeOH ▪ 100% PVP ▪ 20% DL ▪ 50% DL ▪ 80% DL ▪ 100% DL
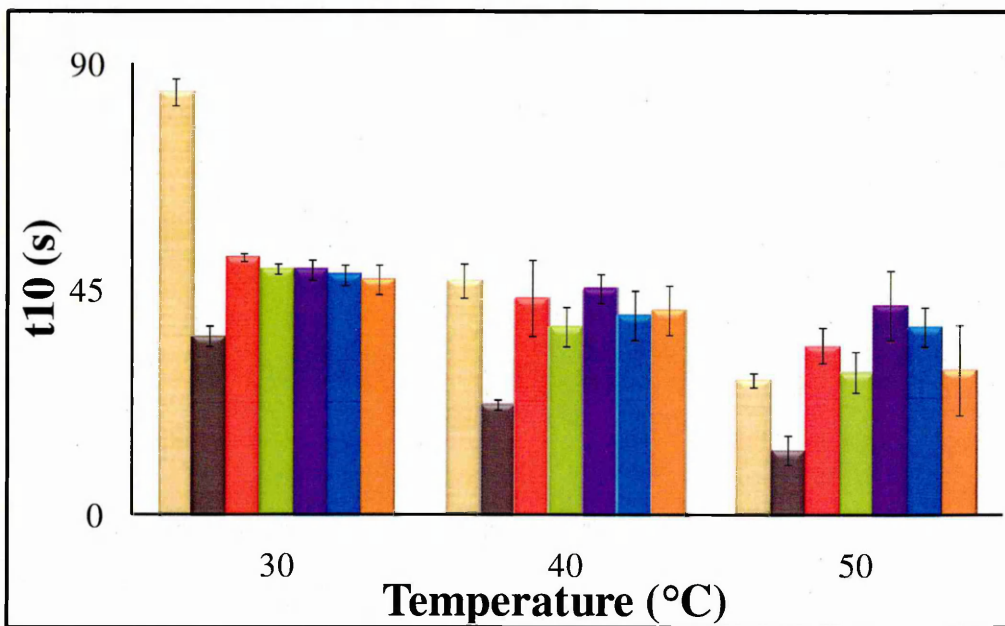
Figure 4.9B Comparison of t_{10} methanol results from pure and acetone/MeOH (DL: Drug Loading)

Methanol ▪ Acetone/MeOH ▪ 100% PVP ▪ 20% DL ▪ 50% DL ▪ 80% DL ▪ 100% DL
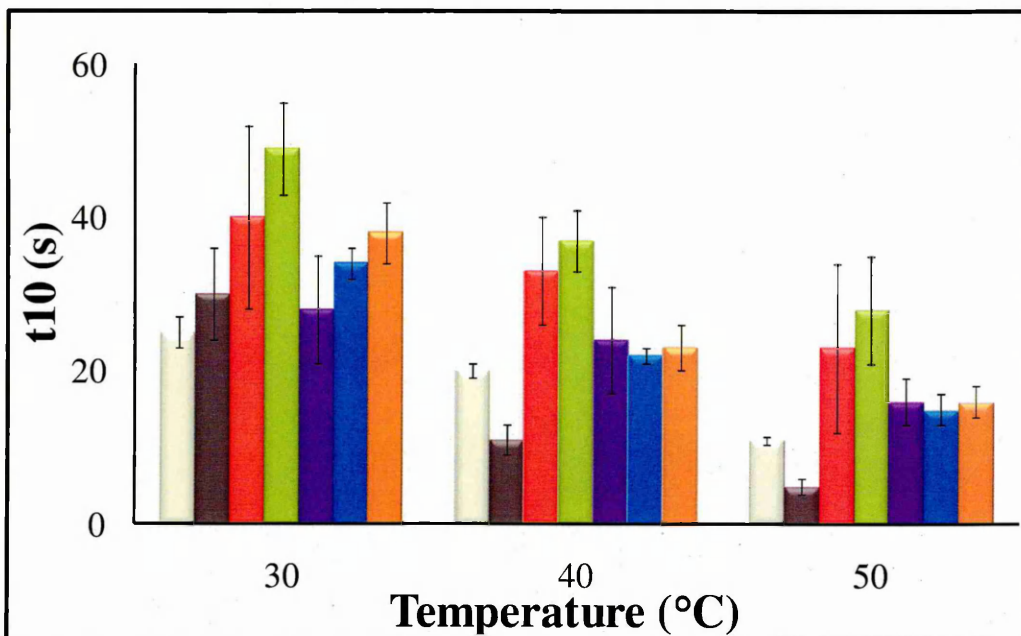
Figure 4.9C Comparison of t_{10} acetone results from pure and DCM/acetone BSM

Acetone   DCM/Acetone   100% PVP   20% DL   50% DL   80% DL   100% DL
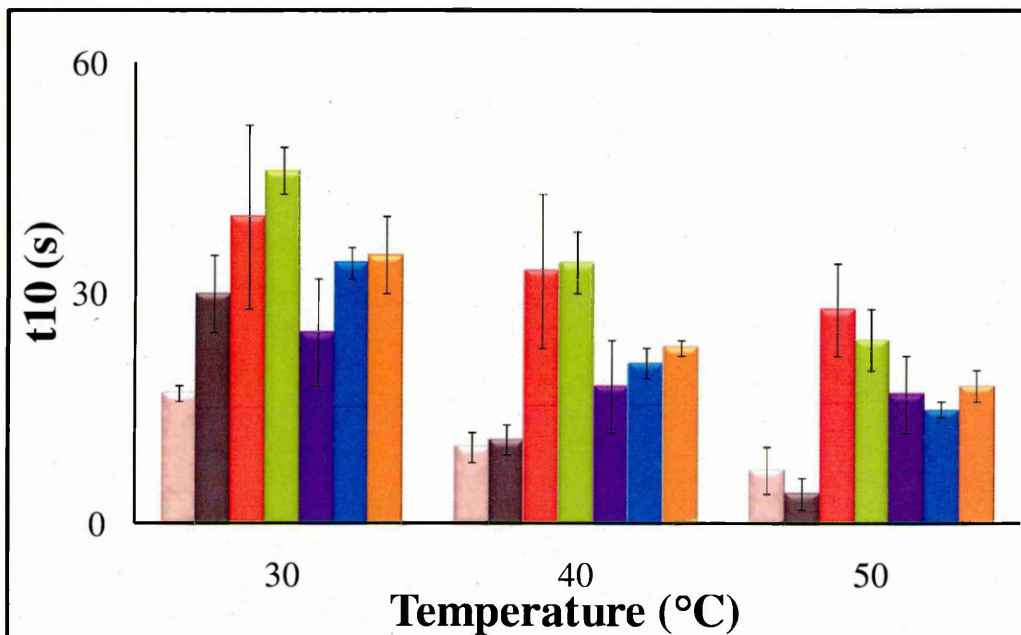
Figure 4.9D Comparison of t_{10} DCM results from pure and DCM/acetone BSM (DL: Drug Loading)

DCM   Acetone/MeOH   100% PVP   20% DL   50% DL   80% DL   100% DL

changed when the solids are incorporated. The t_{10} results and the aforementioned interpretation is supported from ANOVA results (F and P values) and LSD results shown in Tables 4.3A and 4.4A, respectively. The results confirm that temperature has a significant effect on the evaporation, that is, increase in temperature accelerates the acetone evaporation. But acetone evaporation from mixture of binary solvent mixture is not altered when solids are present.

The t_{10} results for the acetone evaporation from the DCM/acetone binary solvent mixtures can be seen in Figure 4.11D. An increase in the temperature increases the DCM solvent evaporation. The evaporation of acetone from the binary solvent mixture at 30 °C is statistically no different in the presence of solids; however, DCM evaporation in the presence of solids is increased at higher temperatures, in this study, 40 °C and 50 °C. Moreover, from the t_{10} results it can be seen that the retardation in acetone evaporation is more pronounced in high polymer loaded samples than high drug loaded samples. That is, the evaporation of acetone is comparatively quicker from the high drug loaded samples than low drug loaded samples. ANOVA results (Table 4.3B) indicate that the evaporation rate of acetone is influenced by temperature and nature of samples. Results from the least significant differences indicate that 30 °C is different to 40 °C and 50 °C but between 40 °C and 50 °C there are no significant differences. Acetone evaporation (Table 4.4B) is significantly retarded when the solids are incorporated. Interestingly, the retardation of acetone from high drug loaded (50%, 80% and 100%) samples are lower than the low drug loaded (0% and 20%) samples. However within high and low drug loadings there are no significant difference at the statistical level. These results are in line with the peak height measurements.

b. Film Formation of Felodipine

The temperature has a significant influence on the rate of film formation of felodipine, as shown in Figure 4.10B. That is, raising the temperature sequentially increases the film formation rate irrespective of 100% drug or polymer loaded samples. Interestingly, the film formation rate of 100% drug loaded samples is no different with polymer loaded samples. However, there are differences in the final products, which will be discussed in the following sections (i.e. molecular interactions). This interpretation is further strengthened by analysing the results from the ANOVA test (F and P values), Table 4.3A. There are significant differences with temperature and samples at the statistical level. Furthermore, LSD (Table 4.4A) indicates that there are significant
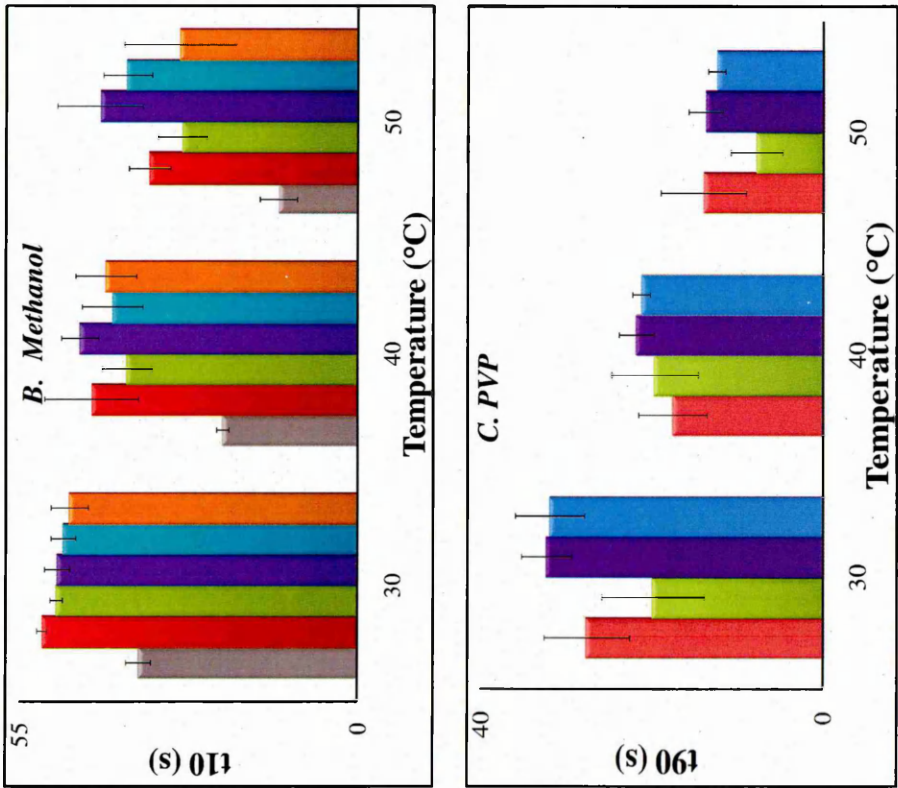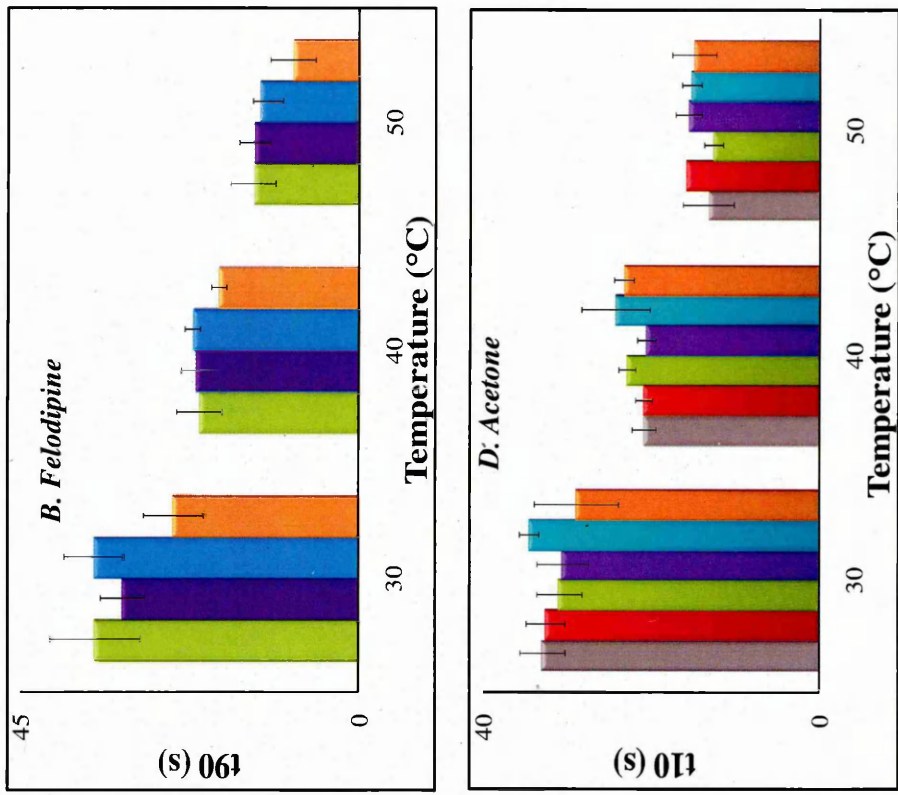
Figure 4.10 t_{10}/t_{90} acetone/methanol binary solvent mixtures (DL: Drug Loading)

63
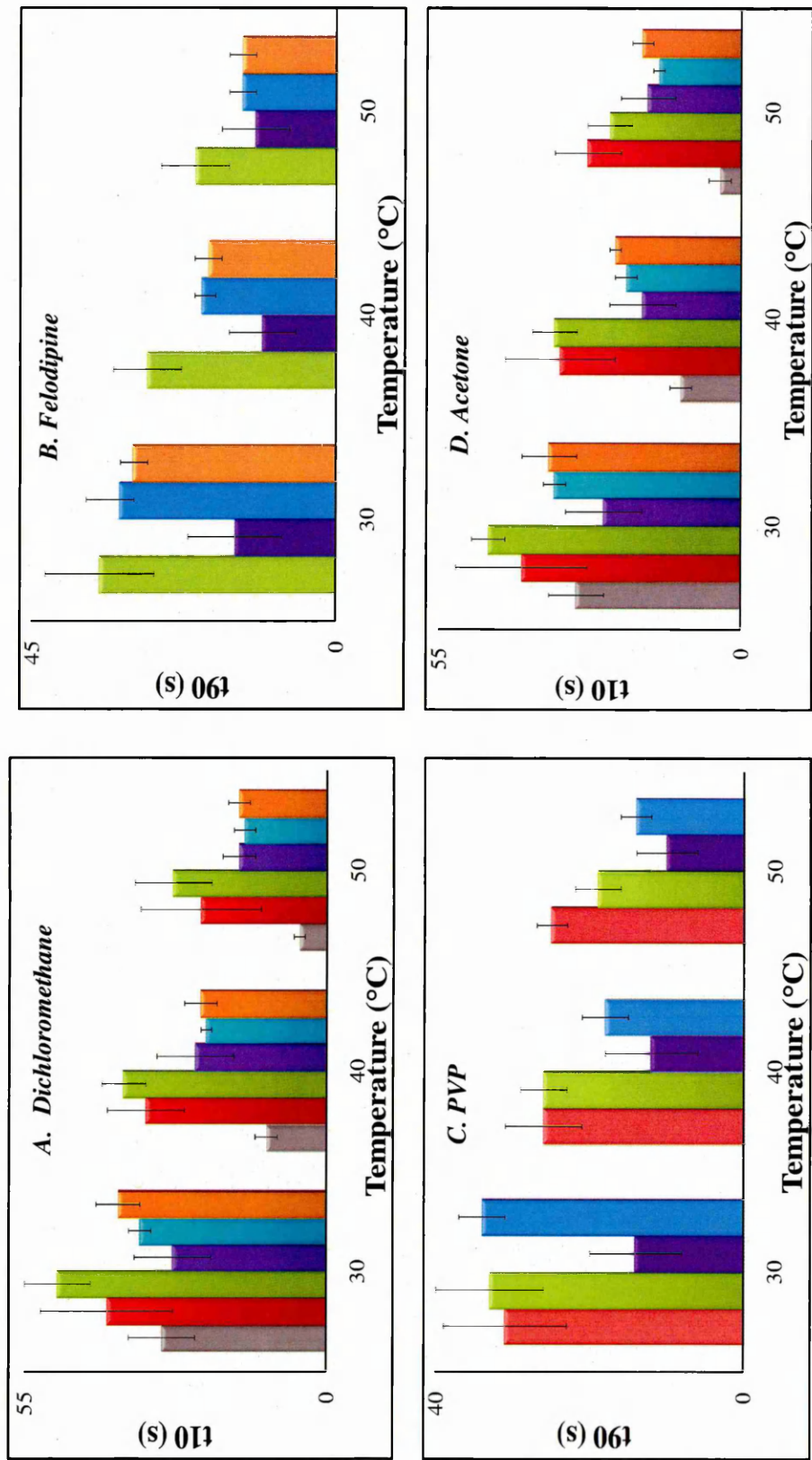
Figure 4.11 t_{10}/t_{90} DCM/acetone binary solvent mixtures
(DL: Drug Loading)

64

differences between the rates at different temperatures at the statistical level. LSD indicates that the rate of formation of 20% drug loaded sample is significantly slower than the 80% and 100% felodipine/PVP concentrations. But within 80% and 100% the formation rates are not statistically significant.

The t_{10} results for the rate of formation of felodipine when cast from DCM/acetone are shown in Figure 4.11B and could be readily inferred that, as there is increase in the temperature, the rate of formation of felodipine is increased. This interpretation is true with 100%, 80% and 20% drug loaded samples but for the 50% drug loaded sample there is no change. ANOVA results shown in Table 4.3B indicate that there is a significant difference between temperature and sample composition at the 95% confidence interval. LSD results (Table 4.4B) indicate that the rate of formation of felodipine at 30 °C is slow when compared to 40 °C and 50 °C but no difference between 40 °C and 50 °C. Also, the behaviour of 50% drug loaded samples is different to 20%, 80% and 100% but between these loadings there is no difference at the statistical level.

c. Film Formation of Polyvinylpyrrolidone

The rate of PVP film formation from the acetone/methanol binary solvent mixture is shown in Figure 4.10C. Temperature has a remarkable effect on the film formation rate of PVP when there is high drug loading; raising the temperature increases the film formation rate for these samples systematically. However, with 20% drug loading, the rate of film formation at 50 °C is different to 30 °C and 40 °C, that is, the film formation time is reduced at 50 °C. Apart from the temperature differences, rate of film formation of pure polymer (100% polymer) is not altered when in the presence of drug loading. Furthermore, ANOVA F and P values Table 4.3A, imply that there are significant differences between temperatures and samples at the 95% confidence level. In addition, LSD results (Table 4.4A) indicate that the rates of film formation of PVP at the various temperatures are significantly different, that is, raising the temperature increases the film formation rate. The rate of formation of PVP from 50% drug loaded sample is faster than 20% drug loaded ones, but not with other samples.

From Figure 4.11C (t_{10} results) it could be seen that the rate of formation of PVP is not influenced by the temperature for the 0% drug loaded samples. For the 20% DL the PVP formation is influenced at 50 °C. For the other samples, that is high drug loadings the effect of temperature is systematic, that is, as there is increase in the temperature

Table 4.3A. ANOVA F and P values, Yes: probably significant difference, No: probably statistically no significant difference

Components	Variables	Solvents Mixture		Pure Polymer		20% DL		50% DL		80% DL		Pure Drug	
		F-value	P-value	F	P	F	P	F	P	F	P	F	P
Acetone	Temperature	Yes	Yes	Yes	Yes	Yes	Yes	Yes	Yes	Yes	Yes	Yes	Yes
	Samples	No	No	No	No	No	No	No	No	No	No	No	No
Methanol	Temperature	Yes	Yes	Yes	Yes	Yes	Yes	Yes	Yes	Yes	Yes	Yes	Yes
	Samples	Yes	Yes	Yes	Yes	Yes	Yes	Yes	Yes	Yes	Yes	Yes	Yes
Felodipine	Temperature	-NA-	-NA-	-NA-	-NA-	Yes	Yes	Yes	Yes	Yes	Yes	Yes	Yes
	Samples	-NA-	-NA-	-NA-	-NA-	Yes	Yes	Yes	Yes	Yes	Yes	Yes	Yes
PVP	Temperature	-NA-	-NA-	Yes	Yes	Yes	Yes	Yes	Yes	Yes	Yes	-NA-	-NA-
	Samples	-NA-	-NA-	Yes	Yes	Yes	Yes	Yes	Yes	Yes	Yes	-NA-	-NA-

Table 4.3B. ANOVA F and P values, Yes: probably significant difference, No: probably statistically no significant difference

Components	Variables	Solvents Mixture		Pure Polymer		20% DL		50% DL		80% DL		Pure Drug	
		F-value	P-value	F	P	F	P	F	P	F	P	F	P
Acetone	Temperature	Yes	Yes	Yes	Yes	Yes	Yes	Yes	Yes	Yes	Yes	Yes	Yes
	Samples	Yes	Yes	Yes	Yes	Yes	Yes	Yes	Yes	Yes	Yes	Yes	Yes
DCM	Temperature	Yes	Yes	Yes	Yes	Yes	Yes	Yes	Yes	Yes	Yes	Yes	Yes
	Samples	Yes	Yes	Yes	Yes	Yes	Yes	Yes	Yes	Yes	Yes	Yes	Yes
Felodipine	Temperature	-NA-	-NA-	-NA-	-NA-	Yes	Yes	Yes	Yes	Yes	Yes	Yes	Yes
	Samples	-NA-	-NA-	-NA-	-NA-	Yes	Yes	Yes	Yes	Yes	Yes	Yes	Yes
PVP	Temperature	-NA-	-NA-	Yes	Yes	Yes	Yes	Yes	Yes	Yes	Yes	-NA-	-NA-
	Samples	-NA-	-NA-	Yes	Yes	Yes	Yes	Yes	Yes	Yes	Yes	-NA-	-NA-

Table 4.4A LSD values for various components cast from acetone/methanol binary solvent mixture

		BSM		0% DL		20% DL		50% DL		80% DL	
		Exp	Cal	Exp	Cal	Exp	Cal	Exp	Cal	Exp	Cal
100% DL	Acetone	0	2.74	0.77	2.74	0.22	2.74	0.11	2.74	2.3	2.74
	Methanol	15.66	7.07	3.5	7.07	0.62	7.07	6.23	7.07	2.74	7.07
	Felodipine	-NA-	-NA-	-NA-	-NA-	6.11	5.04	1.2	5.04	0.01	5.04
	PVP	-NA-	-NA-	-NA-	-NA-	-NA-		-NA-		-NA-	
80% DL	Acetone	2.33	2.74	1.55	2.74	2.55	2.74	2.44	2.74		
	Methanol	18.40	7.07	0.75	7.07	2.36	7.07	3.55	7.07		
	Felodipine	-NA-	-NA-	-NA-	-NA-	6.12	5.04	1.19	5.04		
	PVP	-NA-	-NA-	2.16	6.21	6.1	6.21	0.74	6.21		
50% DL	Acetone	0.11	2.74	0.89	2.74	0.11	2.74				
	Methanol	21.96	7.07	2.81	7.07	6.91	7.07				
	Felodipine	-NA-	-NA-	-NA-	-NA-	4.92	5.04				
	PVP	-NA-	-NA-	2.89	6.21	6.84	6.21				
20% DL	Acetone	0.22	2.74	1.01	2.74						
	Methanol	15.03	7.07	4.11	7.07						
	Felodipine	-NA-	-NA-	-NA-	-NA-						
	PVP	-NA-	-NA-	3.95	6.21						
0% DL	Acetone	0.77	2.74								
	Methanol	19.14	7.07								
	Felodipine	-NA-	-NA-								
	PVP	-NA-	-NA-								

Note: Exp-Experimental; Cal-Calculated

67

Table 4.4B LSD values for various components cast from DCM/acetone binary solvent mixture

		BSM Exp	BSM Cal	0% DL Exp	0% DL Cal	20% DL Exp	20% DL Cal	50% DL Exp	50% DL Cal	80% DL Exp	80% DL Cal
100% DL	Acetone	9.01	6.73	9.60	6.73	13.67	6.73	1.07	6.73	0.06	6.73
	DCM	10.27	6.50	8.06	6.50	9.50	6.50	4.67	6.50	1.80	6.50
	Felodipine	-NA-	-NA-	-NA-	-NA-	7.13	6.96	9.13	6.96	1.13	6.96
	PVP	-NA-	-NA-	-NA-	-NA-	-NA-		-NA-		-NA-	
80% DL	Acetone	8.95	6.73	9.63	6.73	13.73	6.73	1.00	6.73		
	DCM	8.47	6.50	9.86	6.50	11.30	6.50	2.87	6.50		
	Felodipine	-NA-	-NA-	-NA-		5.8	6.96	10.46	6.96		
	PVP	-NA-	-NA-	4.93	7.52	3.6	7.52	12.40	7.52		
50% DL	Acetone	7.95	6.73	10.63	6.73	14.73	6.73				
	DCM	5.60	6.50	12.70	6.50	14.10	6.50				
	Felodipine	-NA-	-NA-	-NA-		16.30	6.96				
	PVP	-NA-	-NA-	17.3	7.52	16.00	7.52				
20% DL	Acetone	22.68	6.73	4.10	6.73						
	DCM	19.70	6.50	1.40	6.50						
	Felodipine	-NA-	-NA-	-NA-							
	PVP	-NA-	-NA-	1.30	7.52						
0% DL	Acetone	18.59	6.73								
	DCM	18.34	6.50								
	Felodipine	-NA-	-NA-								
	PVP	-NA-	-NA-								

Note: Exp-Experimental; Cal-Calculated

Figure 4.13. TG data showing % of residual solvent from binary solvent mixture

Figure 4.15. TG data showing % of residual solvent from 100% PVP cast from acetone/methanol binary solvent mixture

Figure 4.12. Mass Chromatograms showing Solvent evaporation from various systems

Figure 4.14. TG data showing % of residual solvent from 100% felodipine cast from acetone/methanol binary solvent mixture

69

there is increase in the rate of PVP formation. ANOVA results shown in Table 4.3B indicate that the differences between the temperature and samples are statistically significant at the 95% confidence interval. Least Significant Differences shown in Table 4.4B, indicate that kinetics at 30 °C are different to those at 40 °C and 50 °C, but, between 40 °C and 50 °C there are no differences. Interestingly, LSD results indicate that any difference within samples only occurs with the 50% drug loaded samples and any differences with other samples are not statistically significant.

4.4.7 Residual solvents

To assess the sensitivity, reproducibility and validity of FTIR measurements, TG-MS analysis was carried out to quantify the amount of residual solvents in the binary solvent mixtures, 100% felodipine cast from acetone/methanol (FAM) and 100% PVP cast from acetone/methanol (PAM) samples. Typical TG-MS ion curves and thermograms are shown in Figures 4.12 to 4.15. The ion curve results show the evaporation of acetone and methanol from various samples. The resulting TG-MS curves are found to be strikingly similar to FTIR kinetic profile curves (cf. Figure 4.4). That is, acetone evaporates first followed by methanol.

From the FTIR (Figure 4.2) the solvents were found to be completely evaporated after ~2 minutes at 30 °C. The TG-MS data (Table 4.5) show more residual solvents in the studied systems (BSM 4%, FAM 8%, PAM 7%) after 14 minutes at 30 °C. The acetone and methanol from the BSM system as found to be completely evaporated after 20 minutes at 32 °C, whilst 2-3 % remained in the FAM or PAM samples. This % was believed to be within the error and was further confirmed by studying another time/temperature interval of 72 minutes/240 °C where the % remaining is equivalent to the % remaining at 20 minutes/32 °C. If these were residual solvents, at the high temperature, the remaining solvent should have been removed. These results indicate that FTIR analysis can be applied to monitor the solvent vaporization in real time with good measurement sensitivity and reproducibility.

4.4.8 Molecular Interactions

FTIR is a powerful tool to study molecular interactions in any form (solid, liquid or gas) and of any type (H-bonding, Vander Waal's or pi interactions, etc). In order to obtain further evidence of the possible interactions, spectral frequency shifts were monitored. Table 4.6 shows the characteristic peaks for starting materials that can be exploited to monitor intermolecular interactions. These ideas will be utilized to study solvent-solvent, solvent-solid interactions by monitoring the solvent induced frequency shifts

70

(SIFS) and solid-solid interactions from peak shifts of the pure material (cast and solid dispersion). In infrared spectroscopy, the NH, OH and C=O bond absorptions and their molecular vibrations are usually very strong.[189] Moreover, their peak positions or intensities are specific and sensitive to the infrared local environment. Thus, any alterations in peak positions due to inter and intramolecular interactions are representative.

Table 4.5. Residual solvents for various samples

Temperature	Time	BSM			FAM			PAM		
		R1	R2	R3	R1	R2	R3	R1	R2	R3
27 °C	5 min	60	64	62	63	59	58	66	63	59
			62% ± 2			60% ± 3			63% ± 4	
30 °C	14 min	0.5	8	4	11	6	7	10	6	6
			4% ± 4			8% ± 3			7% ± 2	
32 °C	20 min	0.0	0.3	0.1	6	6	6	8	6	6
			0.1% ± 0.2			6% ± 0			7% ± 1	
240 °C	72 min		-NA-		5	5	5	8	5	5
						5% ± 0			6% ± 2	

a. Solvent-solvent interactions

The spectra recorded during the initial stages of the experiment are dominated by the solvents: spectral signatures confirm this. Any frequency shifts during this stage can be attributed to solvent-solvent interactions. In the acetone/methanol binary solvent mixture, methanol acts as a proton donor and acetone acts as a proton acceptor. This can be shown from the acetone carbonyl band which normally appears at 1711 cm^{-1} but in the presence of methanol the carbonyl band is broadened and found to shift to lower wavenumbers (1707 cm^{-1}), Table 4.7. These changes can be attributed to intermolecular hydrogen bonding (H-bonding) between methanol and acetone.

In a DCM/acetone binary solvent mixture, the acetone carbonyl peak appears close to the unperturbed value which is 1711 cm^{-1} (but peak shape is perturbed). Moreover, there is increase in the peak intensity and narrowing of the peak compared to the pure acetone carbonyl peak. Also, in DCM, the $v_{(CH)}$ is found to shift by 5 cm^{-1} to a higher peak position, together with a simultaneous change in the DCM $\delta_{(CH)}$ vibrations. The

observed high frequency shift[190] and narrowing of acetone carbonyl peak[191] is attributable to induced dipole-induced dipole or dipolar interactions between DCM and acetone (Figure 4.16 and Table 4.7).
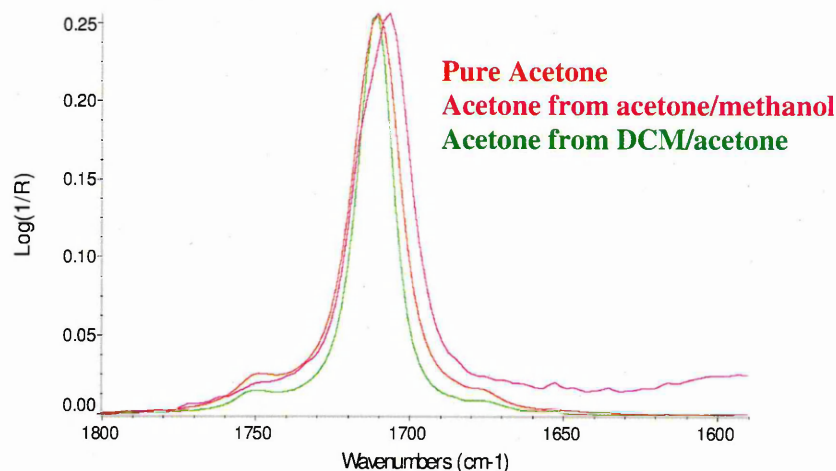
Figure 4.16. Solvent-solvent interactions

b. Solvent-Solid interactions

In order to understand more about nature of interactions between solvents and solids, ternary mixtures (that is, 100% drug or 100% polymer cast from acetone/methanol or DCM/acetone) were studied in detail. As the intensities of solvent bands decrease, there is an increase in the intensity of either the drug or polymer bands. At this stage, any frequency shifts can be ascribed to solvent-solid interactions (Table 4.8). In the acetone/methanol binary solvent mixture, acetone evaporated rapidly (cf. t_{10} results). From peak height measurements and ANOVA it is inferred that acetone does not interact with solids. This statement is supported by tracing the spectral changes and there is no significant changes observed with the acetone carbonyl peak. In addition, acetone is more volatile than methanol and evaporates rapidly before it can interact with the solids (cf. t_{10} acetone results Figure 4.10D).

Now, any shift in the frequency of drug or polymer bands (in acetone/methanol BSM) indicates that methanol is interacting with the solid and is attributable to methanol-solid interactions. Since methanol is a polar protic solvent or proton donor, it can interact with proton acceptors like acetone, felodipine and PVP through H-bonding. Felodipine is known to interact with methanol[31] through hydrogen bonding and this is evident from the ethyl ester carbonyl band appearing at 1680 cm^{-1} (in felodipine starting material ethyl ester carbonyl band appears at 1686 cm^{-1}) during film formation, indicating a solvent-induced frequency shift. Formation of intermolecular H-bonds retards the

72

evaporation rate of methanol, compared to the binary solvent mixture (absence of solids) and is evident from the t_{10} measurements. PVP can also interact with methanol through the formation of intermolecular hydrogen bonds. The carbonyl peak in the PVP starting material appears around 1654 cm^{-1}. When PVP is cast from the acetone/MeOH binary mixture there is 4 cm^{-1} shift to lower wavenumber and the carbonyl peak appears at 1650 cm^{-1}. This indicates that methanol and PVP can also interact, the evaporation of methanol is retarded when compared to the rate in a binary solvent mixture, which agrees well with the t_{10} results.

Results from the peak height measurements and ANOVA indicate that the methanol evaporation is retarded when solids are incorporated. Within sample variations (that is, different felodipine/PVP concentrations) are insignificant, which means drug and polymer interact with methanol to the same extent and LSD supports this. This retardation can be attributed to the aforementioned molecular interactions. From these findings, it is concluded that although methanol interacts with the felodipine and PVP, there is no evidence for acetone to interact with the solids. Besides, to support this conclusion kinetics and molecular interactions of felodipine and PVP in the second binary solvent mixture (DCM/acetone) was studied in detail and will be discussed further.

In the DCM/acetone binary solvent mixture, when felodipine is detected it is found to interact with DCM and acetone at different stages. This can be substantiated by further considering the peak position changes of both NH and C=O stretching of felodipine and acetone, respectively. When the NH stretching peak of felodipine appears at 3344 cm^{-1} the corresponding carbonyl peak of acetone appears around 1703 cm^{-1}. The 8 cm^{-1} shift of $\nu_{(CO)}$ to lower wavenumber is indicative that felodipine interacts with acetone through the formation of H-bonds. Also before there is complete evaporation of acetone and DCM, the felodipine NH stretching peaks, fluctuate markedly and appear between 3351 cm^{-1} to 3344 cm^{-1}. This could be due to interaction of felodipine with both the solvents. The main objective for studying the second BSM is to better understand whether acetone interacts with felodipine. With the peak position changes, t_{10}, MCR and statistical data analytical tools, we are quite happy to conclude that there is clear retardation in acetone evaporation when in DCM/acetone BSM but there is no retardation of acetone with solids in the acetone/methanol BSM.

As previously discussed PVP is insoluble in acetone and hence there could be no interaction. Any retardation in acetone evaporation indicates only physical effects like

viscosity, etc. However, PVP interacts with DCM. Since dichloromethane is a polarisable solvent, it interacts with PVP through strong dipole-dipole or dipolar interactions. These interactions change the conformation of PVP wherein there is shift of carbonyl group to 1662 cm^{-1} (cf. the starting material where it appears at 1654 cm^{-1}). Also evidenced from the DCM peak shifts $\nu_{(CH)}$ 3049 cm^{-1} (due to N$^+$=C-O$^-$ reorientation of PVP and interaction with Cl$^-$ in DCM) and $\delta_{(CCl)}$ 697 cm^{-1}. The PVP-solvent interactions thus change the conformation of the polymeric matrices and can influence the incorporation of the drug or formation of solid dispersions. These will be discussed in Chapter 7 "The Application of Vibrational Spectroscopy to Solid Dispersions: Final Product Characteristics". Moreover, PVP-felodipine intermolecular interactions, drying kinetics and distribution, etc will also be discussed.

4.5 Conclusion

Variable temperature ATR-FTIR can be successfully used to monitor the formation of solid dispersions *in situ* and is a suitable technique to study evaporation rates on this time scale (seconds). Detailed kinetic information is obtainable; t_{10} (the time taken for solvent concentration to drop to 10% of its original value) and t_{90} (the time taken for the solid concentration to rise to 90% of its final value) are suitable parameters. The use of the t_{50} parameter was found to be less useful as it did not allow us to distinguish between systems. MCR has been successfully used to extract t_{10} values for acetone. Raising the temperature increases the rates of solvent evaporation. Acetone evaporates fastest causing an increase in the methanol proportion in the sampling zone. Subsequently, methanol evaporates, leaving the felodipine/PVP solid dispersions. The rate of acetone evaporation is independent of the presence of solids indicating little or no interaction with PVP or felodipine. However, there is clear evidence of interaction of methanol with solids. The rate of evaporation of methanol is significantly retarded when the solids are incorporated. This indicates interaction of methanol with the solids, most probably by hydrogen bonding.

Moreover, monitoring the peak shifts, peak shapes and widths were very useful to track the molecular interactions between solids and solvents successfully. There is no evidence for molecular interactions of solids with acetone (in acetone/methanol BSM) but there are clear indications that both felodipine and PVP interact with methanol. Drug loading and temperature affect the drying rate that is, increasing the temperature and lowering the drug loading increases the drying rate of solids from acetone/methanol BSM.

The investigated conditions could mimic the formation and preparation of solid dispersions, behaviour of different components in solid dispersions, association through intermolecular interactions and phase behaviour. Moreover, these results would be a starting point to better understand the distribution of various components in solid dispersions, phase transition, phase separation resulting to physical, thermal and chemical instabilities. The molecular interpretation of Raoult's law, monitoring spectral peak shifts and TG-MS analysis indicate that t_{10} data analysis can be a promising approach to extract kinetic information.

Table 4.6. Characteristic peaks used to interpret molecular interactions

	Acetone	Methanol	DCM	Felodipine	PVP
ν_{NH}	-	-	-	3364 cm^{-1}	-
$\nu_{anti(CH)}$	-	-	3054 cm^{-1}	-	-
$\nu_{sym(CH)}$	-	-	-	-	
$\nu_{(C=O)}$	1711 cm^{-1}	-	-	1694 cm^{-1} 1686 cm^{-1}	1657 cm^{-1}
δ_{CH}	-	-	731 cm^{-1}	-	-

Table 4.7. Solvent-solvent interactions (note: NA-Not Applicable)

	Acetone	Methanol	DCM
Acetone ($\nu_{C=O}$) and	1711 cm^{-1}	1707 cm^{-1}	1711 cm^{-1}
Full width at half height	15 cm^{-1}	20 cm^{-1}	13 cm^{-1}
DCM (ν_{CH}, δ_{CH})	3059/733 cm^{-1}	-NA-	3054/731 cm^{-1}

Table 4.8. Solvent-solid interactions (note: NI-No Interactions)

	Acetone/Methanol BSM		DCM/Acetone BSM	
	Acetone	Methanol	DCM	Acetone
Felodipine (ν_{NH})	-NI-	3337 cm^{-1}	3351 cm^{-1}	3344 cm^{-1}
PVP ($\nu_{C=O}$)	-NI-	1650 cm^{-1}	1662 cm^{-1}	-NA-

CHAPTER 5.
EVALUATION OF IMAGE PROCESSING TOOLS FOR MID-INFRARED IMAGING

5.1 Introduction

FTIR imaging is a relatively new technique which provides spectral and spatial information for microscopic chemical characterisations.[109] With the imaging investigations, apart from the conventional spectroscopic benefits, the distribution and location of the individual components within the mixture can be established.[107,113] These advancements enhance the chemical characterization of the samples on a microscopic scale including its morphological form (typically polymorphs and hydrates).[2,7,113] Thousands of infrared spectra with near-diffraction limited spatial resolution and moderate spectral resolution can be acquired in minutes depending on the instrumentation type.[1]

In recent years, it has been shown that FTIR-reflectance imaging can be applied to a multitude of fields from biomedical applications,[192-194] single cells,[195,196] polymer research,[107,118,121,197,197-203] agricultural industries[204,205] and identification of artistic materials.[206] Real time analysis of complex systems involving fast infrared imaging has also been reported.[107] Although, FTIR imaging has found immense applications in the aforementioned industries, in the pharmaceutical field except for a few publications[121,207] the widely used sampling technique is ATR imaging.[173,208-211] Those few publications were made at the early stages of the infrared imaging applications. The main reason could be the complexity of pharmaceutical materials. However, considering the widespread use of mid-infrared imaging in the single cell and biomedical fields (considerably complex),[212] understanding and developing data analysis protocols should benefit the pharmaceutical industries. This work presents the application of chemometric approaches to reduce and analyse large amounts of data from FTIR chemical images acquired from pharmaceutical materials.

5.2 Materials and Methods

Three samples with different compositional distributions were studied. Model system I, a high contrast sample (chemical contrast) contains cinnarizine (CIN) cast from dichloromethane and felodipine (FEL) cast from methanol (4% w/v), showing the interface. Model system I serves as a known phase separated system. It was selected to optimise the data pre-processing and data processing procedures. The optimised data analytical tools were extended to study two other systems. Model system II or low

76

contrast sample (chemical contrast) contains felodipine/PVP solid dispersion spray coated from acetone/methanol (4% w/v) and then stored in a dessicator which yields a system that is intimately mixed.[49,91] Model system II serves as a homogeneous system. The other sample is model system III, a medium contrast sample (chemical contrast) containing felodipine and PVP spray coated from dichloromethane and acetone (4% w/v). The prepared sample was stored at high relative humidity (98%) for a period of 12 hours to induce phase separation and will be discussed in detail in Section 5.6.3. Model system III serves as a system of unknown distribution.

These three optical/brightfield and total intensity chemical images samples are shown in Figure 5.1. A Varian 620 FTIR imaging instrument in reflection-absorption mode was used for data collection with a focal plane array (FPA) of 64 x 64 mercury-cadmium-telluride detectors. This provided an image size of ~350 µm x 350 µm (i.e. 64 x 5.5 µm). Spectra were collected averaging 64 scans at a 4 cm^{-1} spectral resolution in the 4000-920 cm^{-1} spectral range. The acquired chemical images were manipulated using Resolution pro (Varian system in-built software) to perform peak height or univariate analysis. Then the images were converted to .spc files to be studied in Isys 50 (chemical image software) and MCR version 2.1 (Courtesy: Thomas Hancewicz, Unilever ltd).[140,178,179]

5.3 ˙ Understanding the Raw Data

Although much literature has been published, chemical imaging is still in its nascent stage; especially to extract useful information from the raw intensity image. That is, artefacts can be introduced at different stages of chemical image collection. For example, the sampling mode or measurement geometry was found to have a remarkable effect on the data quality as well as on the data purity or contamination.[213] Here the contamination refers to optical artefacts or dispersion artefacts.[214] Except for the transmission and attenuated total reflectance mode, other methods like reflection-absorption, grazing angle or diffuse reflection were found to be seriously influenced by the particle size; especially when the wavelength of radiation and the particle size are similar in size, leading to well known Mie-type scattering issues.[212-214] These spectral distortions can be corrected using a modified version of extended multiplicative signal correction algorithms (RMieS-EMSC).[215,216] That said, the issues are a major concern when materials with varied particle size, such as biological materials containing nucleus, protein and lipids in a single substrate, are studied. In the pharmaceutical industry, although variations in particle size are present, these would not pose serious

issues because the particle size of the pharmaceutical products is either smaller or larger in size than the wavelength of radiation. In the following section, methods to tackle these issues are discussed.

Model systems	Brightfield images	Total intensity images
Model system I or High contrast sample		
Model system II or Low contrast sample		
Model system III or Medium contrast sample		
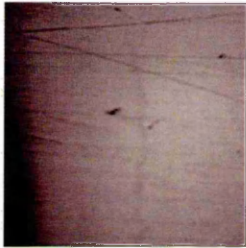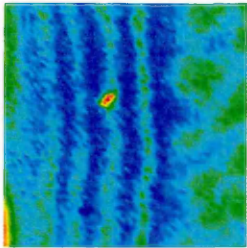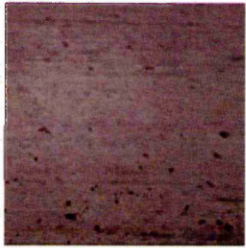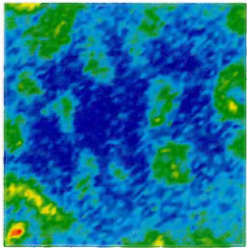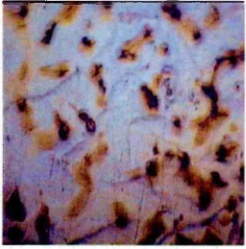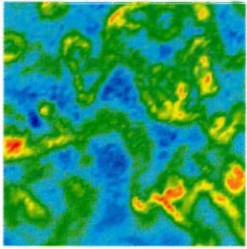
Figure 5.1. Brightfield and total intensity images of the model systems studied

Spectra from the chemical images vary significantly in intensity and shape.[106] The so-called hyperspectral images contain a wealth of information both in quality and quantity. Hence it is prerequisite to reduce the large amount of data before proceeding to interpret the results. It is then possible to separate genuine chemical effects from the optical artefacts. For example, in the solid dispersion the things to be understood and interpreted are drug bands, polymer bands, drug + polymer mixture effects or other interactions (H-bonded, non-polar interacting mixtures, etc.), residual solvent, scattering or dispersion artefacts, optical artefacts like dead pixels or saturated pixels, baseline variations or thickness or pathlength variations and/or atmospheric interferences (water vapour or carbon dioxide). It is evident that the total intensity images acquired mostly

features physical variations rather than chemical signatures.[104,136,217] Understanding these would help in formulating better data analysis procedures.

5.4 Data Pre-processing

The first step in the data pre-processing is to truncate to the region of interest. This enhances the separation of the components as well as reducing the storage memory. The selected bands should be non-interacting, non-saturating and ideally not influenced by optical artefacts.[195,196] The regions of interest used in this study are shown in Table 5.1. Moreover the regions of interest selected are free from the atmospheric interferences like water vapour and carbon dioxide.

Table 5.1. Regions of interest

Samples	Region studied or truncated
Model system I	2850 to 2780 cm^{-1}
Model system II	1125 to 1090 cm^{-1}
Model system III	1125 to 1090 cm^{-1}

In the model systems selected, the commonly encountered optical artefacts were saturated or anomalous pixels, baseline variations and thickness variations. The spikes, anomalous, dead or saturated pixels, if present, are converted as Not-a-number (NaN)[218] and then spectral masking is applied. In order to facilitate a better analysis and interpretation, absorbance values above ~1.5 are masked as NaN's.

The baseline variations were removed by performing a second derivatisation on each spectrum/pixel.[136] In order to correct for thickness variations, the derivatised spectra was scaled with respect to the most intense peak in the spectrum. This normalisation scales spectra to a maximum "intensity" of 1 and a minimum of 0. Minimal preprocessing is preferred,[136] but if artefacts are significant new algorithms are being developed to handle these problems effectively.[105,214-216,219]

After pre-processing the data, the key question then to be answered is to determine how many components contribute to the signal. To achieve this, spectral variations need to be understood. The spectral variations can be important to understand the morphology, the shape and size of features and the presence of molecular interactions.[106] In order to understand molecular interactions at least at the optimisation level, a typical sample prepared by casting the felodipine/PVP sample (50μl) using a Finnpipette was used. For model system II, felodipine/PVP is cast from acetone/methanol while for model system III; felodipine/PVP is cast from dichloromethane/acetone. The peak positions, peak

widths and the intensities were of good quality to be representative for any molecular interactions.

5.5   Data Processing

The pre-processed data must be of sufficiently good quality to extract chemically significant information. There are several potentially useful data processing methods available from classification or clustering techniques to pixelwise data extraction methods. However, the types of data processing procedures depend upon the objective in extracting relevant information from the chemical images. The following four data processing procedures will be critically evaluated for their usefulness in identifying the components of interest in the hyperspectral data cube.

(a).   Univariate analysis : Peak Height Measurements (PHM)

(b).   Supervised Pattern recognition techniques : Compare Correlation (CC)

(c).   Exploratory data analysis : Principal Component Analysis (PCA)

(d).   Image Resolution Methods : Multivariate Curve Resolution (MCR)

When the raw image data for model system I in any type (full or truncated) were analysed using univariate or multivariate tools, erroneous results were obtained (this will be discussed in detail in the following sections). Moreover, this was also the same case when pre-processed data of full spectral range (4000 to 920 cm-1) were considered (data not shown). The scenario was different when the data was truncated to the region of interest (2850 to 2780 cm-1) followed by pre-processing steps and then the processing steps were applied. That is, optical artefacts like thickness variations and particle size are separated and any observed variation is now due only to chemical properties.

5.6   Results and Discussion

5.6.1   Model system I or High Contrast sample or Pharmaceutical Alloys

Model system I had strips of material with known composition (cinnarizine and felodipine) right half is pure felodipine, but the left half is a mixture of cinnarizine and felodipine. Exploratory investigation of the spectra, that is, $v_{(CH)}$ 2807 cm^{-1}, indicated by an arrow mark in Figure 5.2, revealed the presence of three chemically distinct regions. That is, model system I contains regions where there is pure felodipine, felodipine rich and cinnarizine rich mixture regions. Images were generated using discrete peaks at 2807 cm^{-1} and 1099 cm^{-1} to evaluate the distribution of these regions using peak height measurements (Figure 5.3A). The regions in red indicate high concentration of

components while blue indicates low or zero concentration. Figure 5.3A, shows that both the components are present at the same spatial co-ordinates. That is, the univariate measurements were successful in extracting mixed regions of cinnarizine and felodipine; but failed to extract the distribution of pure felodipine layer, because the image has mixed regions of cinnarizine and felodipine of high absorbance. The distribution images extracted using univariate analysis of the raw data is not pre-processed to remove any previously mentioned optical artefacts. Typical spectrum of pure cinnarizine and felodipine are presented in Figure 5.3A under cross-validation. The results of univariate analysis will be used as a control to understand the impact of data pre-processing and data processing procedures.

From Figure 5.3B, the results of the compare correlation maps (extracted from the spectra of pure components) indicate high contrast between the two components, cinnarizine and felodipine. Here a correlation value of 0.99 to 0.80 (assigned red to yellow) indicates that the regions in the image belong to the reference product to which it is compared; whereas a correlation value less that 0.5 indicates the absence of similarity (assigned blue). The intermediate values would require cautious interpretation. From this, it is clear that there is a strong relationship between correlation coefficient value, distribution of components and concentration of analytes in the mixture. However, in order to have a better understanding of the compare correlation results, the "Histogram" is studied in detail. "Histogram" is a useful tool to study the distribution of various components within the mixture. "Histogram" analysis for model system I (Figure 5.3B, cross-validation) shows bi-modal or two different kinds of distribution. The results indicate that the model system I contains two components that are highly phase separated. Although the results from compare correlation maps and "Histogram" seem to be very interesting, the unavailability of the pure spectrum for mixed felodipine shows the major limitations of the supervised data analysis approach.

Before interpreting the distribution of various components within the processed images, the extracted pure components from PCA and MCR are analysed. Figure 5.4, shows the comparison of the results from univariate, PCA and MCR data analysis in the spectral range between 2850 cm^{-1} and 2750 cm^{-1}. In all these data analyse the spectrum is second derivatised. From univariate analysis, three components are identified as; cinnarizine rich, felodipine rich, pure felodipine and are assigned the colours black, red and green, respectively. The respective spectra were collected from cinnarizine rich, felodipine rich and pure felodipine regions. The corresponding results in PCA analysis are labelled PC

I, PC II and PC III whereas in MCR data analysis these are labelled MCR factor I, II and III, respectively. Strong correlation between the 'spectra' can be observed in the following spectral regions 2807 cm^{-1} for cinnarizine rich region (PC1 and MCR1), 2820 cm^{-1}/2790 cm^{-1} for felodipine rich region(PC2 and MCR2) and 2840 cm^{-1}/2790 cm^{-1} for pure felodipine regions (PC3 and MCR3).

From the Figure 5.3C, the results of the principal component analysis are shown. The principal component corresponding to cinnarizine rich region shows 91% of the variance, the second principal component corresponding to felodipine rich region shows 7% variance while third principal component (pure felodipine region) shows 0.6% of the variance. The first three principal components (PC's) explain 98.6% of the total variance. Although, this does not account for more than 99%, the results from the PRESS plot, a cross-validation scheme[220] to measure the descriptive ability of the PCA analysis is applied. The PRESS plot is generated by plotting predicted residual error of sum of squares versus number of principal components and the minimum value in the plot indicates the correct number of principal components to be predicted. PCA PRESS plot (Figure 5.3C) indicates that three principal components will account for all variability in this data set.

The results for model system I using MCR-ALS is shown in Figure 5.3D. Data analysis using MCR-ALS is based on hard or white modelling approach.[221] That is, chemical knowledge of the sample and the number of components within the system is well known. The Figure 5.3D shows the MCR distribution maps for cinnarizine rich, felodipine rich and pure felodipine regions. The cross validation scheme applied for MCR is the direct comparison of the extracted pure components with the real pure components. Moreover, from univariate and PCA analysis it is established that model system I contains three factors.
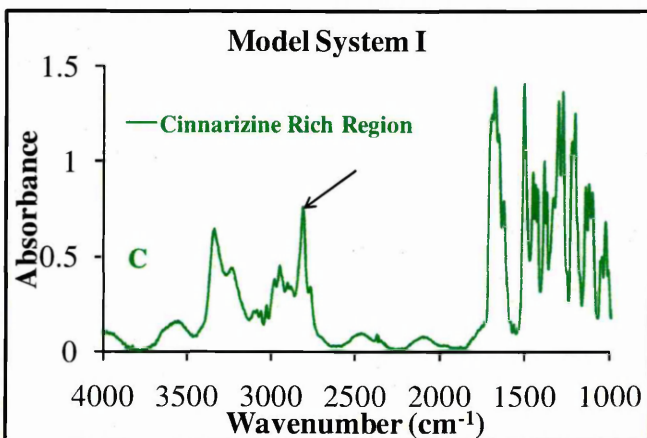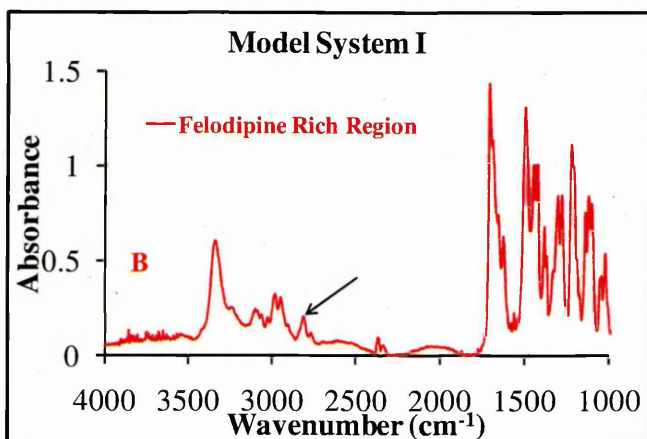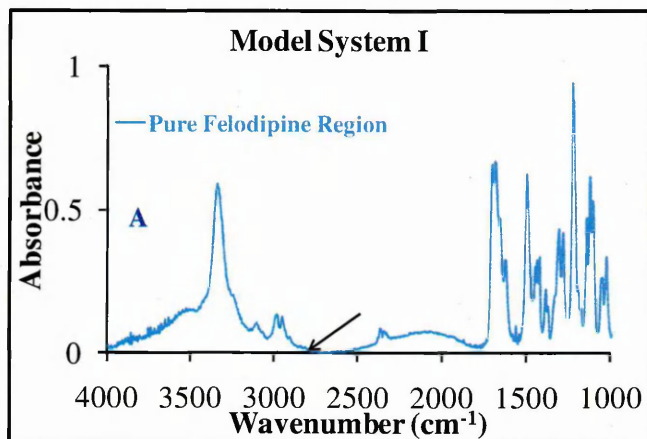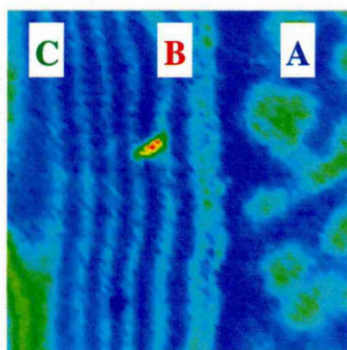
Figure 5.2. Raw image data for model system I (Left) and Spectra from various regions (Right)

As already mentioned the results from the univariate measurements and compare correlation needs careful interpretation and shows the need for the data pre-processing approaches. The results generated using PCA and MCR are in good agreement, reliable and meaningful. The results show that this simple model system consists of three components and is highly phase separated.

5.6.2 Model system II or Low Contrast sample

This model system of felodipine/PVP cast from acetone/methanol was studied to extend the data analysis in a way to better understand the optimisation tools. Moreover, a great deal of work in bulk and microscopic analysis of solid dispersions revealed that a drug dispersed in the polymeric material is in an amorphous state.[28,222] The disappearance of the NH stretching band at 3376 or 3337 cm^{-1} or appearance of the NH stretching peak at 3292 cm^{-1} indicates the formation of solid dispersions.[88] That said, the results from the unprocessed univariate analysis (Figure 5.5A) appear to be quite contradictory. Images were generated using discrete peaks at 2886 cm^{-1} and 1099 cm^{-1} to evaluate the distribution of PVP and felodipine using univariate or peak height measurements and Figure 5.5A underlines to indicate significant separation of the components.

The raw data cube acquired was pre-processed in a similar way to that previously discussed (cf. pre-processing of model system I). The pre-processed data was then processed using chemometric data processing steps. The results from compare correlation are shown in Figure 5.5B. Moreover, comparing the correlation images of pure felodipine, pure PVP and a mixture shows that the intensity range is from 0.88 to 0.99. This indicates that the pure components and a felodipine/PVP mixture are highly correlated; offering a reliable qualitative indication that the components are uniformly distributed. Moreover, the "Histogram" (Figure 5.5B) fit a Gaussian like or unimodal distribution for the pure components. Hence, it can be concluded that the model system II is homogeneously distributed.

Figure 5.3. Comparison of chemometric data analytical tools in extracting distribution maps from the model system I
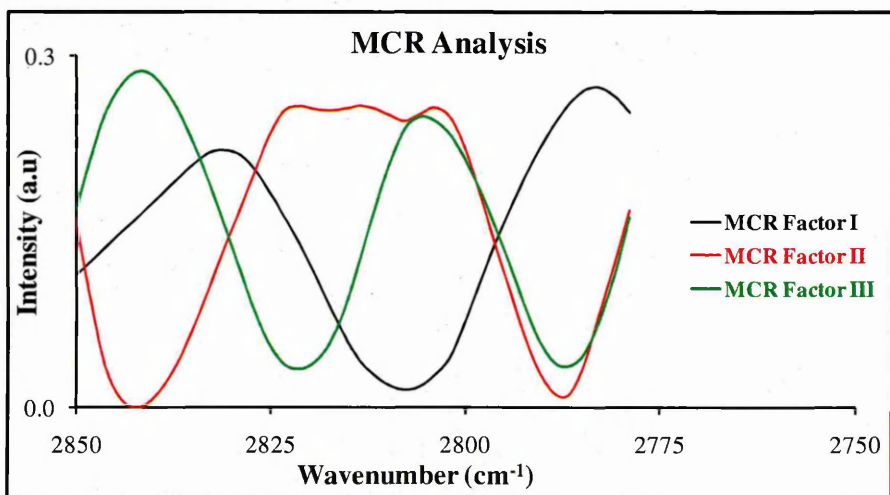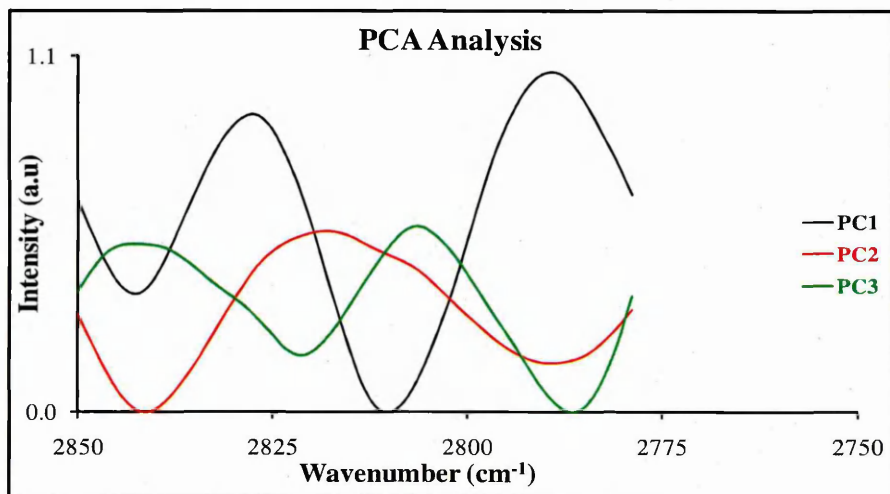
Figure 5.4. Comparison of 'Real' pure component spectra and 'Extracted' pure components for Model system I

Figure 5.6, shows the comparison of the results from univariate, PCA and MCR data analysis for model system II in the spectral range between 1125 cm^{-1} and 1090 cm^{-1}. In all this data the spectra are second derivatised. From univariate analysis, two components are identified as; solid dispersion rich region and PVP rich region and are assigned colours red and blue, respectively. The corresponding results in PCA analysis are labelled PC I and PC II whereas in MCR data analysis these are labelled MCR factor I and II, respectively. Strong correlation between the 'spectra' can be observed in the following spectral regions 1099 cm^{-1}/1114 cm^{-1} for solid dispersion rich regions and 1099 cm^{-1}/1116 cm^{-1} (shoulder peak) for PVP rich regions.

The results from PCA are shown in Figure 5.5C. The score images indicate that 99.6% of the total variability is explained with the first principal component (PC I) or solid dispersion rich region, the second principal component (PC II) or PVP rich region explains 0.36% of the variability. The PRESS plot also shows that only two principal components are required to characterise the data.

The chemical knowledge of the sample and the number of components expected within the model system II is well known and predicted that the system contains two factors (solid dispersion and PVP rich regions). The distribution of the MCR factors are shown in Figure 5.5D. The obtained images matched well with the PCA results which gave us the confidence in predicting the results. Each of the compare correlation images look similar and resemble the image to PC 1 and MCR factor 1. The distribution of each component cannot be precisely calculated if there is uniform distribution, at least with the statistical pattern recognition methods like compare correlation. PCA is an exploratory approach and estimates concentration of analytes based on the global pixel variations whereas MCR estimates the concentration of each factors or analyte based on pixel to pixel variations.[136] That is, the distribution of solid dispersions is dominant in the chemical image and only a few pixels indicate the presence of pure polymer.

The results from PCA and MCR are in good agreement and reveal that the felodipine/PVP solid dispersions cast from acetone/methanol are homogeneously distributed. This example clearly illustrates the need for data pre-processing and sophisticated data analytical tools to avoid misinterpretation when components are homogeneously distributed.
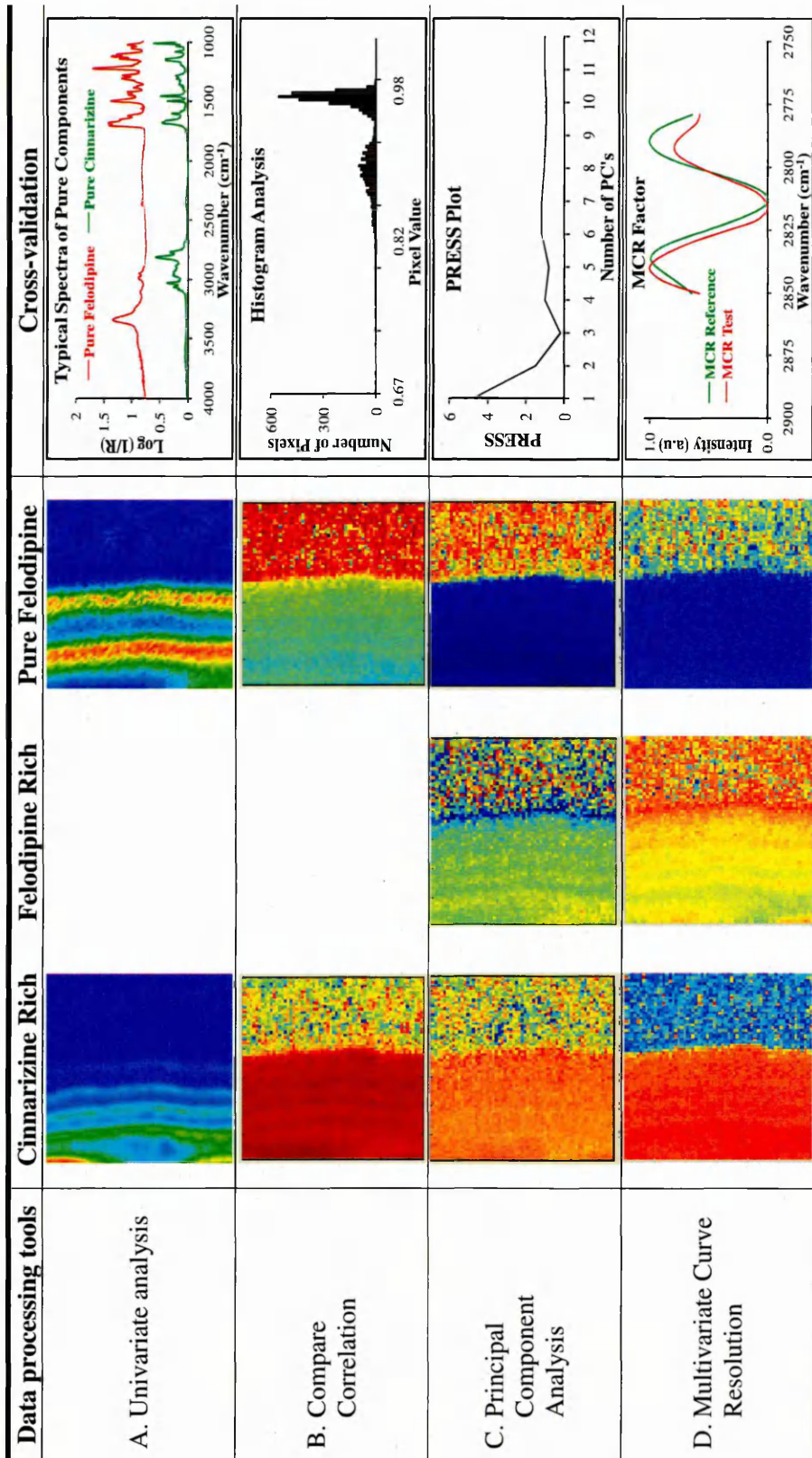
**Figure 5.5. Comparison of chemometric data analytical tools in extracting distribution maps from the model system II**

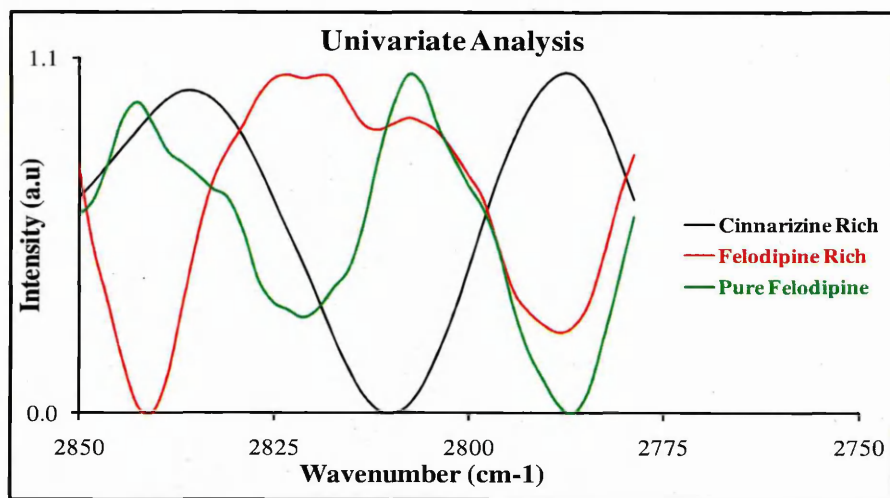**Figure 5.6.** Comparison of 'Real' pure component spectra and 'Extracted' pure components for Model system II

5.6.3 Model System III or Medium contrast sample

The data pre-processing and data processing procedures were then extended to felodipine/PVP solid dispersions cast from DCM/acetone binary solvent mixture, hereafter called model system III. The sample was stored at high relative humidity (98%) for a period of 12 hours and then studied. The raw data cube acquired was pre-processed in a similar way to that previously discussed (cf. pre-processing of model system I). Before interpreting the results it is worth detailing the storage conditions and their impact on the prepared solid dispersions. When a prepared solid dispersion is stored at an elevated relative humidity of 98% (using a saturated salt solution of potassium hydrogen sulphate), the absorbed moisture induces phase separation and subsequent recrystallization of the drug.[48,88,91]

Figure 5.7A shows images generated using peaks at $v_{(NH)}$ 3376 cm^{-1}, $v_{(CH)}$ 2886 cm^{-1}, and $v_{(CO)}$ 1099 cm^{-1}, to evaluate the distribution of (i) crystalline felodipine rich region (represented as drug rich) (ii) polymer rich regions with crystalline felodipine (represented as polymer rich) and (iii) homogeneous felodipine/PVP solid dispersion regions, respectively from the univariate measurements. A summary of the peaks used to describe the regions is presented in Table 5.2..

Table 5.2 Peak information used to interpret various regions in Model system III

Region	Peaks
Drug Rich	$v_{(CO)}$ 1099 cm^{-1} (no $v_{(CH)}$ 2886 cm^{-1})
Polymer Rich	$v_{(NH)}$ 3372 cm^{-1} and $v_{(CO)}$ 1099 cm^{-1}
Solid Dispersion Rich	$v_{(CH)}$ 2886 cm^{-1} (no $v_{(NH)}$ 3372 cm^{-1})

"Histogram" from compare correlation for the model system III shows that the sample contains at least three different components and the corresponding image planes for felodipine, PVP and solid dispersion are shown in Figure 5.7B.

Figure 5.8, shows the comparison of the results from univariate, PCA and MCR data analysis for model system III in the spectral range between 1125 cm^{-1} and 1090 cm^{-1}. In all this data, the spectra are second derivatised. From univariate analysis, three components are identified as; solid dispersion rich region, PVP rich region, felodipine rich region and are assigned red, blue and green respectively. The corresponding results in PCA analysis are labelled PC I, PC II and PC III whereas in MCR data analysis these

are labelled MCR factor I, MCR factor II and MCR factor III respectively. Strong correlation between the 'spectra' can be observed in the following spectral regions 1097 cm^{-1}/1114 cm^{-1} for solid dispersion rich regions, 1099 cm^{-1}/1120 cm^{-1} (shoulder peak) for PVP rich regions and 1097 cm^{-1}/1112 cm^{-1} for felodipine rich regions. Although there are slight deviations in the results the extracted components are mathematical results, the region selected is a narrow window; moreover these results are from a single pixel (that is, pixel to pixels variations are not included). Within these errors, the comparison between the results is satisfactorily accepted.

The PCA results are shown in Figure 5.7C, and the results indicate that 3 principal components are required to explain 98% of the total variability. The addition of two more PC's would account for 99.6% of the variability. However, since the PRESS plot indicates that the sample contains only three PC's, any further addition could lead to over-fitting. This gives us the confidence in deducing that only 3 PC's are present within the sample.

The MCR results are shown in Figure 5.7D. Previous analysis of the number of components (from PCA results) showed that model system III contains three factors. The areas obtained for factor I, factor II and factor III matched well with the PCA results which gave us the confidence in the results and clearly show that, under unsuitable storage conditions, phase separation can be induced in this system. Compare correlation shows similar polymer rich and felodipine/PVP solid dispersion images to those of PCA and MCR but the drug rich regions show poor agreement; probably indicating the requirement of an additional training data set.

5.7 Image visualisation tools

Once the data dimensionality is reduced and the distribution of components is established, the next step is to explore the spectral and spatial characteristics within the hyperspectral data.[104] Moreover, summarizing the image results provides a useful means of understanding the complex data. This is imperative because we use vision to process[193] approximately 75% of the incoming information and it is proven to be very useful in fields such as photography and histopathology. In this context, image enhancement tools are applied to better understand the distribution of various components within the model systems investigated.
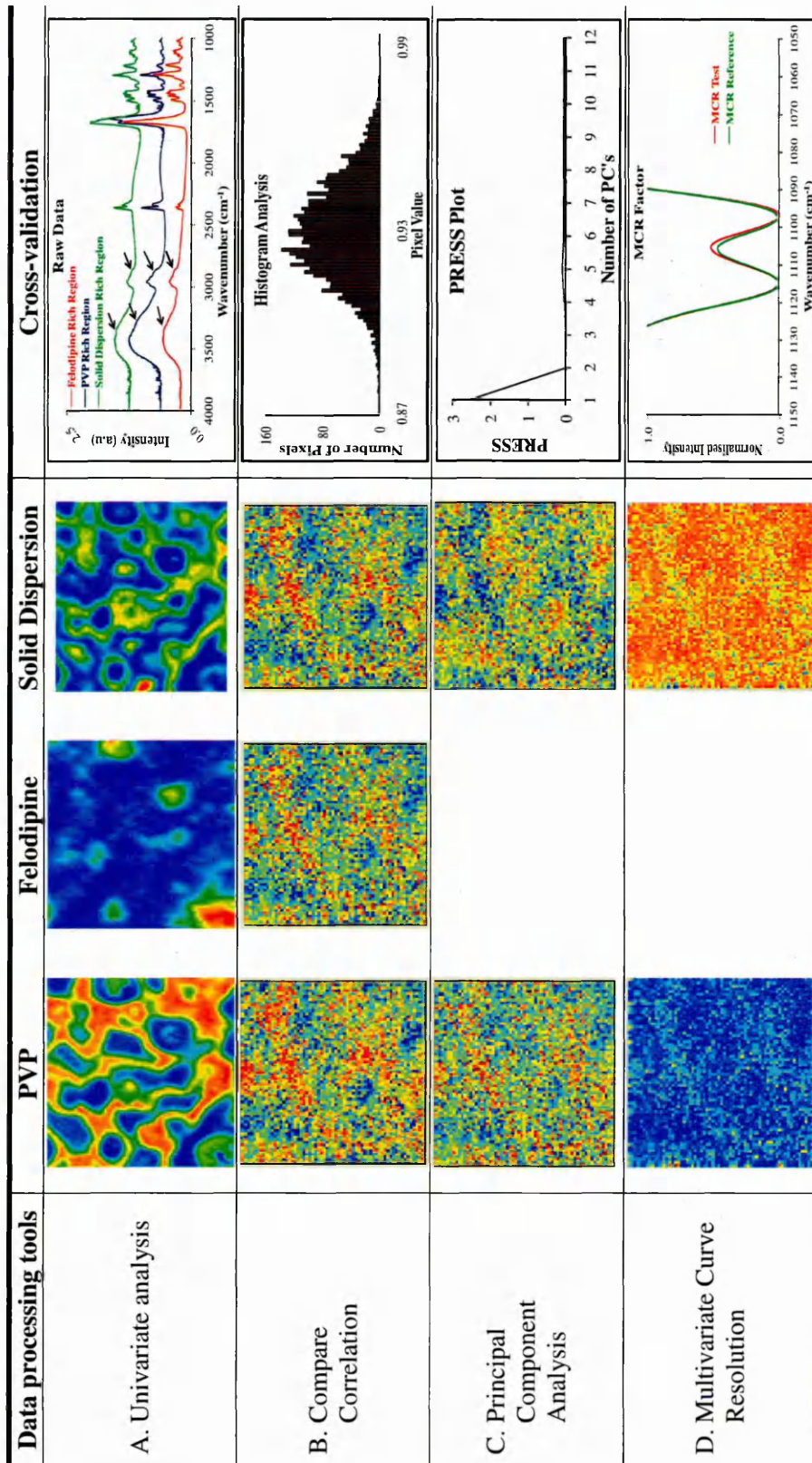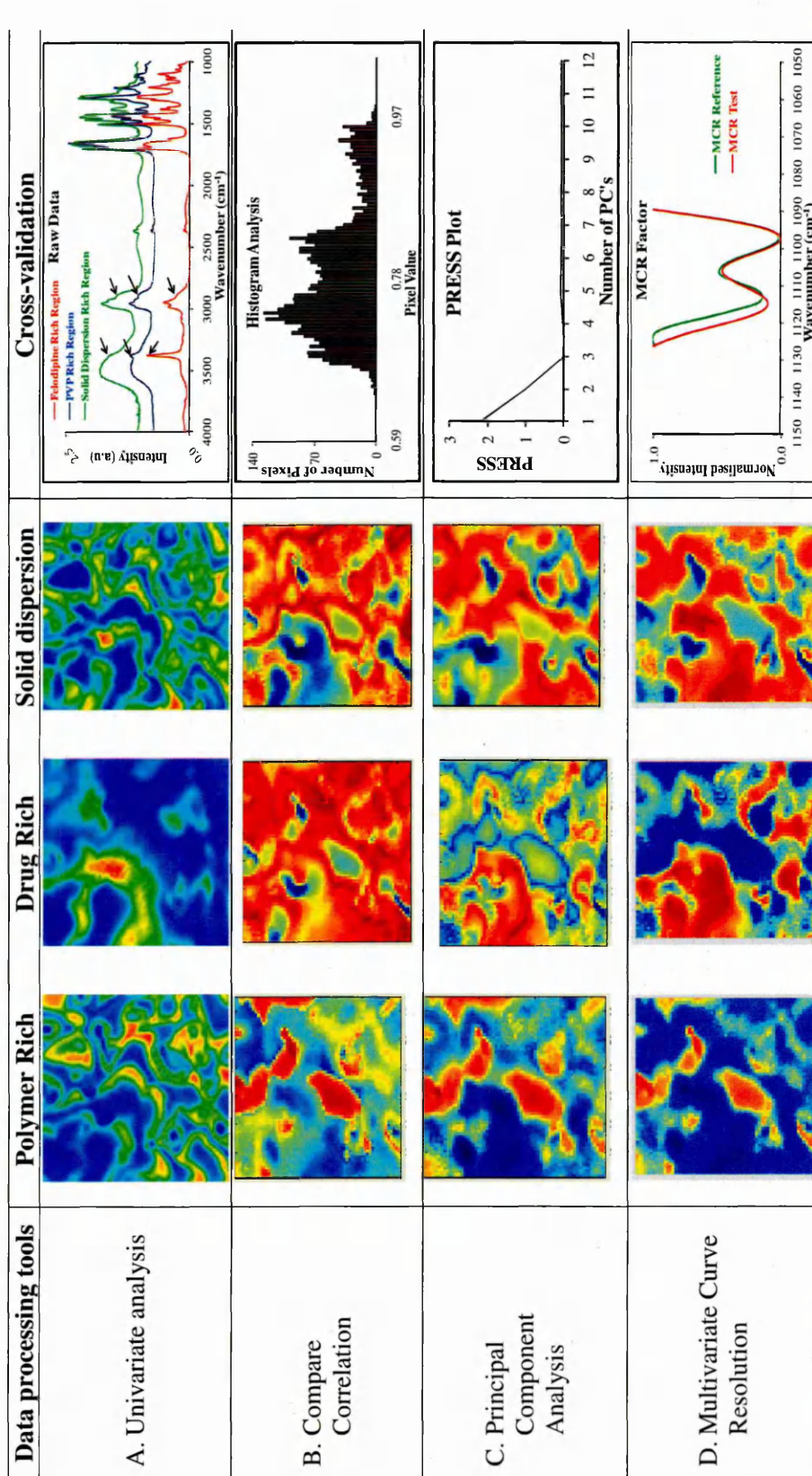
Figure 5.7. Comparison of chemometric data analytical tools in extracting distribution maps from the model system III

92

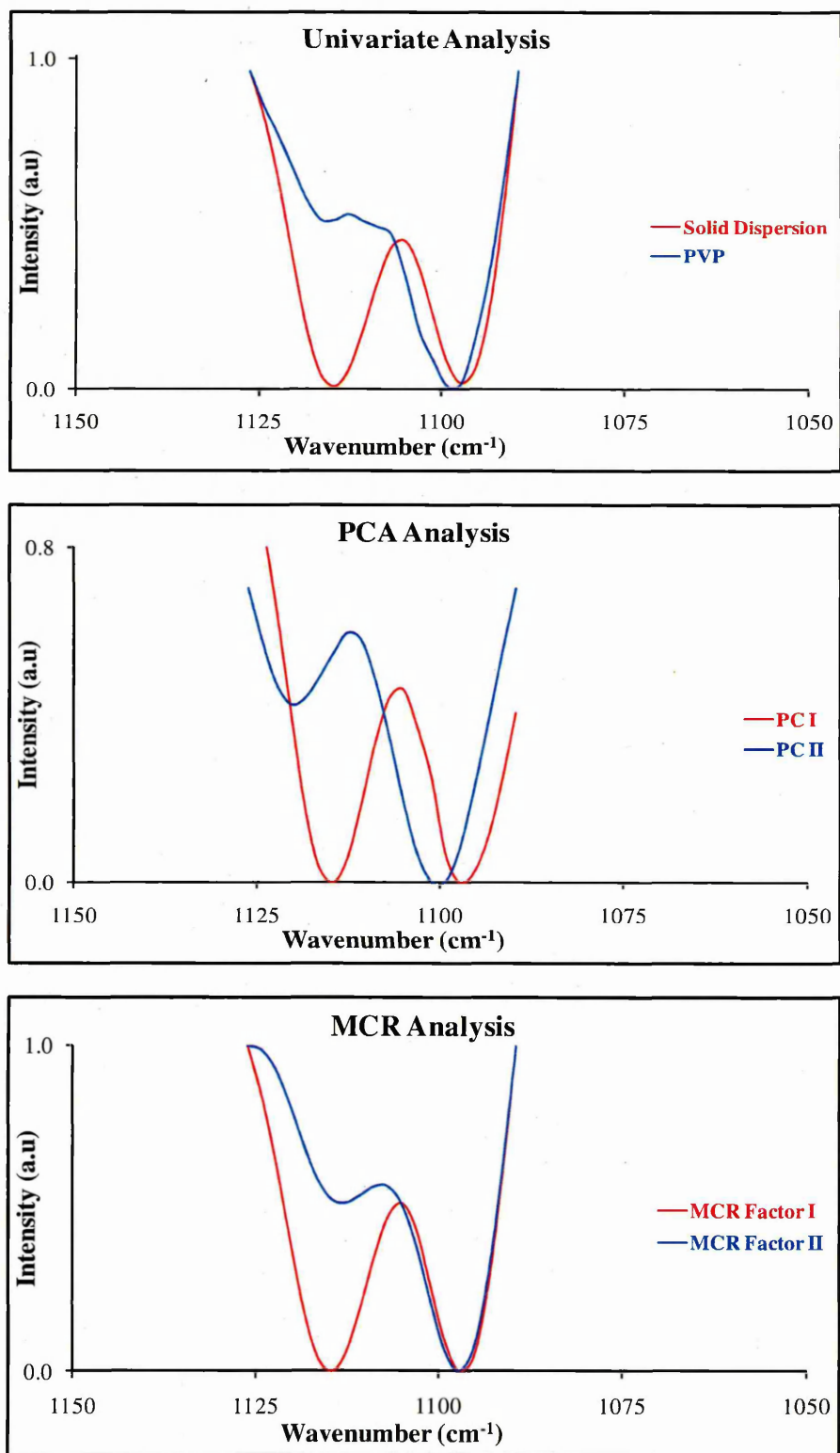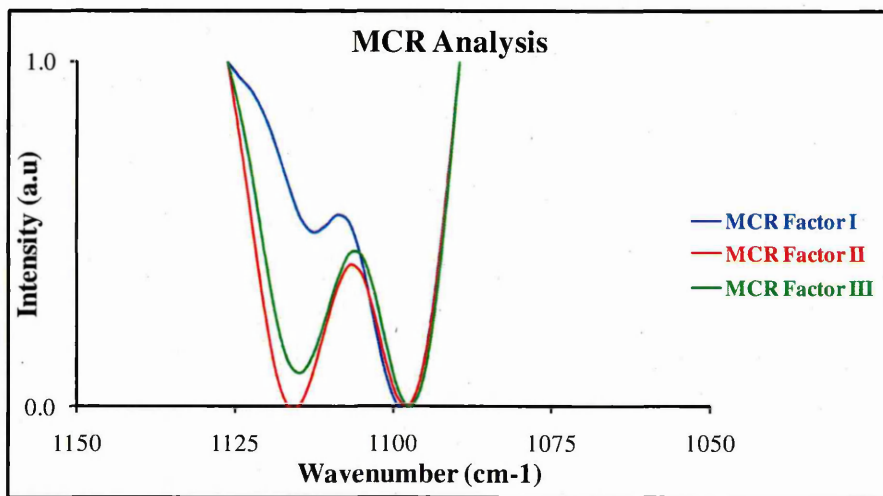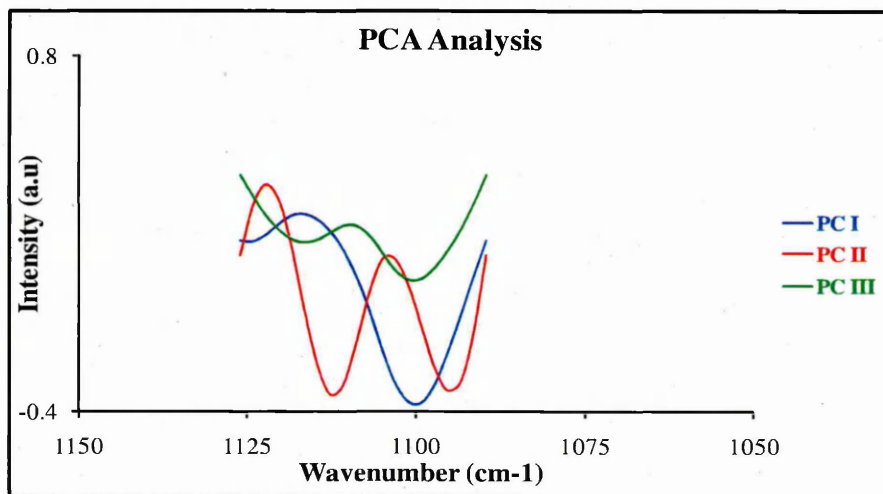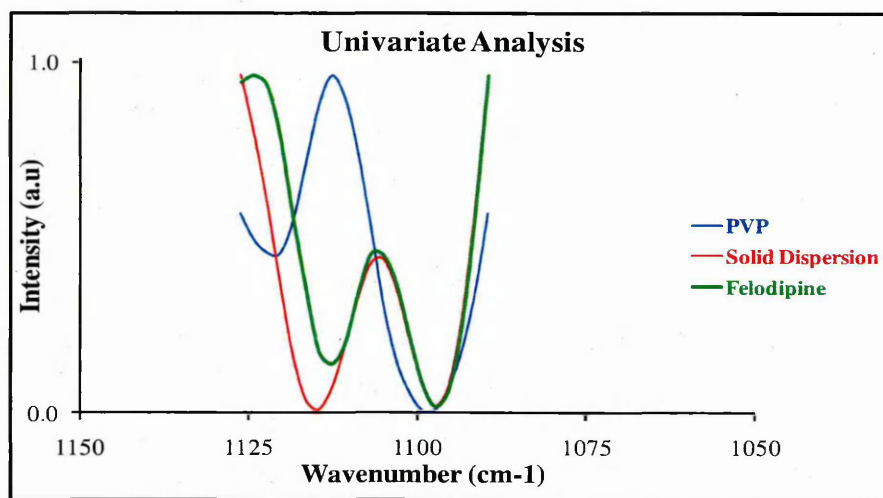**Figure 5.8.** Comparison of 'Real' pure component spectra and 'Extracted' pure components for Model system III

5.7.1 Red-Green-Blue (RGB) reconstruction

The RGB image is a composite image produced to enhance the visualising ability of the resulting images.[104] RGB interpretation is a colour model in which three single channel images are created. It is created by overlaying each constituent distribution images derived from the principal component analysis and then assigning one of the three colours red, green or blue.[223] These image enhancement tools help to better visualise the location of various components within the sample and also provide an insight into the uniformity and distribution (homogeneity or heterogeneity) of these constituents. . The RGB images are shown in Figure 5.9A, B and C for the model systems I, II and III, respectively.

5.7.2 Scatter plots with colour representation

The scatter plot with colour representation is one other visualisation tool that is used to extract the number of components present within the sample and their distribution. The results of PCA, scores or loadings, can be visualised by representing them in a scatter plot. The resulting scatter plot summarizes the relation or correlation between the loadings. Figure 5.10A, B and C are the scatter plots for the model systems I, II and III, respectively. The scatter plots represent the plot of principal component I (PC I) vs. principal component II (PC II). For example, in model system I, cinnarizine rich regions are found to be PC I and felodipine rich region is PC II. A set of data points in the scatter plot can be defined as an ellipse (shown in Figure 5.10A). While doing so the extracted individual features or regions from the principal component analysis can be marked by selecting one of the available colours (red, green, blue magenta, cyan, or yellow).[223] A different colour is used for each of the loadings and referenced in the table, so that different components and their distribution can be discriminated in the graph and in the image, respectively.

The graphical display of the variables can be used to identify whether different spectral features are related. If the two loadings are strongly related, then the data points form a systematic shape (e.g., a straight line or a clear curve). The straight line can be upwards meaning positive correlation between the loadings or negative correlation, if downwards. If the variables are not related, then the points form an irregular "cloud". The resulting composite image and scatter plot can be used to understand the distribution between the various components within the acquired image.

5.7.3 RGB vs. Scatter plots

The RGB and scatter plots were produced after PCA analysis and are shown in Figure 5.9 and 5.10, respectively. The resulting variables or the principal components were assigned specific colours, shown in Table 5.3. With model system I, cinnarizine rich regions, felodipine and mixed felodipine were assigned red, green and blue, respectively. For model system II, red was assigned to solid dispersion rich region and PVP rich region was assigned blue. With model system III, PVP rich, drug rich and solid dispersions rich regions were assigned blue, green and red, respectively. These representations were the same both in RGB and scatter plots.

The RGB reconstruction for model system I, II and III are shown in Figure 5.9A, B and C, respectively. From the RGB representation for model system I, II and III, the composite image derived shows two components, one component and possibly three components respectively. However there is no marked discrimination between components for model system III within the image.

The scatter plots (image visualisation) for model systems I, II and III are shown in Figure 5.10D, E and F, respectively. The loading scatter plot (Figure 5.10B) for model system II has data points forming a systemic shape in downward direction meaning the solid dispersion rich region and PVP rich region form a uniform distribution but are anti-correlated to each other. The loading scatter plot (Figures 5.10A and C) for model system I and III shows clear discrimination between the components. From the loading scatter plot, PRESS plot (Figures 5.3C and 5.7C) and composite images it is evident that model systems I&III contain at least three components. That is, model systems I and III are phase separated to different degrees, while model system II is homogeneously distributed, which agrees well with the data processing results.

Table 5.3 Colour assigned to individual components in composite image

	Model System I	Model System II	Model System III
Red	Cinnarizine Rich regions	Solid Dispersion	Solid Dispersion
Green	Felodipine	-Not Applicable-	Felodipine
Blue	Diffused Felodipine	PVP	PVP

Although conclusions from the scatter plot are similar to RGB reconstruction, the advantages obtained using scatter plot options are multitude. Firstly, with RGB only three components can be used while with scatter plot reconstruction at least six components can be used. Secondly, the discrimination between various components is better in a scatter plot than RGB reconstruction model.

5.7.4 Validation of MCR scatter plot

Although multivariate curve resolution extracts spectra from unresolved data, the problem of rotational ambiguity within the obtained results is a serious issue.[142,144,224,225] That is, MCR can produce solutions (called principal factors) that fit mathematically, but do not carry any physical or chemical meaning and this uncertainty is called rotational or intensity ambiguities. In line with this, in order to overcome these issues we applied multivariate statistical tools like scatter plot to MCR concentration data and this will be discussed in detail comparing the results from three model systems. In Section 5.7.2 image visualisation tools, the scatter plot was described. The scatter plot can be used to obtain component distribution images, graphical displays of the variables and a means to understand the relationship or correlation between the variables. The obtained results are then cross-validated with PCA results.

In this point of view, the MCR concentration images for various model systems were plotted as MCR factors vs. pixel response, as shown in Figure 5.11A. This generates a MCR score scatter plot. The generated score scatter plot indicates the relationship between the factors. If the separation between the factors is large it indicates different chemical entities. The results indicate that there are three different factors with a cross over point signifying there is an interface. The MCR loading scatter plot can be generated and interpreted the same way as PCA loading scatter plot (cf. Section 5.7.2). When two MCR factors are plotted to understand the correlation between them they signify the distribution of the components in the sample. Scatter plot of PF1 (cinnarizine) vs. PF2 (felodipine) of the model system I, shows clear separation between the components and this is cross validated against the PCA scatter plot shown in Model system I (Figure 5.11B) and Model system II (Figure 5.11C), respectively. The score scatter plot, loading scatter plot thus indicate that the model system II is highly phase separated.

In this context, the concept of the aforementioned discussion was extended to model system II and model system III where the MCR loading plot results indicate there are

two and three components respectively. Moreover, the MCR score scatter plot indicates homogeneous and heterogeneous distribution, model system IIB and model system IIIB respectively. This is in good agreement with the PCA scatter plot results, shown in model system IIC and model system IIIC.

These results show that with confidence scatter plots can be applied to estimate the number of components and its distribution in order to avoid ambiguities in MCR results.

5.8   Conclusions

In this chapter, several image processing tools have been evaluated in an attempt to better extract distribution maps of various species in the multi-component mixtures. Three model systems, that is high, low and medium contrast samples, were included in the study. Of the three systems, the number of components and their identity were fully known for the high contrast sample or model system I and low contrast sample or model system II. Then, the developed data pre-processing and data processing tools were extended to the medium contrast sample or model system III whose identity was unknown or sparsely known.

Univariate analysis, for example peak height measurements, is the simplest approach used to generate an intensity or distribution map of various components in the mixture. That said, it is not always straight forward when systems under study are prone to optical artefacts like thickness variations, optical artefacts like scattering and importantly when overlapping bands in multi-component mixtures are present. We have clearly demonstrated that even with the simplest model system studied, in the absence of data pre-processing steps, the results can be very misleading.

Compare Correlation mapping is a useful tool for studying the distribution or homogeneity of various components within the multi-component mixtures. In the present study, the correlation co-efficient scale was applied successfully to trace the distribution of each component and "Histogram" was used to study the uniformity in the distribution of components. Since pixel-wise correlation of each component within the hypercube was made, this provides an insight into the sample uniformity and this was directly related to the number of components present in the sample. However, compare correlation was successful only with the low contrast model systems. With the high and medium contrast sample it showed poor agreement with the other approaches. Compare correlation probably requires additional training data. Furthermore, it also requires prior

knowledge about the sample which restricts its wide spread application especially in stability and degradation studies or reaction monitoring etc.

	Model System I	Model System II	Model System III
	A	B	C
Composite Images			
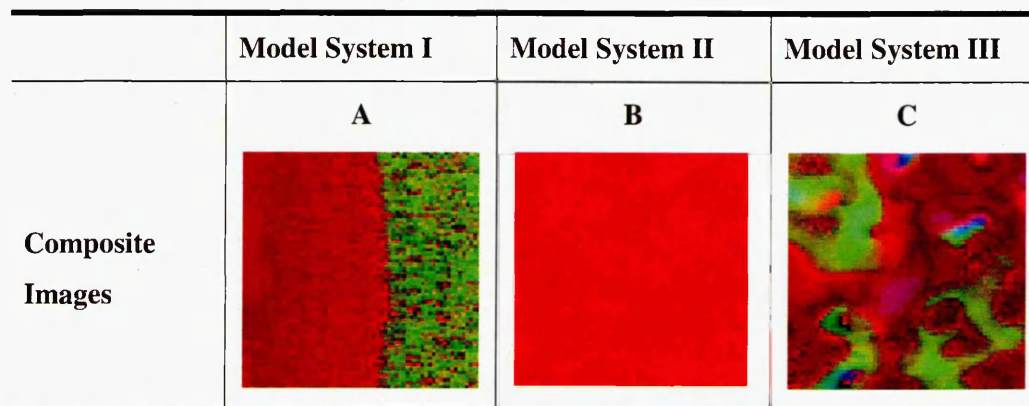
Figure 5.9. Image Enhancement Tools (RGB Reconstruction)

	Model System I	Model System II	Model System III
	A	B	C
Loading plot			
	Plot of Cinnarizine vs. Felodipine	*Plot of Solid dispersion vs. PVP rich regions*	*Plot of Solid dispersion vs. PVP rich regions*
	D	E	F
Composite Images			
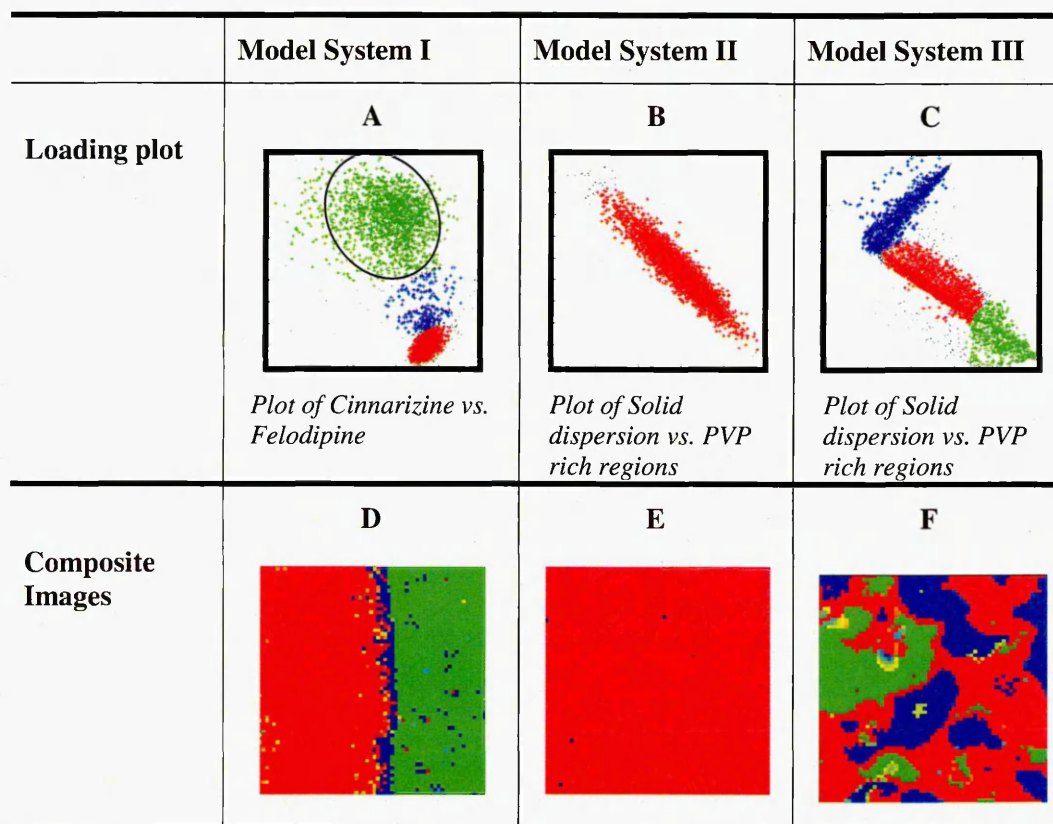
Figure 5.10. Image Enhancement Tools (Scatter Plot)

Principal Component Analysis (PCA) has been demonstrated to be an effective tool to study the sample when only an exploratory type of data analysis is required. PCA identifies the number of pure components present in the sample without supervision or

98

without prior information. Mostly, the loading image cannot be a good starting point to extract the information about the sample because any principal components (PC's) do not necessarily correspond to one specific chemical component in the mixture.[136] Instead, in our studies the predicted residual error of sum of squares (PRESS) plot was successfully used. Additionally prior knowledge about the sample together with the compare correlation results was validated while determining the number of components that are expected to be present within the sample. Multivariate curve resolution (MCR) extracts straightforward information about the identity and the distribution map of 'pure' components in the mixture. Such resolution methods do not require any prior information about the sample and do not suffer from any inteferences.[4] Moreover, the MCR results are in good agreement with the PCA results.

More detailed analysis has shown that data pre-processing is vital in order to avoid misinterpretation. Through the application of chemometrics to FTIR chemical images, the optical artefacts are separated and chemically significant information is extracted[226]. Additionally, a synergistic combination of FTIR imaging and chemometric tools unravels the wealth of information contained in the resulting images. Optimised image preprocessing, processing and a flow chart of the various steps involved in the extraction of information from the mid infrared chemical images are shown in Table 5.4 and Figure 5.12 respectively.

Table 5.4. Optimised image preprocessing and processing tools

Factors	Comments
Sampling Method	Depend upon the analysis need
Data Preprocessing	
Spikes, Bad Pixels	Pixel (NaN) mask
H_2O, CO_2	Truncate data to region of interest **(T-ROI)**
Baseline correction	Second derivative
Thickness variations	Peak Height Normalisation
Scattering	Truncation
Data Processing	MCR/PCA preferred (depends on the need)
Image Visualisation	Scatter Plot
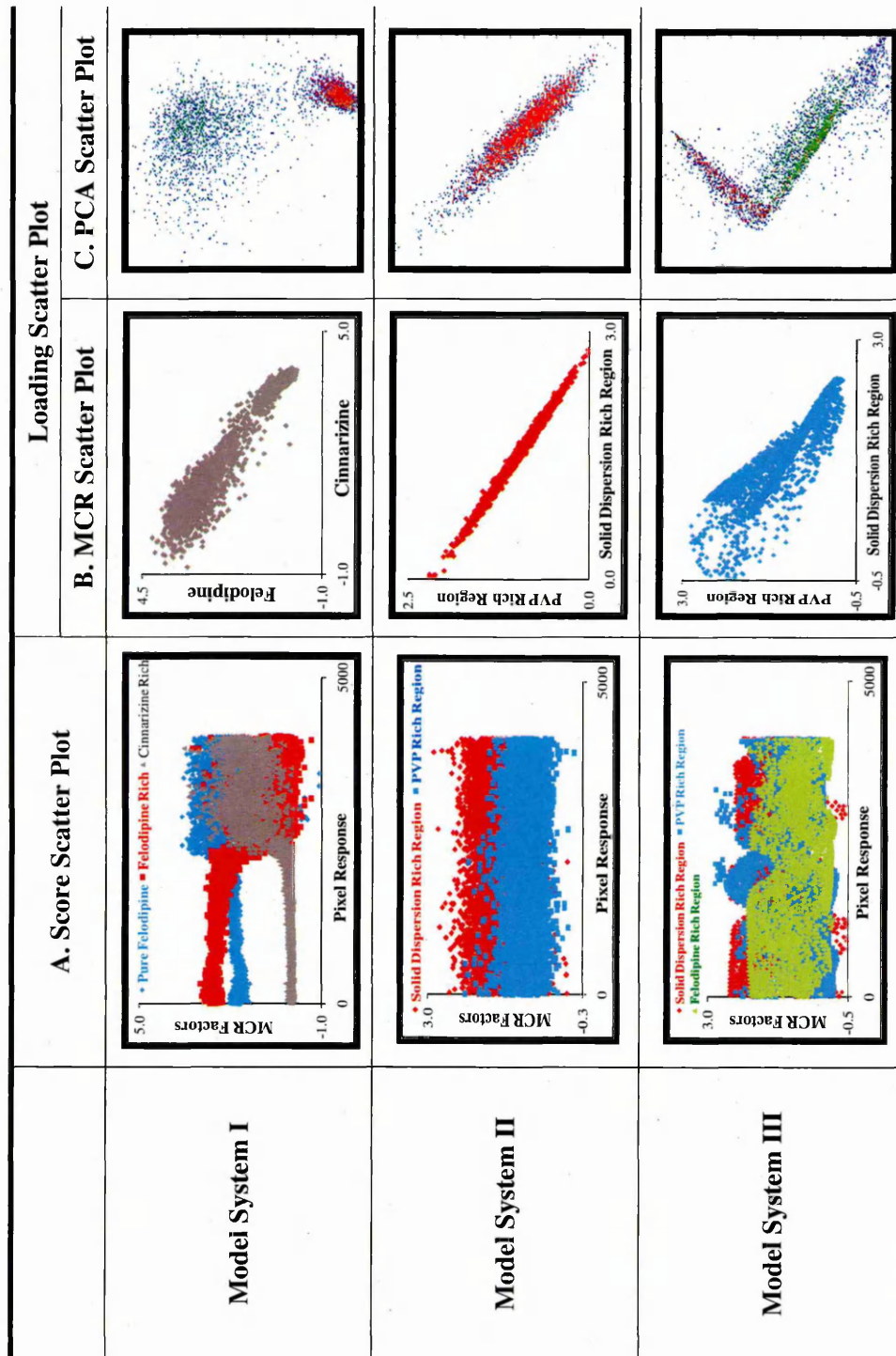
Figure 5.11. Comparison of MCR and PCA scatter plots

100
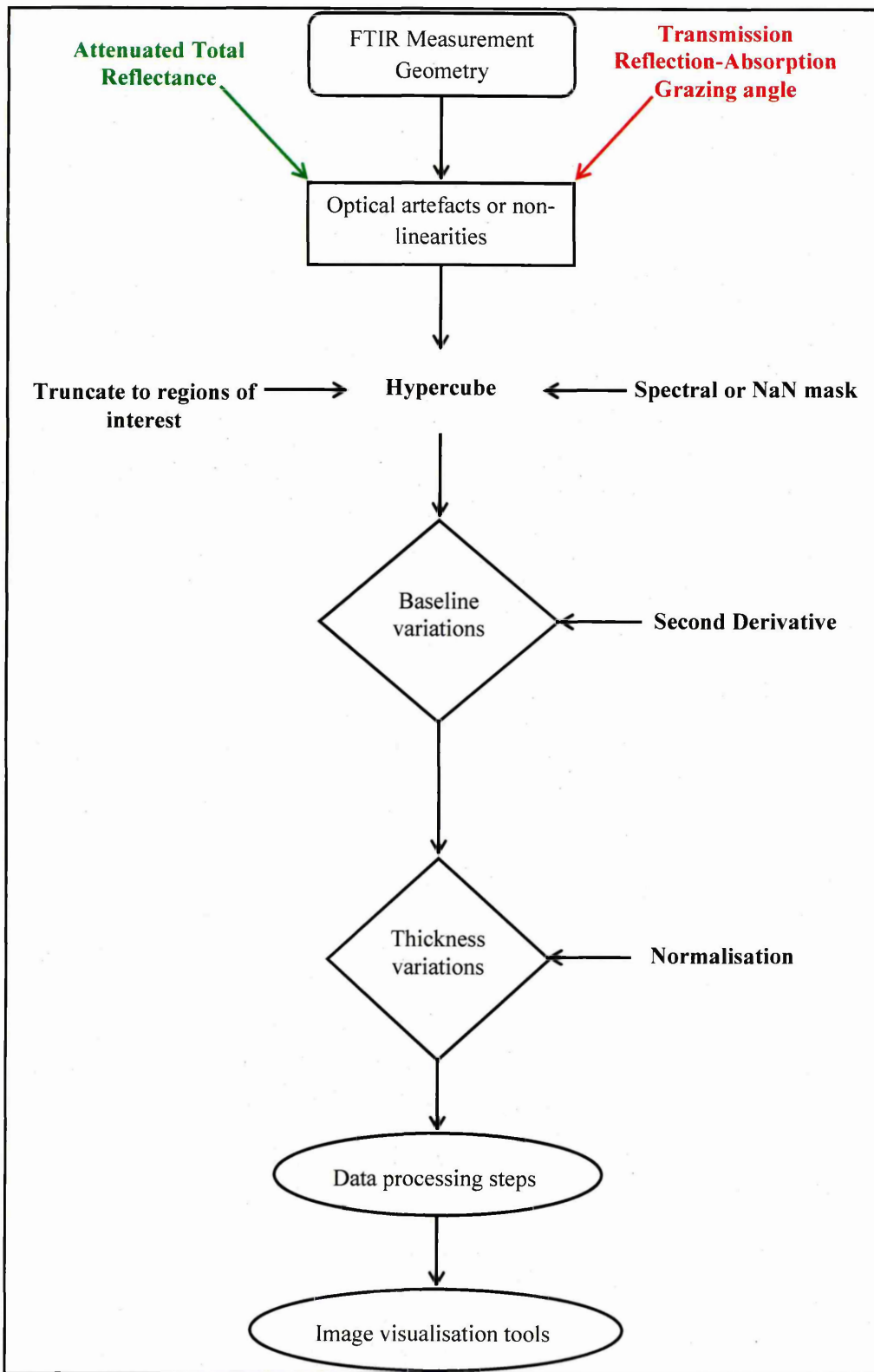
Figure 5.12. Overview of various steps involved in extracting information from mid infrared chemical images

CHAPTER 6.
THE APPLICATION OF VIBRATIONAL SPECTROSCOPY TO SOLID DISPERSIONS: FINAL PRODUCT CHARACTERISTICS

6.1 Introduction

Even though large numbers of studies on spray drying,[29,52,227-230] rotary evaporation[39,61,64,231] or rapid solvent evaporation[46,93] are available only a limited number of articles are dedicated to study the effect of solvents on the resulting solid dispersions. The distribution of various components within the solid dispersions will be influenced by the solubility of individual components within the dissolving solution. To the best of our knowledge, to date, there has been no work reported describing the importance of solvent induced component distribution with respect to preparation of solid dispersions. The goal of this work is to understand the relation between the kinetics derived from the bulk spectroscopy studies and microscopic chemical characterisation. In this regard, the work described in this Chapter is carried out to answer the following questions;

1. Can FTIR imaging be applied to complement the findings of *in situ* monitoring to study the impact of solvent interaction on the distribution of the felodipine and PVP within the prepared solid dispersions?

2. Can FTIR imaging be applied to study the phase separation in the resulting solid dispersions?

This Chapter is divided into two parts. In order to provide insight into solid-solid interactions and its relevance in the formation of intimately mixed solid dispersions, firstly, the results from Chapter 4 are further investigated. The bulk spectroscopic results (ATR-FTIR measurements) are discussed to understand the drug-polymer interactions in detail. Secondly, mid infrared imaging is applied to extract microscopic and spatial information on the distribution of various components within the solid dispersions. Then the results are combined and correlated to understand the impact of adhesive and cohesive interactions on the compositional distribution, hence the phase behaviour of the prepared solid dispersions.

6.2 Experiments

6.2.1 Materials

Materials used are a model drug, felodipine (AstraZeneca, U.K) and the polymer, Polyvinylpyrrolidone (Plasdone, K29/32), purchased from International Speciality

Products (ISP). Acetone, dichloromethane and methanol (HPLC grades) were obtained from Sigma-Aldrich, Switzerland. Unless stated, the drug, the polymer and the solvents received were used as obtained.

6.2.2 Sample preparation

For ATR-FTIR measurements, three different drug-carrier weight ratios (20:80, 50:50 and 80:20) for binary systems, 100% drug or 100% polymer and two different mixed solvent systems (acetone/methanol and DCM/acetone at 50:50 v/v) were used. 1g of the solid was dissolved in 25ml of the solvents to yield 4 wt% solutions. 50 µl of each solution was cast directly onto a pre-heated ATR crystal using a Gilson pipette. Studies were carried out at 30°C, 40°C and 50°C respectively. Each experiment was conducted with 5 replicates to ensure reproducibility.

For spectroscopic imaging studies, drug-carrier weight ratios for binary systems were 20% felodipine and 80% PVP which were dissolved in the mixed solvent (acetone/methanol and DCM/acetone) systems (50:50% v/v) to yield 4% w/v solution. The prepared solutions were spray coated (using a Badger air brush) on to a 316 stainless steel reflective substrate and stored in the dessicator.

6.2.3 Experimental Parameters

Fourier Transform Infrared spectra were collected using a Specac ATR system attached to a Thermo Nicolet Nexus bench equipped with a Mercury-Cadmium-Telluride detector. The spectra were collected between 4000-650 cm^{-1} at a resolution of 4 cm^{-1} using 4 co-added scans. The spectra were collected in the series mode (continuous collection of spectra over a pre-determined period for 5 minutes), a method available within the instrumental software. All the spectra during the kinetic study were collected in the Log1/R format. Background spectra of the clean ATR crystal were collected before each sample spectrum.

Chemical Images were obtained using a Varian FTIR Imaging spectrometer in reflection-absorption mode. The images were collected between 4000-920 cm^{-1} at a resolution of 4 cm^{-1} and 64 co-added scans. Data analysis was performed using peak height and chemometric approaches (data preprocessing, data processing (MCR-ALS) etc) were performed as described in image processing tools (cf. Chapter 5).

6.3 Results and Discussion

6.3.1 PVP Final Product Characteristics

From the *in situ* or kinetics of solvent evaporation experimental results (cf. Chapter 4) it was evident that the solvents evaporated rapidly and the dry film was formed well within 100 seconds. So we considered that data studied around 5 minutes is representative of a dry film. At this stage, any frequency shifts observed indicates solid-solid interactions.

a. *Effect of solvents*

The final product characteristics are different when PVP is cast from an acetone/methanol or DCM/acetone binary solvent mixture as shown in Figure 6.1 and Table 6.1. Since, PVP contains tertiary amide it is susceptible to the nature of the solvents.[176] When PVP is cast from acetone and methanol the final film is brittle, thin and transparent. This is attributable to the conformational changes due to the pyrrolidone ring reorientations and H-bond interactions, hence, increased PVP segmental motion when PVP interacts with proton donor systems.[232,233] As previously stated, the carbonyl peak of PVP undergoes a lower wavenumber shift and appears at 1650 cm^{-1}. Moreover the appearance of the $\delta(CH_2)$ at 1436 cm^{-1} indicates that the carbonyl environment is influenced by molecular interactions[234] through the formation of H-bonds. Since there is hydrogen bond formation with methanol, there is increased PVP segmental motion.

However, when PVP is cast from DCM/acetone the scenario is quite different (Figure 6.1 and Table 6.1). That is, the final product formed is rubber like, thick and opaque. These changes indicate that there is volume and hence the PVP dimension changes and assumes a globular structure.[235] The carbonyl group in the final product appears at 1664 cm^{-1} which indicates that there is increase in the dipolar interactions and increase in the rigidity of the pyrrolidone rings which also leads to the formation of the globular structure to minimize the contacts between the PVP segments and the solvent molecules.[235,236]

b. *Effect of temperature*

As discussed in the previous section, temperature has a marked effect on the kinetics of PVP formation and also on the final product characteristics. When PVP is cast from the acetone/methanol binary solvent mixture the carbonyl band appears at 1650 cm^{-1}, 1658 cm^{-1} and 1661 cm^{-1} at 30°C, 40°C and 50°C, respectively (Figure 6.2A and Table 6.2). These shifts indicate the effect of temperature, that is, as there is increase in the temperature, the rate of solvent evaporation is increased thereby decreasing the

solvation[237] and hence the higher wavenumber shift in the carbonyl peak. Moreover, it has been shown that methanol is a good solvent for PVP at 25°C, which ties up well with our results.[238]

In comparison, when PVP is cast from DCM/acetone, the carbonyl peak appears around 1664 cm^{-1}, 1670 cm^{-1} and 1667 cm^{-1} at 30°C, 40°C and 50°C, respectively. This upward shifts indicate that there is little or negligible solvation of PVP by this system and hence the final product is waxy or globular in structure. It should be noted that, the intensities of the PVP carbonyl peak cast from DCM/acetone compared to acetone/methanol (Figure 6.2B and Table 6.2) are weak, which means that there is no close contact with the crystal or the sample is washed away (also cf. the CH and OH stretching is weak as shown in Figure 6.1).

6.3.2 Felodipine final product characteristics

a. Solvent Effects

From the Figure 6.3A, B and Table 6.3, it can be seen that in the starting material of felodipine, the NH stretch peak appears around 3363 cm^{-1}. Moreover, the carbonyl region has multiple peaks, of which one appears around 1694 cm^{-1} and another around 1686 cm^{-1}, these being assigned to ethyl ester carbonyl and methyl ester carbonyl respectively.

When felodipine was cast from the acetone/methanol binary solvent mixture, the peaks broadened and there was an approximately 25 cm^{-1} shift in the NH peak position. Simultaneously, there were changes in the carbonyl region in which the ethyl ester carbonyl had an 8 cm^{-1} downward shift, whereas the methyl ester carbonyl had a 4 cm^{-1} upward shift. These results indicate that there is stronger drug-drug intermolecular hydrogen bonding when felodipine is cast from solvents, than in the starting material, which is a pharmaceutical solid. Moreover, the ethyl ester carbonyl forms a stronger H-bond than the methyl ester carbonyl.[175]

b. Effect of temperature

Although temperature is having a marked effect on the kinetics of felodipine film formation, from Figure 6.4 A, B and Table 6.4, it can be seen that temperature is not having any marked effect on the final product characteristics. Any change in the felodipine NH stretching and carbonyl peak positions can be used as a spectral signature to indicate the effect of temperature. From Figure 6.4A, B and Table 6.4, it can be seen that the felodipine NH and carbonyl peak position cast from the two different binary solvent mixture at three different temperature (30°C, 40°C and 50°C) was found to have

no significant difference on the final product. Marsac *et al.*,[88] showed that drug-drug intermolecular hydrogen bonding interactions show a gradual and systematic shift in peak position from 3337 cm^{-1} at 5°C to 3350 cm^{-1} at 160°C. The change in peak position versus temperature was dependant on the glass transition temperature of the system investigated.[88, 175] The T$_g$ of felodipine is 43°C. We might anticipate a shift of ~1.6 cm^{-1} (based on a 13 cm^{-1} shift over 15°C to 160°C range) and our working spectral resolution was 4 cm^{-1}. However, in our studies the spectral changes reported by Marsac were not observed because the temperature range studied was narrow and the expected shift was smaller than the spectral resolution. This observation is independent of the nature of the solvents used for casting felodipine.

c. Effect of Polymer loading and Drug Loading

The presence of polymer influenced the final product characteristics of felodipine. felodipine is a proton donor and interacts with a proton acceptor molecule like PVP.[11,22,71,86,239] In the absence of polymer, the NH stretching peak appears at 3363 cm^{-1} or around 3337 cm^{-1} as in the case of starting material or cast film respectively. When the polymer is incorporated there is at least a 45 cm^{-1} red shift and the NH stretching peak appears around 3292 cm^{-1} in the final product (Figure 6.5 A, B and Table 6.5). This clearly illustrates the existence of strong hydrogen bonding between the drug and the polymer and indicates the formation of solid dispersions.

When PVP is cast from DCM/acetone the final product formed is rubber like, thick and opaque evidenced from the carbonyl group appearing at 1670 cm^{-1} (cf. effect of solvents on PVP characteristics, Chapter 4.4.1). The drug loading (20%, 50% and 80% w/w) was found to have an effect on the final product characteristics of polymer when cast from DCM/acetone (Figure 6.5 B and Table 6.5). Firstly, the final product formed is brittle, transparent and it appeared similar to the final product cast from acetone/methanol binary solvent mixture. In the presence of drug, there is appearance of NH stretching peak (due to hydrogen bond formation) in the final product (Figure 6.5A and Table 6.5) which indicates formation of solid dispersions. The formation of solid dispersion alters the final product characteristics of PVP from rubber like to brittle.

The drug loading was found to have a remarkable effect on the intermolecular interactions between the drug and the polymer, shown in Figure 6.5 A, B and Table 6.5. When the drug loading was low (20% drug loading) the NH stretching peak appeared around 3292 cm^{-1} which indicates that there are strong H-bonding interactions between the drug and the polymer when compared to cast felodipine or the felodipine starting

material. As the drug loading is increased the drug-polymer interactions become disrupted and there is increase in drug-drug interactions.[240] This was tracked using the changes in the peak intensities, peak widths and peaks shifts as shown in Figure 6.5 and Table 6.5.

The nature of amorphous states depend on the drug-polymer ratio and with low drug loading concentrations, the drug-polymer interactions yield stable and miscible solid dispersions.[50,51,240] As the concentration of drug is increased there is reduction in the drug-polymer interactions, potentially leading to physical instability. Although the final product characteristics of 20% drug loaded felodipine/PVP solid dispersions cast from both the solvents were similar, in order to understand the impact of solvents on the hase behaviour, mid infrared imaging studies will be carried out.

Table 6.1. Characteristic bands to study the effect of solvent on the PVP final product characteristics

Compound	$\nu(CH_2)$	$\nu(C=O)$	$\delta(CH_2)$	$\nu(N\text{-}C)/ \delta(CH_2)$	$\delta(CH_2)$
PVP starting material	2889	1659	1460/1422	1283/1269	734
PVP cast from acetone/methanol	2891	1650	1460/1436/1422	1286/1274	734
PVP cast from DCM/acetone	2881	1664	1459/1422	1285/1271	730

NH and CH stretching region (3800 to 2600 cm^{-1})   C=O stretching region (1800 to 1600 cm^{-1})
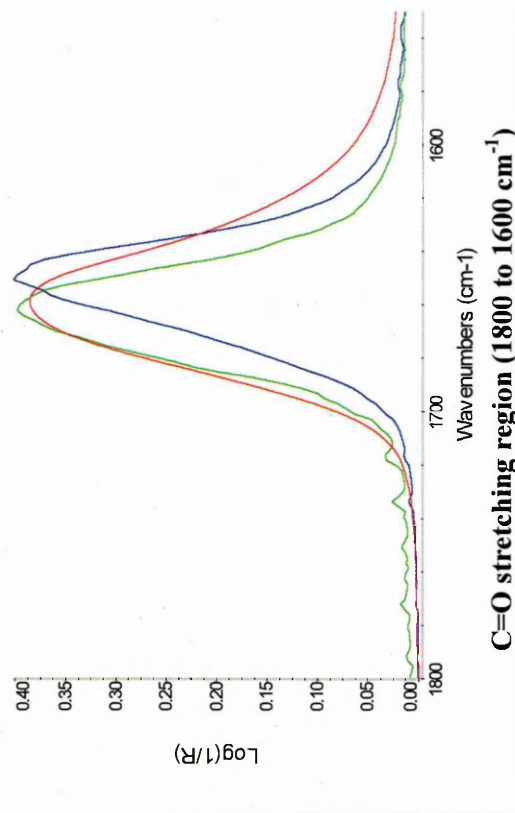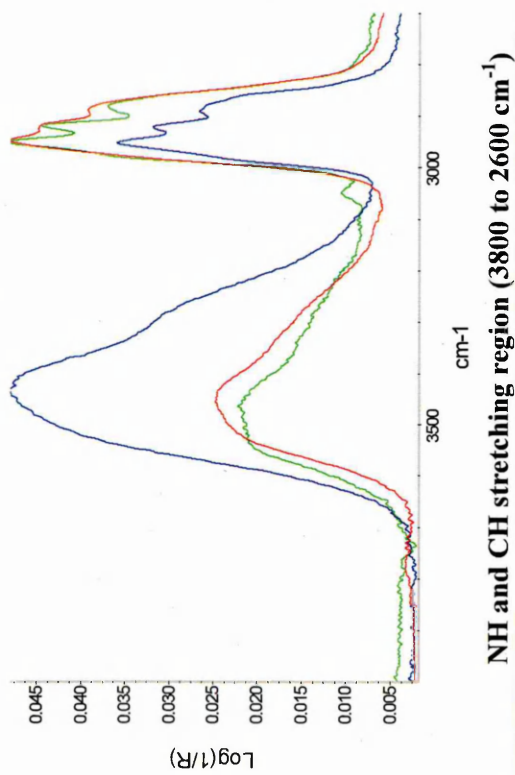
Figure 6.1. Typical representation on the effect of solvent on polymer final product characteristics at 30°C (PVP starting material; PVP cast film from Acetone/Methanol and PVP cast film from DCM/Acetone)

Table 6.2. Characteristic bands to study the effect of temperature on the PVP final product characteristics

Compound	$\nu(CH_2)$	$\nu(C=O)$	$\delta(CH_2)$	$\nu(N-C)/\delta(CH_2)$	$\delta(CH_2)$
PVP cast from acetone/methanol					
At 30°C	2891	1650	1460/1436/1422	1286/1274	734
At 40°C	2887	1658	1460/1421	1285/1271	734
At 50°C	2881	1661	1460/1421	1283/1270	733
PVP cast from DCM/Acetone					
At 30°C	2881	1664	1459/1422	1285/1271	730
At 40°C	2880	1670	1460/1422	1285/1272	731
At 50°C	2880	1667	1460/1421	1283/1270	730

A. Acetone/Methanol

B. Dichloromethane/Acetone
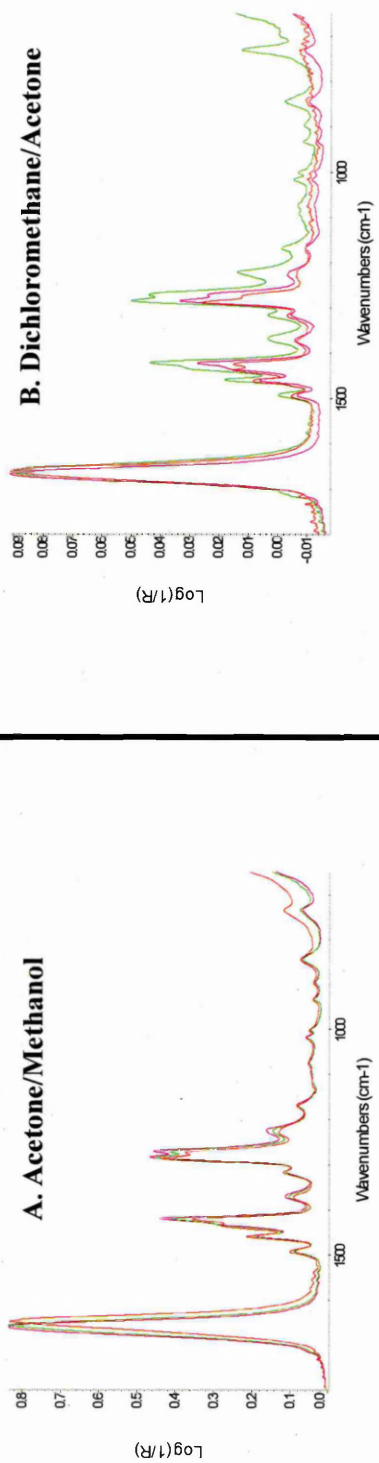
Figure 6.2. Typical representation on the effect of temperature on PVP film cast from different BSM's (30°C; 40°C and 50°C)

Table 6.3. Effect of solvent on drug crystallinity

Compound	ν(NH)	ν(C=O)	ν(C=O)	Band I	δ (N-C)	ν(C-O)	Band II	Band III
Felodipine starting material	3363	1694	1686	1644	1202	1097	770	669
Felodipine cast from acetone/methanol	3337	1698	1679	1650	1208	1099	777	-
Felodipine cast from DCM/acetone	3338	1697	1679	1655	1209	1099	777	-
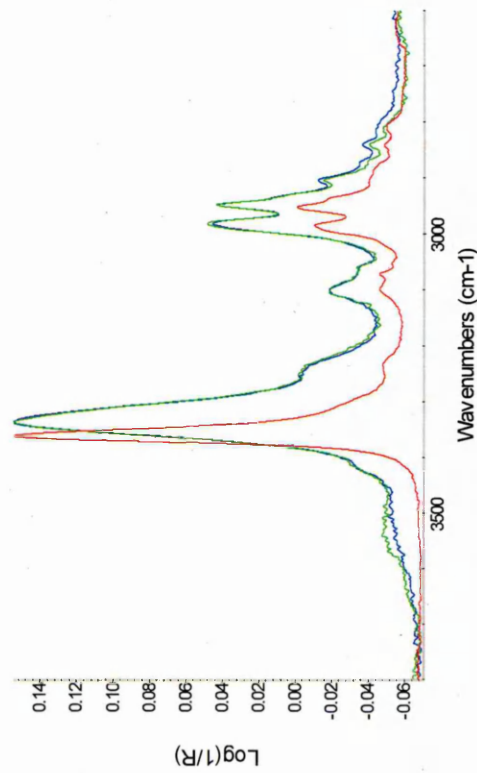
A. NH and CH stretching region (3800 to 2600 cm⁻¹)
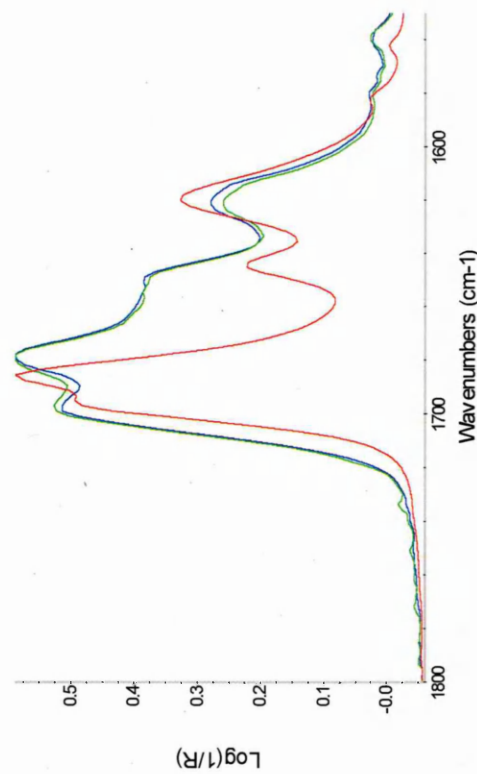
B. C=O stretching region (1800 to 1600 cm⁻¹)

Figure 6.3. Typical representation on the effect of solvent on drug crystallinity (Felodipine starting material; Felodipine cast film from Acetone/Methanol and Felodipine cast film from DCM/Acetone)

Table 6.4. Effect of temperature on Felodipine cast film from Acetone/Methanol and cast film from DCM/Acetone.

Compound	ν(NH)	ν(C=O)	ν(C=O)	Band I	δ (N-C)	ν(C-O)	Band II	Band III
Felodipine cast from acetone/methanol								-
At 30°C	3337	1698	1679	1650	1208	1099	777	
At 40°C	3338	1698	1679	1650	1207	1097	777	
At 50°C	3339	1698	1679	1650	1206	1098	777	
Felodipine cast from DCM/acetone								-
At 30°C	3338	1697	1679	1655	1209	1099	777	
At 40°C	3338	1698	1680	1655	1210	1097	777	
At 50°C	3337	1697	1679	1655	1208	1098	777	
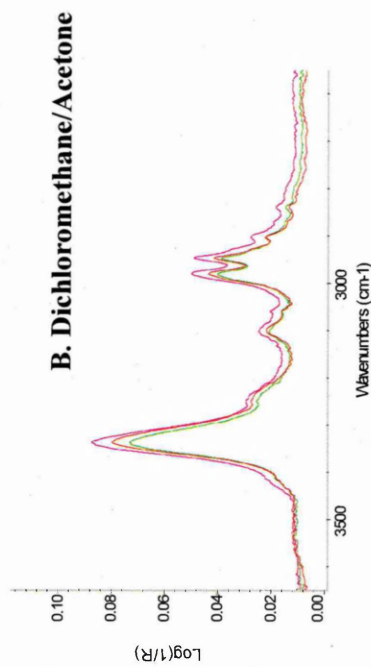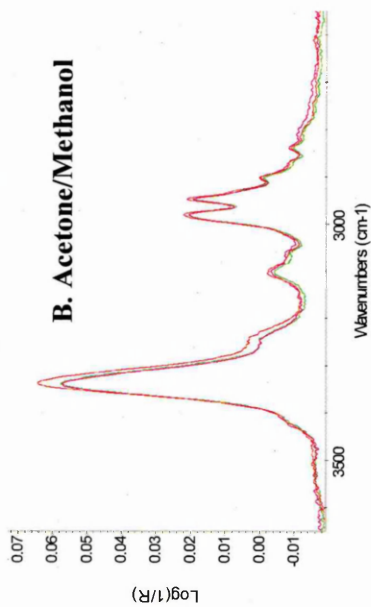
Figure 6.4. Typical representation on the effect of temperature on felodipine film cast from different binary solvent mixture's (30°C; 40°C and 50°C)

Table 6.5. Effect of drug loading on Felodipine/PVP cast film from Acetone/Methanol and cast film from DCM/Acetone.

	20 DL FPAM 30°C		50 DL FPAM 30°C		80 DL FPAM 30°C			20 DL FPDA 30°C		50 DL FPDA 30°C		80 DL FPDA 30°C	
	Position	Intensity	Position	Intensity	Position	Intensity		Position	Intensity	Position	Intensity	Position	Intensity
$\nu(N\text{-}H)$	3291	0.037	3292	0.034	3333	0.047		3292	0.054	3292	0.052	3337	0.029
$\nu(C{=}O)$	1657	0.685	1675	0.481	1678	0.402		1657	0.587	1661	0.41	1681	0.301
$\nu(C\text{-}O)$	1099	0.129	1099	0.290	1099	0.541		1100	0.064	1099	0.177	1100	0.339

A. Acetone/Methanol

B. Dichloromethane/Acetone
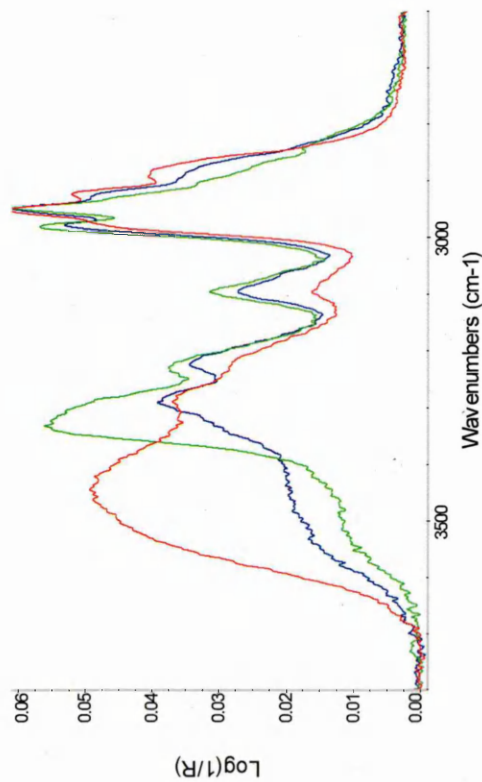
A. 20DL; 50DL; 80DL (Film cast from acetone/methanol)   B. 20DL; 50DL; 80DL (Film cast from DCM/acetone)
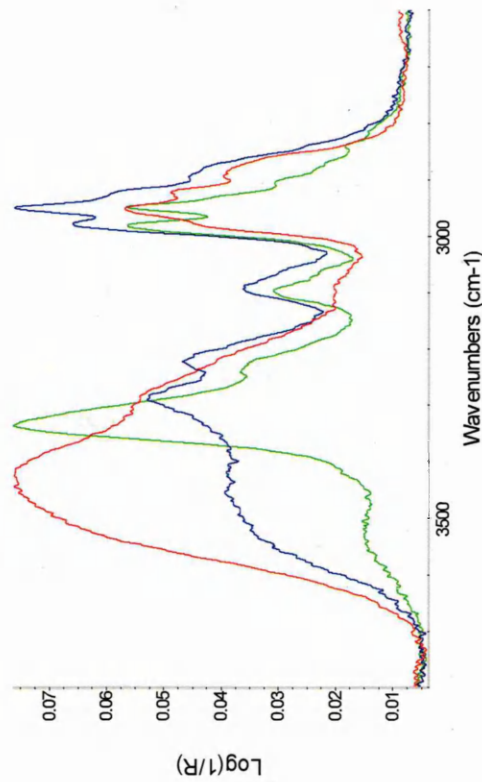
Figure 6.5. Typical representation of effect of drug loading on Felodipine/PVP cast film from Acetone/Methanol and DCM/Acetone at 30°C (20DL; 50DL; 80DL)

6.3.3 Spectroscopic Imaging

Felodipine/PVP solid dispersions spray coated from the two binary solvent mixtures (optical images) are shown in Figures 6.7A and 6.8A. Initially the spectra (from chemical images) are monitored for a classical comparison to look for similarity in results between the bulk and microscopic evaluations. From the spectra it can be clearly seen that irrespective of the solvents (acetone/methanol, Figure 6.6A and DCM/acetone Figure 6.6B) there is strong drug/polymer intermolecular interactions like the presence of felodipine ($v_{(CO)}$ 1099 cm^{-1}) along with PVP ($v_{(CH)}$ 2885 cm^{-1}) and absence of crystalline felodipine peak and will hereafter be termed as "homogeneous felodipine/PVP solid dispersion regions".

The spectra from the chemical images of felodipine/PVP solid dispersion cast from DCM/acetone sample showed two additional types of distribution. In both types, the drug deemed to be amorphous (due to the appearance of NH stretching peak, positioned at ~3338 cm^{-1}). The appearance of the NH stretching peak, and partially interacting PVP (evidenced from the $v_{(CH)}$ 2885 cm^{-1}) is visualised. This will hereafter be termed as "polymer rich regions with amorphous felodipine (represented as polymer rich)". And there is also another type of felodipine distribution wherein there is no evidence of PVP bands and this will be thereafter termed as "amorphous felodipine rich region (represented as drug rich region)". These initial observations show that the FTIR image of the final product differs depending upon the solvent mixture. However, no conclusions can be derived on the compositional distribution for the reason discussed under Chapter 6 on image processing tools. This is because the raw image data is prone to physical artifacts like baseline drifts, saturated/noisy pixels, thickness effects etc. Firstly, the data is pre-processed to remove the aforementioned artifacts and then was analysed using multivariate curve resolution approach (discussed in Chapter 3.).

Figure 6.9A and Figure 6.9B show the resulting 'pure component' factors from the MCR-ALS analysis compared to 'real' pure components. Figure 6.9A shows the comparison of MCR factor 1 with the second derivative spectrum of pure PVP prepared from acetone/methanol solution. Strong correlation between the 'spectra' can be observed in the following spectral regions $v_{(CH)}$ 1465-1425 cm^{-1}, $v_{(CN\ or\ CC)}$ 1322-1276 cm^{-1}, $v_{(CO)}$ 1022 cm^{-1}. Similarly, from Figure 6.9B we can observe that MCR factor 2 has similarities to the pure spectrum of PVP, the pure spectrum of felodipine, but the greatest correlation to the real pure component spectrum of a felodipine/PVP solid dispersion. This can be shown by closely looking at the spectral regions corresponding

to reference felodipine/PVP solid dispersion $v_{(CN, \text{ or } CC)}$ 1322-1276 cm^{-1} and $v_{(COC)}$ 1145 cm^{-1}-1103 cm^{-1} regions. Thus MCR factor 1 and MCR factor 2 can thus be assigned to PVP rich and solid dispersion rich regions, respectively.

The distribution of the pure component spectra generated from the MCR-ALS analysis (i.e. MCR factor 1/PVP rich region and MCR factor 2/solid dispersion rich region) are shown in Figure 6.7B and 6.7C. To further substantiate these findings, the results from loading scatter plot generated from MCR principal factors (Figure 6.11A), score scatter plot generated from MCR concentration images (Figure 6.11B) and image visualisation tool (Figure 6.7D) are used. This is because, MCR estimates the concentration of each factor or analyte based on pixel to pixel variations.[136] The loading scatter plot of MCR factor 1 and 2 describe a negative trend which implies that the two factors show negative correlation. Also the score scatter plot of MCR factors vs. pixel response show good separation between them (Figure 6.11B) which indicates that they are derived from separate chemical entities. These two components are identified to be pure PVP and solid dispersion (felodipine/PVP) and are merged to a single composite image using image visualisation tool and is shown in Figure 6.7D. The PVP rich region is indicated in green and solid dispersion rich region is indicated in red. The resulting composite image shows that the distribution of solid dispersions is dominant in the chemical image and only a few pixels indicate the presence of pure polymer (indicated in green).

When the solid dispersions are cast from acetone/methanol, results from *in situ* measurements indicate that drug does not interact with acetone and neither does polymer. The drug and polymer interacts with methanol which correlates well and ties in with the imaging results; that felodipine/PVP solid dispersion cast from acetone/methanol binary solvent mixture are found to be homogeneously distributed, hence relatively low number of pure PVP pixels.

When the felodipine/PVP solid dispersion is prepared from DCM/acetone solution, the final product, that is, the compositional distribution of felodipine and PVP are quite different. Figure 6.10A, Figure 6.10B and Figure 6.10C show the resulting 'pure component' factors from the MCR-ALS analysis compared to 'real' pure components. Figure 6.10A shows the comparison of MCR factor 1 with the second derivative spectrum of pure PVP prepared from DCM/acetone solution. Strong correlation between the 'spectra' can be observed in the following spectral regions $v_{(CH)}$ 1465-1425 cm^{-1}, $v_{(CN \text{ or } CC)}$ 1322-1276 cm^{-1}, $v_{(CO)}$ 1022 cm^{-1}. From Figure 6.10B we can observe that MCR factor 2 has similarities to the pure spectrum of felodipine prepared from

DCM/acetone in spectral regions corresponding to $v_{(CN, CC)}$ 1506 cm^{-1}, $v_{(COO)}$ 1253-1174 cm^{-1}, $v_{(COC)}$ 1143-1103 cm^{-1} and $v_{(CC, CH)}$ 1076-1043 cm^{-1}. Similarly MCR factor 3 shows good correlation to the real pure component spectrum of a reference felodipine/PVP solid dispersion. This can be shown by closely looking at the spectral regions corresponding to felodipine/PVP solid dispersion $v_{(CN, or CC)}$ 1322-1276 cm^{-1} and $v_{(COC)}$ 1143 cm^{-1}-1103 cm^{-1} regions. Thus MCR factor 1, MCR factor 2 and MCR factor 3 can thus be assigned to PVP rich, felodipine rich and solid dispersion rich regions, respectively.

The distribution of the pure component spectra of MCR factor 1/PVP rich region, MCR factor 2/felodipine rich region and MCR factor 3/solid dispersion rich region generated from the MCR-ALS analysis are shown in Figure 6.8B, Figure 6.8C and Figure 6.8D respectively. In order to validate these findings, the results from loading scatter plot generated from MCR principal factors (Figure 6.12A), score scatter plot generated from MCR concentration images (Figure 6.12B) and image visualisation tool (Figure 6.8E) are used. The loading scatter plot indicates heterogeneous distribution and score scatter displays that these three components are chemically similar. The three components are 1. "amorphous felodipine rich region (represented as drug rich region)" 2. "polymer rich regions with amorphous felodipine (represented as polymer rich)" and 3. "homogeneous felodipine/PVP solid dispersion regions" (cf. Chapter 6.3.3). These three major components were merged to a single composite image using image visualisation tool and is shown in Figure 6.8E. The PVP rich region is indicated in green, felodipine rich regions in blue and solid dispersion rich region is indicated in red. These results indicate that there is significant phase separation of drug and polymer.

In considering the mechanism of phase separation, this is better explained when considering and combining the results from the *in situ* measurements of DCM/acetone binary solvent mixture. We have already shown that in the DCM/acetone binary solvent mixture felodipine interacts with acetone and with dichloromethane. However, PVP interacts only with the dichloromethane. Effects of solvent on the phase behaviour of the polymer blends have been studied and reported extensively within the polymer industry.[241-245] When the interaction parameters between the solvent and two miscible components are very different, the solvent induces phase separation.[246] In DCM/acetone the interaction parameters between the solvents, felodipine and PVP are different (cf. solvent acceptor number and donor number discussed in Chapter 4). Also the

conformational states of the polymers vary significantly in solution and this dictates the solid-solid miscibility and the drug-polymer interactions.

Mandal and Woo, have discussed in detail the effect of solvents and casting temperatures on the phase behaviour of poly (vinyl methyl ether)/poly (benzyl methacrylate).[247] They reported that phase separation can be induced at high temperatures between weakly interacting miscible polymer mixtures and poor solvents.

6.4 Conclusions

Variable temperature ATR-FTIR, Spectroscopic imaging along with chemometric data analysis are powerful tools to investigate the molecular interaction and distribution of various components within the prepared solid dispersions. Preparation methods and solvents can induce phase separation and we have shown the applicability and strength of combining bulk and microscopic measurements. Moreover we have shown that properly processed and analysed chemical images are invaluable. In most of the literature it has been shown that phase separation is generally explained by calculating the T_g or dielectric measurements or molecular mobility. In this chapter we have presented the novel way for interpreting the drug-polymer or solvent induced drug-polymer phase separation.
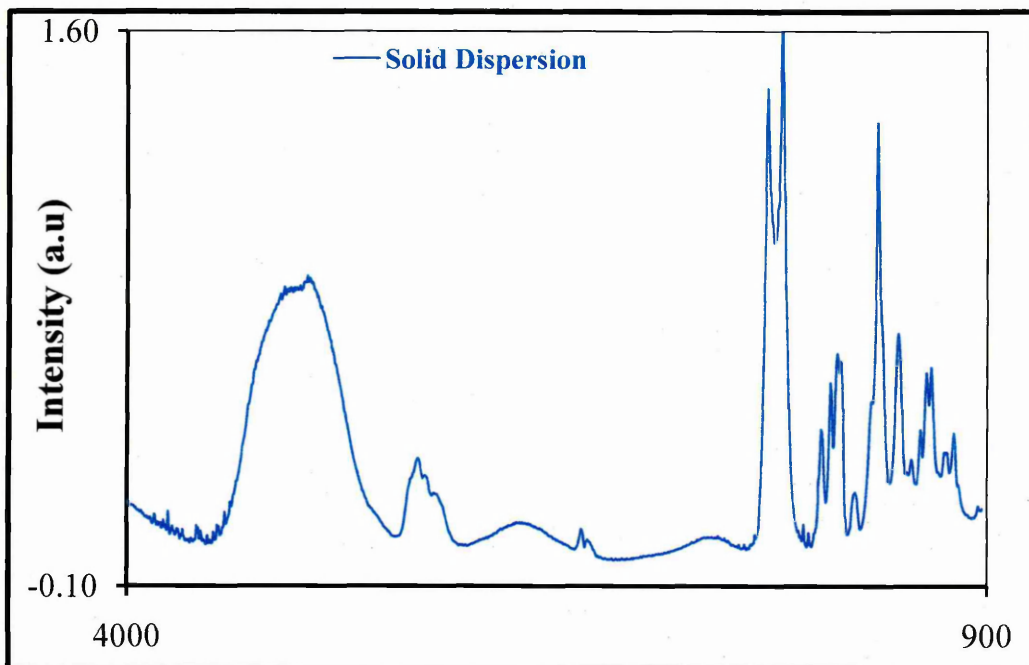
Figure 6.6A. Typical spectra extracted from the various regions of Fel/PVP prepared from acetone/methanol
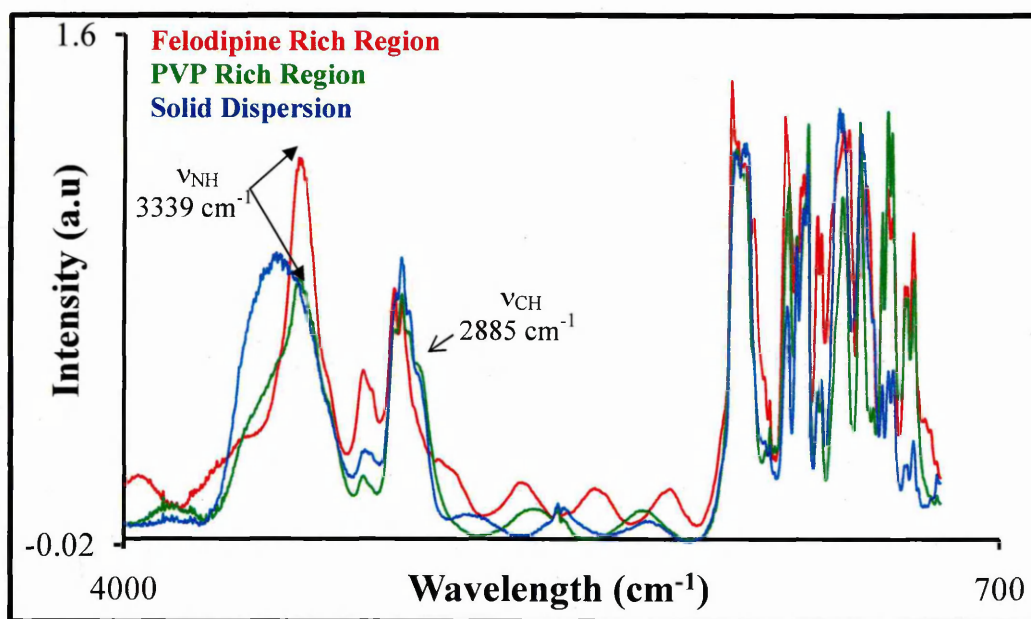
Figure 6.6B. Typical spectra extracted from the various regions of Fel/PVP prepared from dcm/acetone

A. Optical Image	B. Polymer rich (Green)	C. Solid Dispersion rich (Red)	D. Image Visualisation

Figure 6.7. Felodipine/PVP Spray Coated from Acetone/Methanol

A. Optical Image	B. Polymer rich (Green)	C. Drug rich (Blue)	D. Solid Dispersion Rich (Red)	E. Image Visualisation
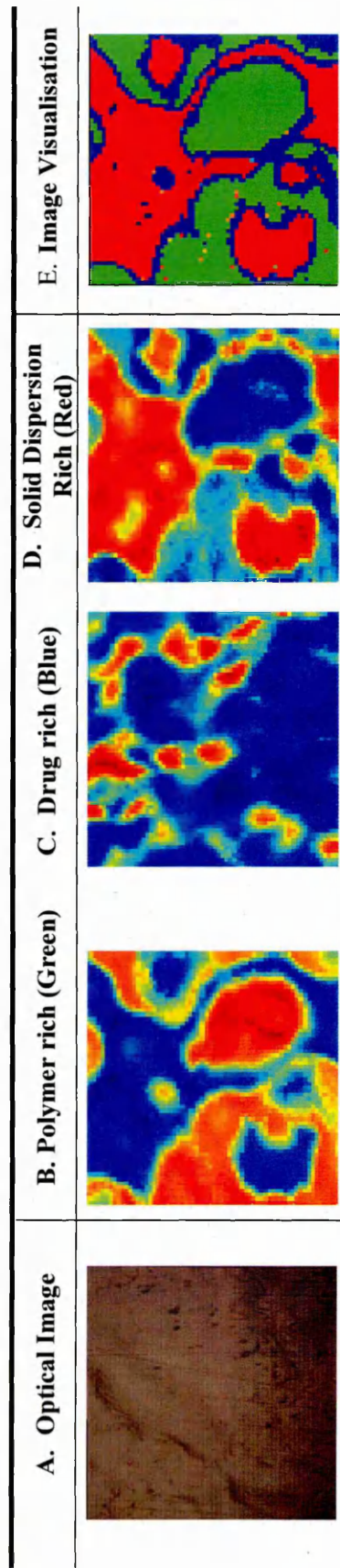
Figure 6.8. Felodipine/PVP Spray Coated from Dichloromethane/Acetone

118

Figure 6.9A Comparison of MCR factor 1 with spectrum of PVP prepared from acetone/methanol
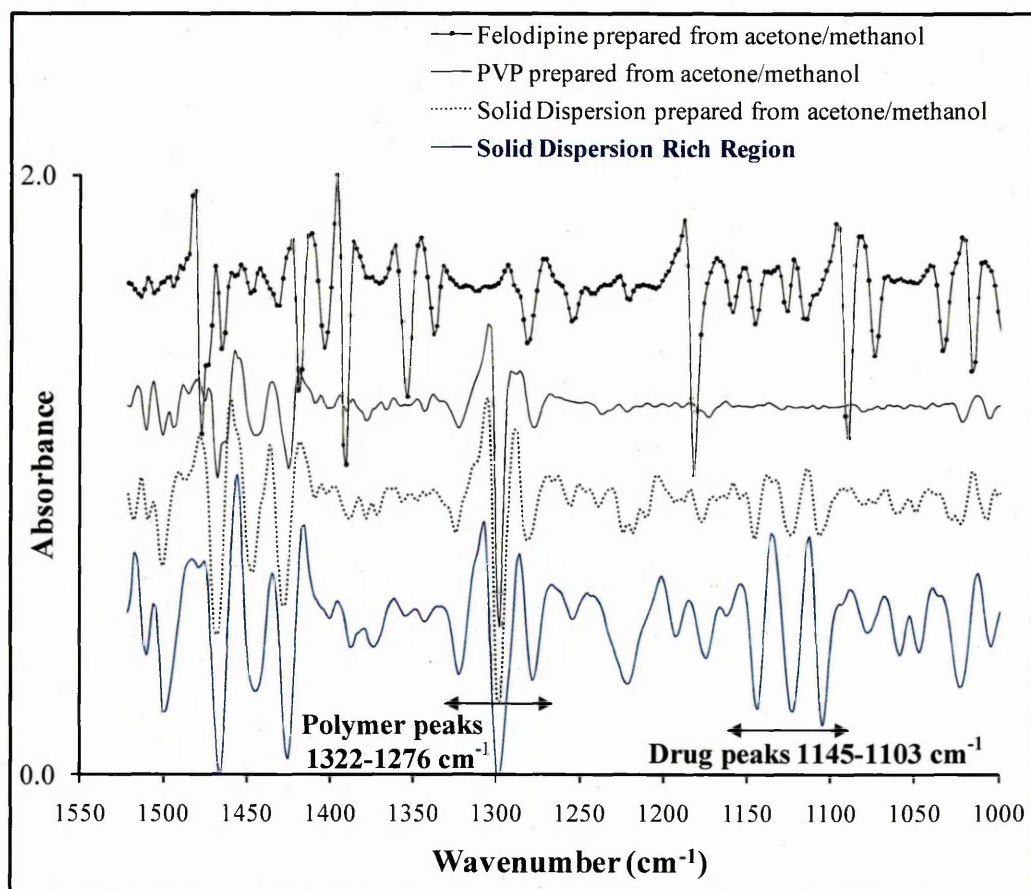
Figure 6.9B Comparison of MCR factor 2 with spectrum of reference solid dispersion prepared from acetone/methanol

119
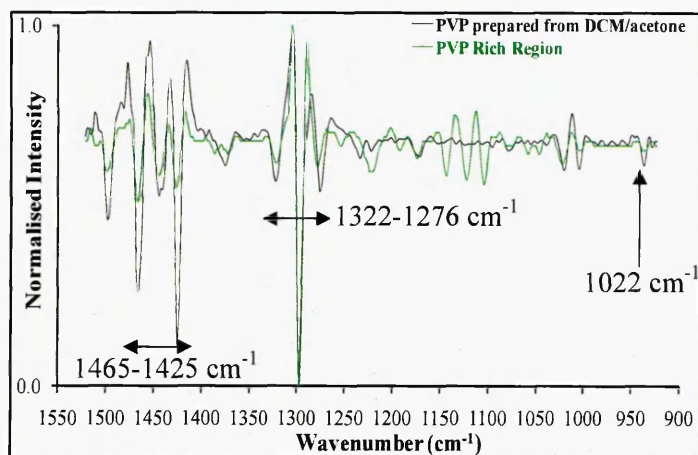
Figure 6.10A Comparison of MCR factor 1 with spectrum of PVP prepared from DCM/acetone
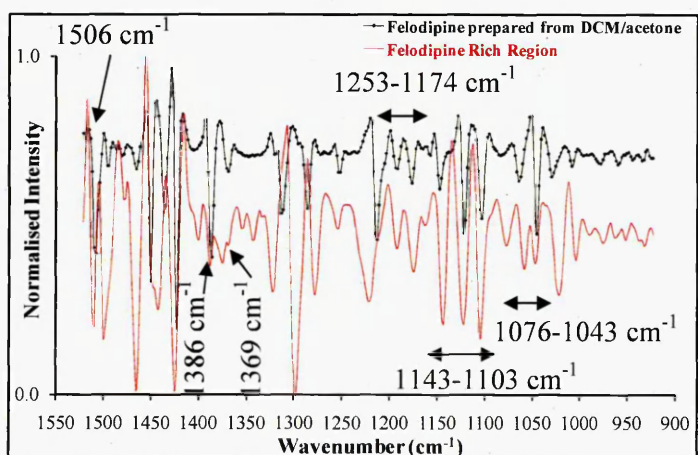
Figure 6.10B Comparison of MCR factor 2 with spectrum of felodipine prepared from DCM/acetone
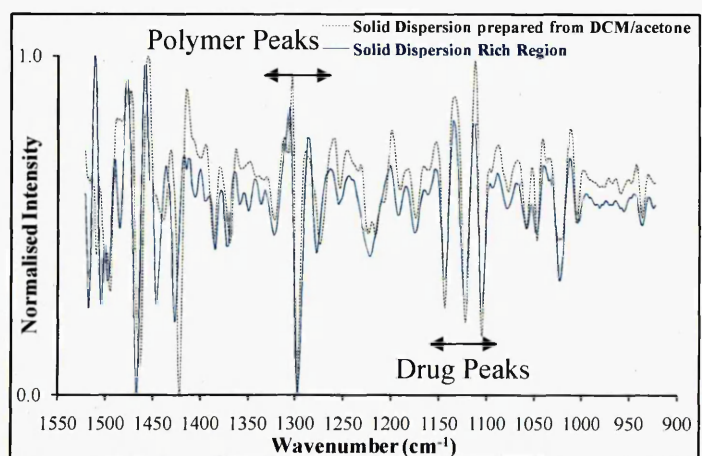
Figure 6.10C Comparison of MCR factor 3 with spectrum of reference solid dispersion prepared from DCM/acetone
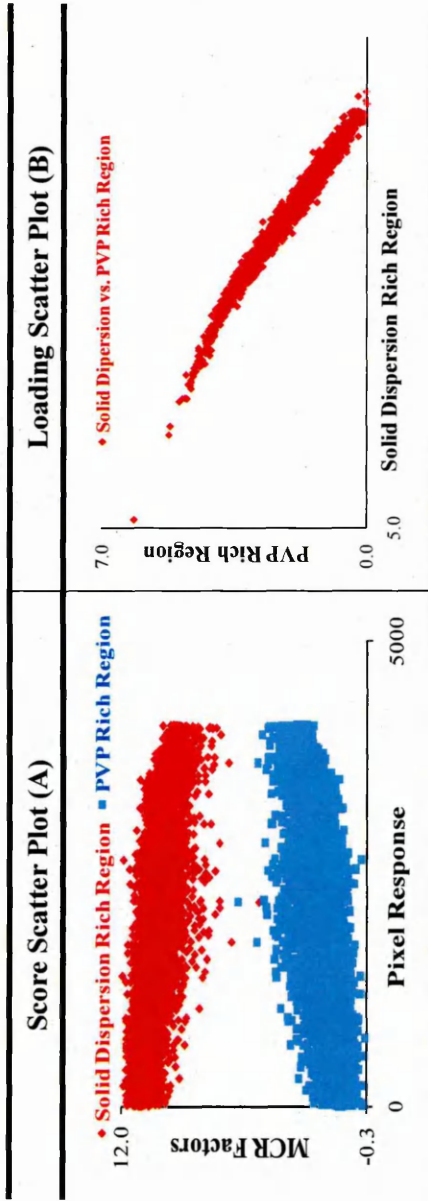
Figure 6.11. Felodipine/PVP Spray Coated from Acetone/Methanol
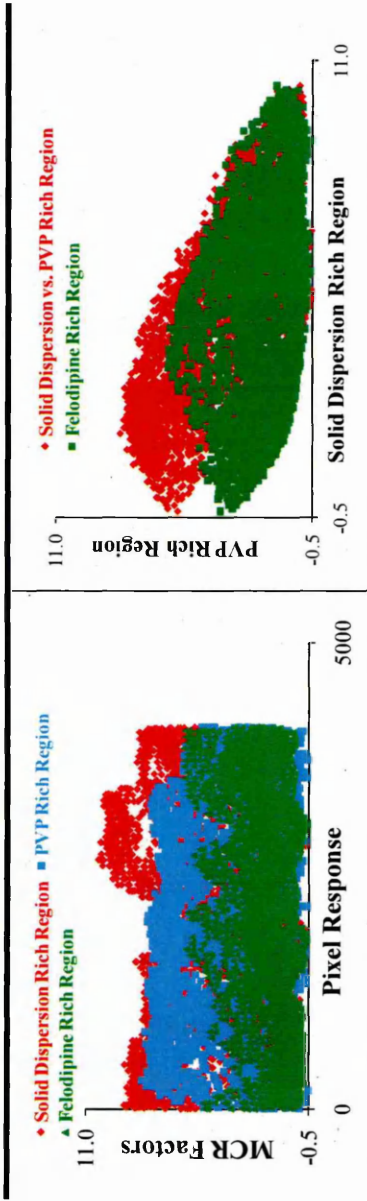
Figure 6.12. Felodipine/PVP Spray Coated from Dichloromethane/Acetone

121

CHAPTER 7.
INFRARED IMAGING IN ASSESSING THE THERMAL STABILITY OF SOLID DISPERSIONS

7.1 Introduction

PVP is an extensively used polymer in a variety of industries. In polymer industries degradation studies are important in understanding the properties of the materials when subjected to extensive storage conditions. PVP behaves differently when exposed to nitrogen, hydrogen or oxygen atmospheres.[248] *In situ* FTIR measurements[248] were successful in showing the degradation of PVP-Rhodium and PVP-Platinum nanoparticles. The results indicated that the PVP bound to surface metal ions underwent degradation faster than the unbound or outer layer of PVP. Moreover, the decomposition of PVP-Pt occurs 100 °C below that of PVP.[59,248,249] Two routes of oxidative degradation of PVP[57] both involving the α-position of N-atom has been proposed.[57] If a secondary carbon atom in the pyrrolidone ring is attacked it forms a complex (imide) cyclic carbonyl structure (Figure 7.1C) with infrared peak position centred around 1772 cm^{-1}. If the tertiary carbon in the back bone is attacked then it forms an a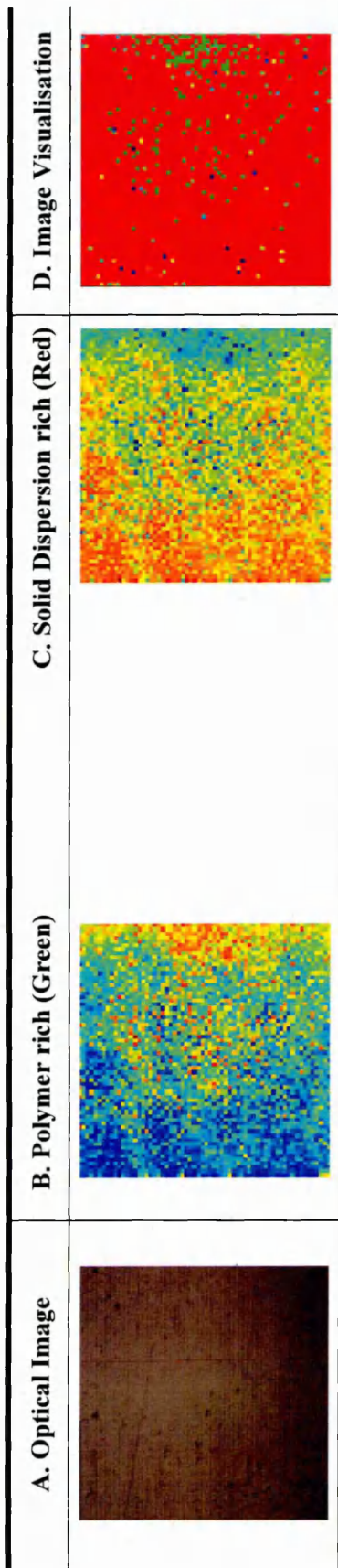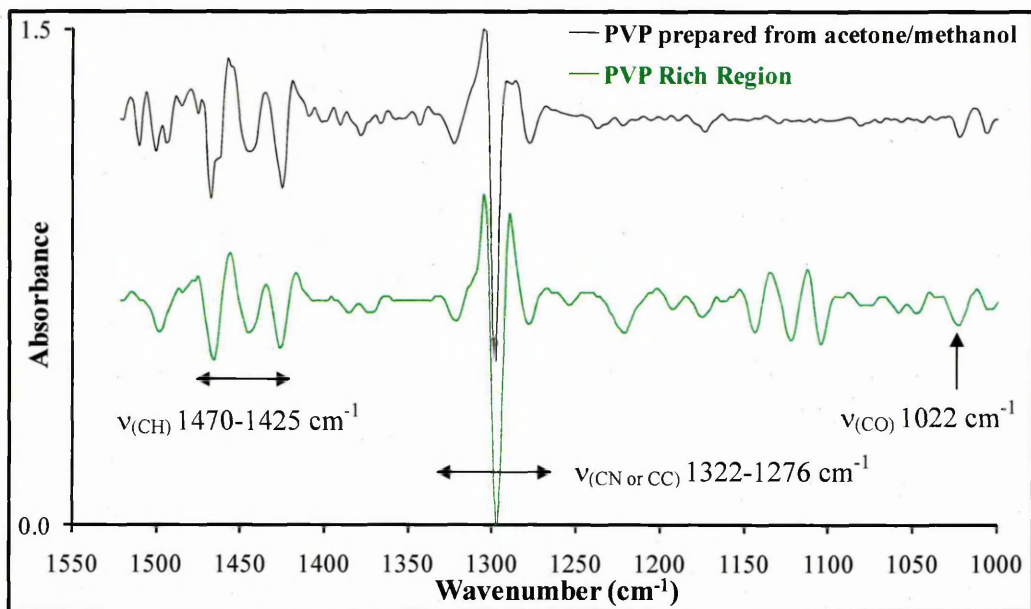liphatic ketone (Figure 7.1D) having a peak at 1729 cm^{-1}. In highly filled PVP silica polymeric systems the formation of imide-like structures was hindered due to the formation of H-bond between PVP and silica.[58]

The chloride containing 1,4 dihydropyridine derivatives like felodipine are thermally stable to dry air temperature at 90 °C for 120 days;[250] however they are very sensitive to ionising (beta and gamma) radiations.[251,252] When felodipine is heated above its melting temperature (145 °C), it forms a (partially) thermally decomposed product. However it is not found in commercial products like Plendil.[68,253]

When PVP and felodipine are solvent cast, the resulting solid dispersion is stable at higher temperatures (160 °C) and cooling to the ambient temperatures shows the reversible (in the absence of moisture) nature of H-bond interactions, that is, the drug-polymer interactions weaken as the temperature approaches the melting point of the drug; subsequent cooling restores the H-bond interactions (which become strong).

FTIR imaging has been applied to study the oxidative degradation of rubber and showed that vulcanisation of rubber starts by forming free radicals; however a self protective coating is formed to resist the decomposition.[254] In a related study addition of antioxidants resisted the decomposition in the beginning stage but degradation was

found to increase as oxygen penetration at later stages aggravates the decomposition of rubber.[255] The spatial selectivity of FTIR imaging was successful in tracing the competitiveness of the antioxidants and the self protective layer to inhibit the oxidation.[254,255]

The identification of small quantities of degradation products can be difficult to observe if there is spectral overlapping or optical artefacts. In these cases, the application of chemometric processing tools like multivariate curve resolution (MCR) can be handy and serves the required purpose by decomposing pure spectra from the mixtures and extracting the corresponding distribution maps. In determining the degradation products of nifedipine, MCR was successful in extracting two components from the sample matrix, one corresponding to nifedipine and other to the photo-decomposition product nitrosopyridine.[137,250]

7.2 Objective of the present study

This work aims to investigate the applicability of mid-infrared imaging in generating the chemical distribution maps of model components, evidence of thermally induced separation and identification of the thermally degraded products from spray coated felodipine/PVP solid dispersions.

7.3 Structures of the starting materials and degradation products
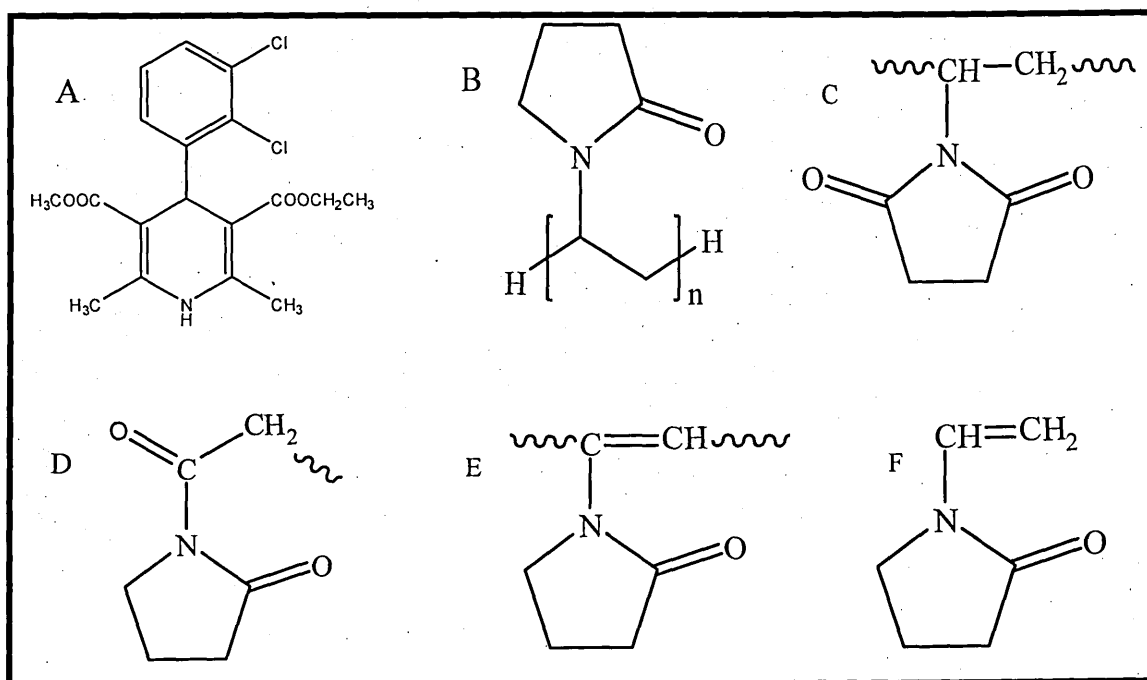
Figure 7.1. Chemical structures of felodipine (A), PVP (B) and PVP degradation products (C, D, E and F)

Table 7.1. Characteristic peaks of starting material and degradation products[59,68,88,248,249,253]

Felodipine (A)		PVP (B)		PVP Degradation Products	
$\nu_{(NH)}$	3354 cm^{-1}	$\nu_{(CH)}$	2873 cm^{-1}	C. $\nu_{(C=O)}$	~1772 cm^{-1}
$\nu_{(C=O)}$	1700 cm^{-1}	$\nu_{(C=O)}$	1673 cm^{-1}	D. $\nu_{(C=O)}$	~1729 cm^{-1}
$\delta_{(COC)}$	1205 cm^{-1}	$\delta_{(CH\ sci)}$	1419 cm^{-1}	E. $\delta_{(C=C)}$	~802 cm^{-1}
$\delta_{(CCO)}$	1095 cm^{-1}	$\delta_{(CN\ or\ CH\ wag)}$	1280 cm^{-1}	F. $\delta_{(RC=C)}$	~966 cm^{-1}

7.4   Experiments

7.4.1   TGA/DTA Measurements

Pure drug and pure polymer were used as obtained (in powder form). A physical mixture consisting of 20% drug and 80% polymer (w/w) was made up by physically mixing the two components. Another 20% drug loaded sample, prepared in a similar manner, was dissolved in mixed solvent (acetone/methanol, %w/v) (FPAM SD) and then cast, dried and pulverised. 10 mg of the pulverised sample was then placed in an alumina crucible. The prepared samples were then analysed using a Netzsch Proteus Thermal Analyser under air in dynamic temperature mode. The flow rate of air was set to be 40 ml/min. The temperature range set was 25 °C to 800 °C (heating rate of 20 °C /min).

7.4.2   In situ FTIR ATR Measurements

50µl of felodipine (100%) and PVP (100%) solutions prepared using acetone/methanol binary solvent mixture were cast onto a preheated ATR diamond crystal at 180 °C and the data was collected continuously (as a function of time) for a period of 12h. Thermo Nicolet FTIR spectroscopy in attenuated total reflectance (Specac) sampling mode was used for data collection with number of scans 64 and spectral resolution of 4 cm^{-1}. Data analysis was done using the Omnic instrument software

7.4.3   Mid infrared imaging

Felodipine-Polyvinylpyrrollidone (Fel/PVP) solid dosage formulations were dissolved in a methanol/acetone mixture. The prepared solutions were then sprayed using a Badger air brush on to a 316 stainless steel substrate. The spray coated samples were stored at different temperatures (room temperature, 60 °C, 100 °C and a temperature of 180 °C, which is above the glass transition temperature (T_g) of polymer and melting temperature (T_m) of the drug. The data were pre-processed to remove any optical

artefacts and data processing done using multivariate approaches (as discussed in Chapter 5 image processing tools). All the data analysis was performed using the Isys chemical imaging software.

7.5   Results and Discussion

7.5.1   Thermogravimetric/Thermal Analysis (TG-DTG-DTA) measurements

From the TG curves, the degradation events for pure drug (Figure 7.2A) occur at 240-370 °C and 370-600 °C; pure polymer shows different number of degradation events in the ranges 300-400 °C, 400-480 °C and 480-660 °C. The differential thermogravimetric (DTG) curves (Figure 7.2B) highlight no additional steps are seen to be involved in the degradation of either drug/polymer or solid dispersions. The physical mixture and solid dispersions shows similar number of degradation events in the ranges 308-371 °C, 375-475 °C and 475-600 °C but different trends. The differential thermal analysis (Figure 7.2C) of pure drug and physical mixture show a transition region centered around 145 °C which correspond to crystalline melting point of felodipine. However, pure polymer and the solid dispersion do not show this transition.

From the TG curve it can be seen that drug on its own begins to degrade at a lower temperature than the physical mixture or the solid dispersion, however, polymer on its own degrades at the slowest rate. Interestingly, the degradation temperature of physical mixture and solid dispersion are found to be similar. However, from the DTA curve it can be seen that felodipine is in the crystalline state when in pure form or in a physical mixture. However, this peak is absent in the solid dispersion which does mean felodipine is in the amorphous form. The initial weight loss around 100 °C is due to loss of water.
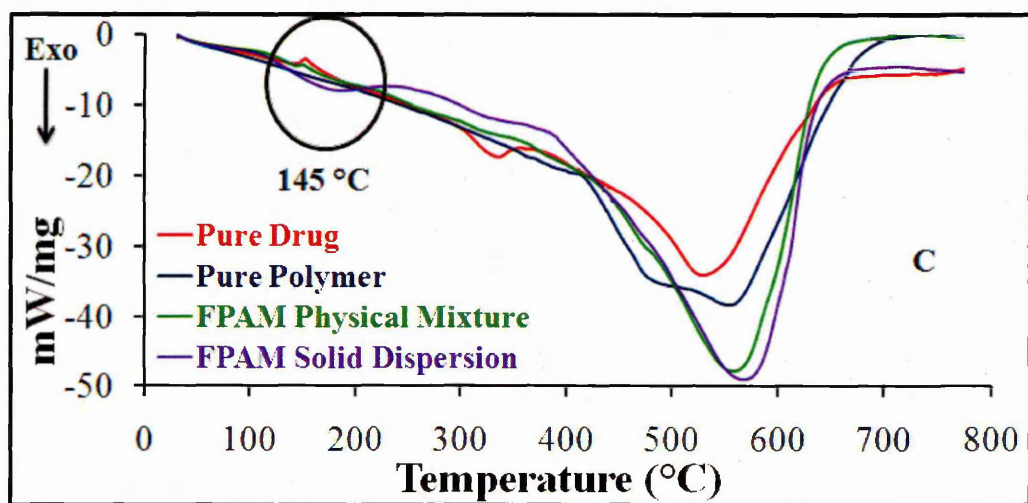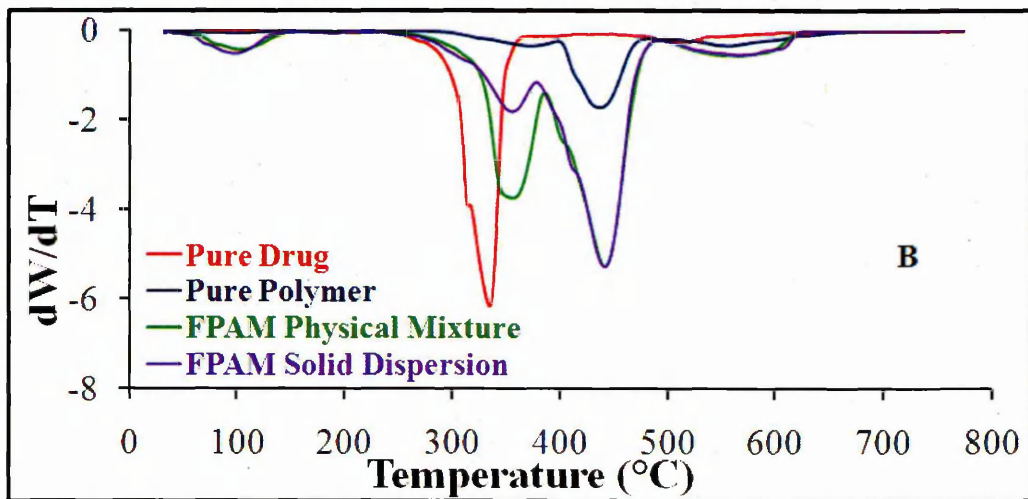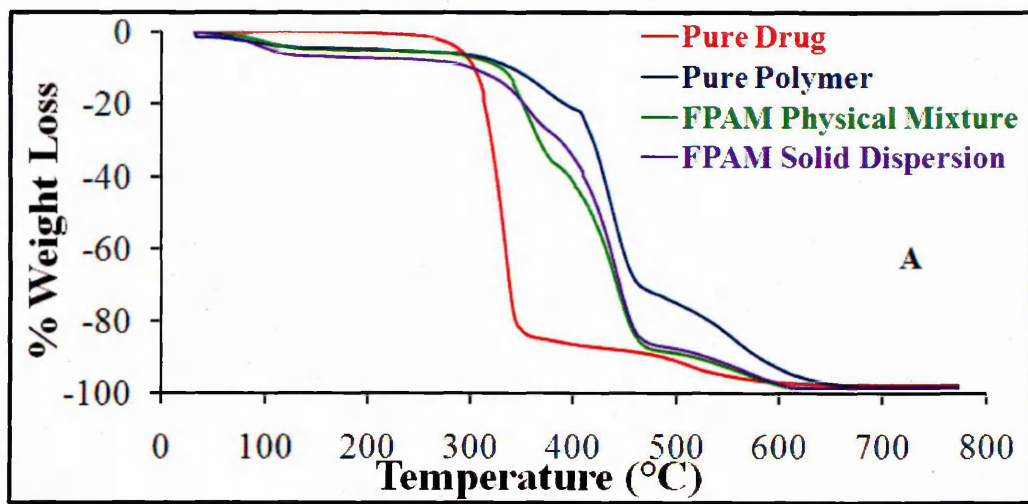
Figure. 7.2. TG-DTG (A&B) and DTA (C) measurements

7.5.2 In situ ATR-FTIR studies

The spectral changes as a function of time, kinetic profiles for felodipine, PVP and solid dispersion are shown in Figures 7.3-7.5. The infrared spectra (Figure 7.3A) at various time intervals for the solvent cast film of felodipine at 180 °C together with the kinetic profile (Figure 7.5A) are shown. The chemical structure of felodipine is shown in Figure 7.1A and the major bands of interest in studying the degradation products are $v_{(NH)}$ 3354 cm^{-1}, $v_{(C=O)}$ 1700 cm^{-1} and $v_{(C-O)}$ 1095 cm^{-1} shown in Figure 7.3 and Table 7.1. However, these bands appeared at 3363 cm^{-1}, 1694 cm^{-1}, 1099 cm^{-1} in the felodipine starting material and 3337 cm^{-1}, 1699 cm^{-1}, 1099 cm^{-1} in the solvent (acetone/methanol) cast film at 30 °C (cf. $v_{(NH)}$, $v_{(C=O)}$, $v_{(C-O)}$ Table 6.4 in Chapter 6). The amorphous state is thermally unstable.[67,256] The NH peak position changes with the temperature at 180 °C and this could possibly indicate the weakening of the drug-drug intermolecular interactions.[88] These changes occur abruptly close to the glass transition temperature. The melting point of felodipine[68] starting material is 145 °C and the glass transition temperature of amorphous felodipine[66,256] is ~43 °C. The studied temperature is well above the T_g and T_m of felodipine. The observed peak shifts with cast film at 180 °C indicates the conversion of amorphous felodipine to liquid form or melt. TG-MS observations indicated that there is liberation of methylene chloride at ~165 °C. The change in NH and CO peak positions together with TG-MS results indicate that there are small volatile breakdown products like CO_2, H_2O, CH_2Cl_2, small chain alcohols and ketones. The spectral changes of felodipine show no new bands appearing (Figure 7.5A), thus indicating that there is no formation of new products that remain on the surface. These observations illustrate that felodipine oxidises (deduced from the disappearance of characteristic felodipine peaks at various time intervals) within 450 mins, which is expected to happen with small molecules.

The infrared spectrum at various time intervals for the solvent cast film of PVP at 180 °C and the kinetic profile are shown (Figure 7.4A and Figure 7.5B respectively). From the spectral features it can be seen that PVP bands reduce in intensity and also show appearance of new bands. The frequencies and structures corresponding to known degradation products are shown in Table 7.1C-F and Figure 7.1C-F. The spectral bands $v_{(CH)}$ 2873 cm^{-1}, $\delta_{(CH\ sci)}$ 1419 cm^{-1} and $\delta_{(CN\ or\ CH\ wag)}$ 1280 cm^{-1} are reduced in intensity on degradation.[58,59,248,249] The observed bands corresponding to degradation products are $v_{(C=O)}$ 1772 cm^{-1}, $v_{(C=O)}$ 1729 cm^{-1}, $v_{(C=C)}$ 802 cm^{-1} and $v_{(CN-O)}$ 966 cm^{-1}. The $v_{(C=O)}$

1772 cm^{-1} and $v_{(C=O)}$ 1729 cm^{-1} peaks indicate the formation of imides (Figure 7.1C) and aliphatic ketones (Figure 7.1D), respectively.

Interestingly, when felodipine/PVP solid dispersions are subjected to similar conditions, the results are quite different. The infrared spectra (Figure 7.3B, 7.4B) and kinetic profile (Figure 7.5C) at various time intervals for the solvent cast film of PVP+felodipine are shown. That is, the imide band at 1772 cm^{-1} is of lower intensity than the 1729 cm^{-1} aliphatic carbonyl. These observations suggest that intermolecular interactions (H-bonding) between felodipine and PVP hinder the rearrangement and formation of complex carbonyl-imide like structures.[58] There is overlapping or contributions from felodipine in the PVP $\delta_{(CH\ sci)}$ 1419 cm^{-1} and $\delta_{(CN\ or\ CH\ wag)}$ 1280 cm^{-1} frequencies. In order to understand whether there is any degradation within the solid dispersion, the carbonyl band will be studied initially.

Although there is degradation in the solid dispersion matrix, the felodipine/PVP H-bond is quite remarkable in that the drug does not carbonise or evaporate as with the cast pure felodipine. Studies have shown that in the absence of moisture when the felodipine/PVP solid dispersions are subjected to a temperature rise from 0 °C to 160 °C and subsequent cooling, there is a reversible strengthening of the H-bonding interactions.[88]

Having established some aspects of degradation conditions, we will now further to assess the applicability of FTIR imaging to complex systems and then focus on using chemometrics to extract the required information.

7.5.3 Mid infrared imaging

FTIR imaging is a relatively new technique which provides spectral and spatial information for microscopic chemical characterisations. In this study, FTIR imaging was used to determine the distribution of the model drug felodipine, the model polymer PVP, degradation products or thermally induced phase separation from the prepared solid dispersions.

Spray dried samples were stored at 60 °C (temperature above the Tg of drug), 100 °C (temperature below the Tg of drug/polymer mixture) and 180 °C (temperature above the melting point of drug and Tg of Polymer). Then the samples were studied as prepared, after 1 day, after 1 week, after 2 weeks and after 3 weeks. The emergence of a peak at 1772 cm^{-1} (ellipse as shown in Figure 7.6) is indicative of the degradation product (Figure 7.1C). This indicates the formation of a complex cyclic structure involving a carbonyl group. The distribution of the degraded product was generated by plotting the

intensity of the discrete peak at 1772 cm^{-1}. The successive images shown at 100 °C and 60 °C are obtained at similar regions in the sample. However, the use of peak height tools to extract information from the raw intensity images should be cautiously used. This is because the raw hyperspectral data from the reflection measurements are prone to optical artefacts.[212-214]

Studies from *in situ* FTIR and TG measurements revealed that any degradation product within the solid dispersion is to be expected from the polymer. Moreover, the degradation of polymer is a quite complex process wherein the backbone and the pyrrolidone carbonyl are involved. In the previous Chapters 5 and 6, the regions of interest for chemometric data analysis for many reasons were restricted to drug bands. However, the preliminary measurements here have shown that the degradation is mostly associated with the polymer; hence in this study a wider region of interest (1520 to 920 cm^{-1}) will be used for chemometrics processing. In order to study the applicability of FTIR imaging and chemometrics in tracing the degradation products, the samples stored at 180 °C (shown in Figure 7.6) was further assessed.

MCR data analysis was done based on hard or white modelling approach, that is, sample chemistry, information from TG-DTA and *in situ* FTIR analysis was used to predict the number of chemical components present in the acquired image. A model constructed with three MCR factors was used. The pre-processed and processed MCR concentration images (cf. Chapter 5 Image processing tools) are shown in Figure 7.7 (bottom). The extracted spectrum was compared with pure component spectrum of 'solid dispersion and PVP' as described in Chapters 5 and 6. Since we did not have the pure spectrum of the PVP degradation products, the idea of cautiously cross-referencing the univariate distribution images (Figure 7.7 top) with MCR concentration images were used in this study. Moreover, the spectrum of pseudo degradation product represented in purple colour (Figure 7.8A) was obtained from the *in situ* thermal stability measurements. This was created by subtracting the spectrum at time '0' which is a non-degraded sample from the final spectrum at time 720 min which was a degraded product. These assumptions were made by carefully assessing the infrared spectrum at various regions avoiding obvious spectral artefacts.

The distribution image of MCR factor 1 (Figure 7.7) was found to resemble univariate image generated using discrete peaks at 1048 cm^{-1}. Figure 7.8A shows the comparison of MCR 'extracted' spectra (MCR factor I) with second derivative spectrum of pure PVP and pseudo degradation product spectrum. Strong correlation between the extracted

spectrum and pseudo degradation product spectrum is interpreted in the following regions 1502 cm^{-1}, 1428 cm^{-1} and $v_{(CO)}$ 1060-1040 cm^{-1}. Similarity between the MCR factor 1 and pure PVP spectrum was observed in $v_{(CH)}$ 1297 cm^{-1}. Furthermore, in Section 7.5.2 *in situ* stability studies we showed that PVP on its own degrades to form new products on long exposure to higher temperatures. These interpretations show that the MCR factor 1 can be assigned to a distribution image of PVP degradation product.

The MCR concentration image 2 (Figure 7.7) was found to resemble univariate image generated using discrete peaks at 1099 cm^{-1}. Figure 7.8B shows the comparison of MCR 'extracted' spectra (MCR factor 2) with second derivative spectrum of solid dispersion. Strong correlation between the extracted spectrum and solid dispersion spectrum was observed in the following regions $v_{(CH)}$ 1465-1425 cm^{-1} and $v_{(CO)}$ 1103 cm^{-1}. These regions are spectral signatures for polymer and drug. Furthermore in Section 7.5.2 *in situ* ATR-FTIR studies showed that drug on its own oxidatively degrades over time; however when the drug is dispersed in the polymer matrix as solid dispersion the carbonisation is prevented. These interpretations show that the MCR factor 2 can be assigned to a distribution image of solid dispersion.

The concentration image of MCR factor 3 (Figure 7.7) was found to resemble univariate image generated using discrete peaks at 1373 cm^{-1}. Figure 7.8C shows the comparison of MCR 'extracted' spectra with second derivative spectrum of 'real' component spectrum of PVP. Strong correlation between the extracted spectrum and solid dispersion spectrum was observed in the following region $v_{(CH)}$ 1525-1425 cm^{-1}. These interpretations show that the MCR factor 3 can be assigned to a distribution image of pure PVP.

The results indicate that long exposures of solid dispersions to high temperatures induce degradation. Interestingly, the drug on its own evaporates at higher temperatures, although in the solid dispersions there are drug rich regions. These two components were homogenously distributed when stored at room temperature (Chapter 6 on final product characteristics). From univariate imaging analysis it is seen that the samples stored at the highest temperature showed evidence of rapid degradation, whereas the degradation was slower with the samples stored at 100 °C and slowest for 60 °C. Unsurprisingly, the samples stored at room temperature showed no degradation.
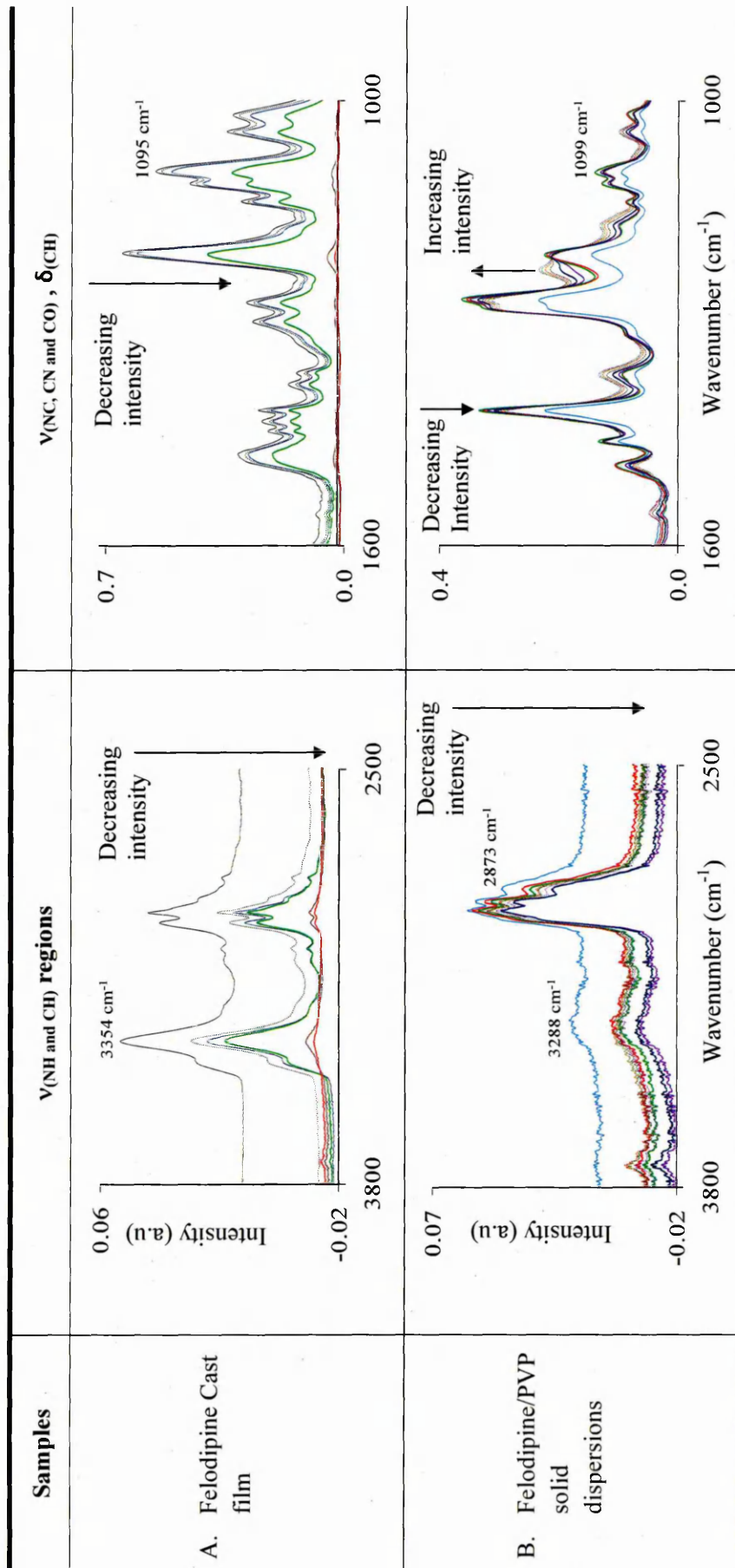
Figure 7.3. Spectral changes as a function of time (felodipine cast film at 180 °C); 4min, 60min(dotted lines), 102 min, 144min, 192 min, 246 min): Felodipine/PVP solid dispersion at 180 °C: 3.5min, 30min, 45min, 135min, 275min, 400min(dotted lines), 500min(dotted lines), 600min(dotted lines), 700min(dotted lines))
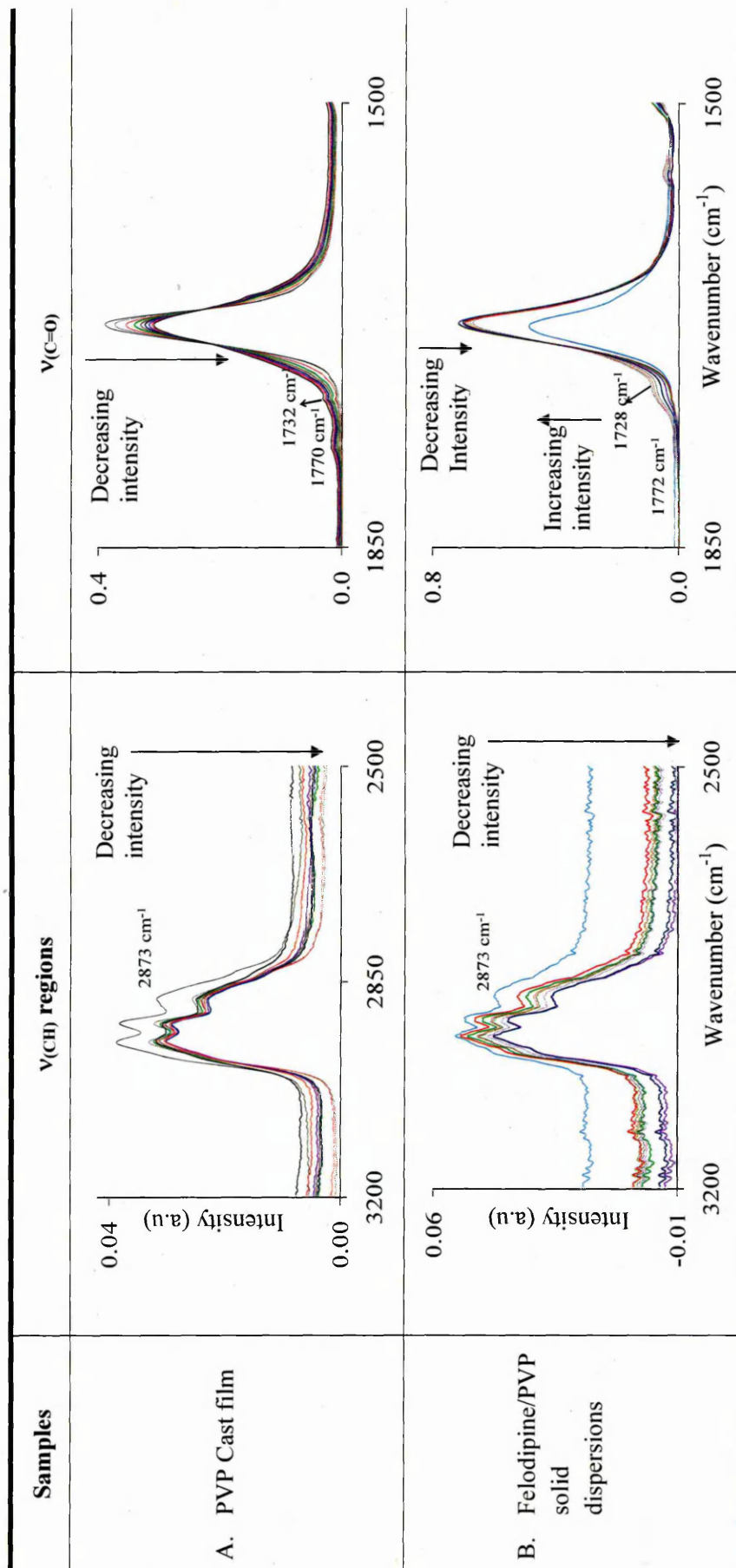
Figure 7.4. Spectral changes as a function of time (PVP cast film at 180 °C); 4min, 60min(dotted lines), 150min, 253min, 345min, 436min, 529min, 625min, 718min): Felodipine/PVP solid dispersion at 180 °C; 3.5min, 30min, 45min, 135min, 275min, 400min(dotted lines), 500min(dotted lines), 600min(dotted lines), 700min(dotted lines))

132
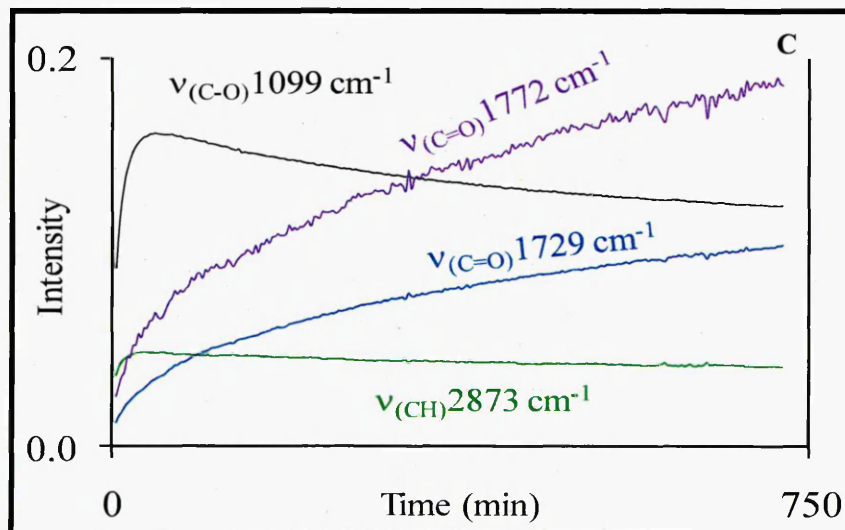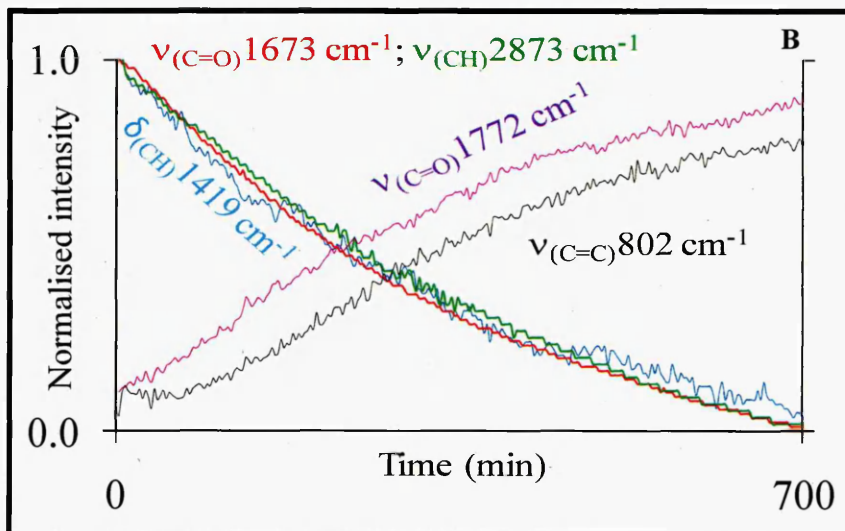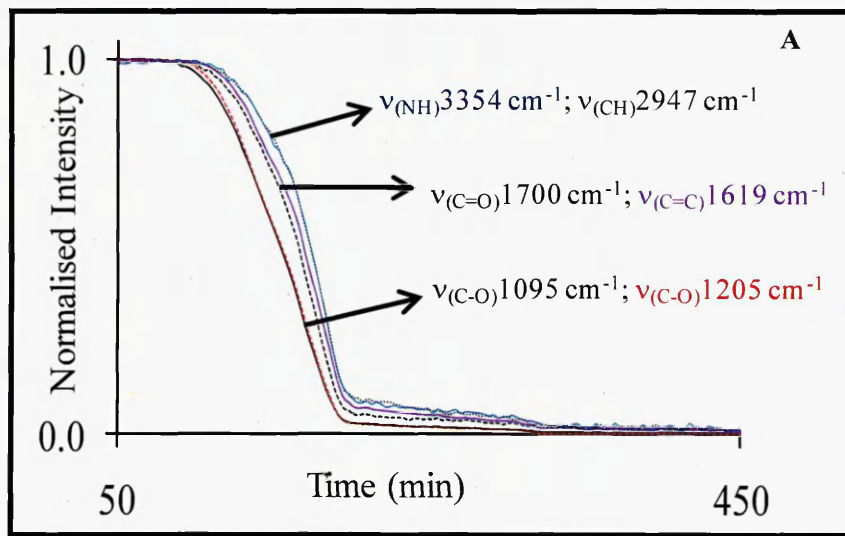
Figure. 7.5 *In situ* FTIR studies at 180 °C; Felodipine solvent cast film
(A), PVP cast film (B) and Fel/PVP solid dispersions (C)

133

However, to investigate temperature induced phase separation, the influence of temperature on the degradation rate or film thickness we need additional pre-processed samples with regions contributing to H-bond or felodipine/PVP interactions etc. This is because, in samples containing unknown degradation products, the idea of extrapolating already interpreted results will not be an ideal approach. This study shows that truncating the spectral bands to regions of interest should be applied cautiously and prior knowledge about the materials included in the study is essential. Future work will be directed towards inclusion of the carbonyl, and pyrrolidone degradation groups or using the entire spectral range and applying other pre-processing steps like mean centre, vector normalisation etc in order to effectively interpret the results of the thermal stability studies of solid dispersions. Moreover, the *in situ* FTIR data (Figure 8.5B) seems reasonable to fit first order kinetics. Hence future work can be directed to extract kinetic information from these measurements.

7.6 Conclusion

Chemical imaging is an effective tool in probing the identification and distribution of the degradation products within the solid dispersions. Spectroscopic imaging in combination with complementary techniques is an effective tool to better understand and locate the degradation products on a micron scale. TGA results revealed that drug, polymer and drug/polymer mixture did not show any indication of degradation until 240 °C. However, *in situ* FTIR spectroscopy and long-term FTIR imaging results suggest that prolonged exposures to dry air induce degradation even at lower temperatures (in our studies it is 60 °C). FTIR Imaging facilitates the successful identification and distribution of degraded products. The samples stored at 180 °C degraded rapidly, whereas the degradation was slower at 100 °C and slowest at 60 °C. Although, the selected conditions are extreme ones, the results provide valuable information about the storage conditions and their importance.
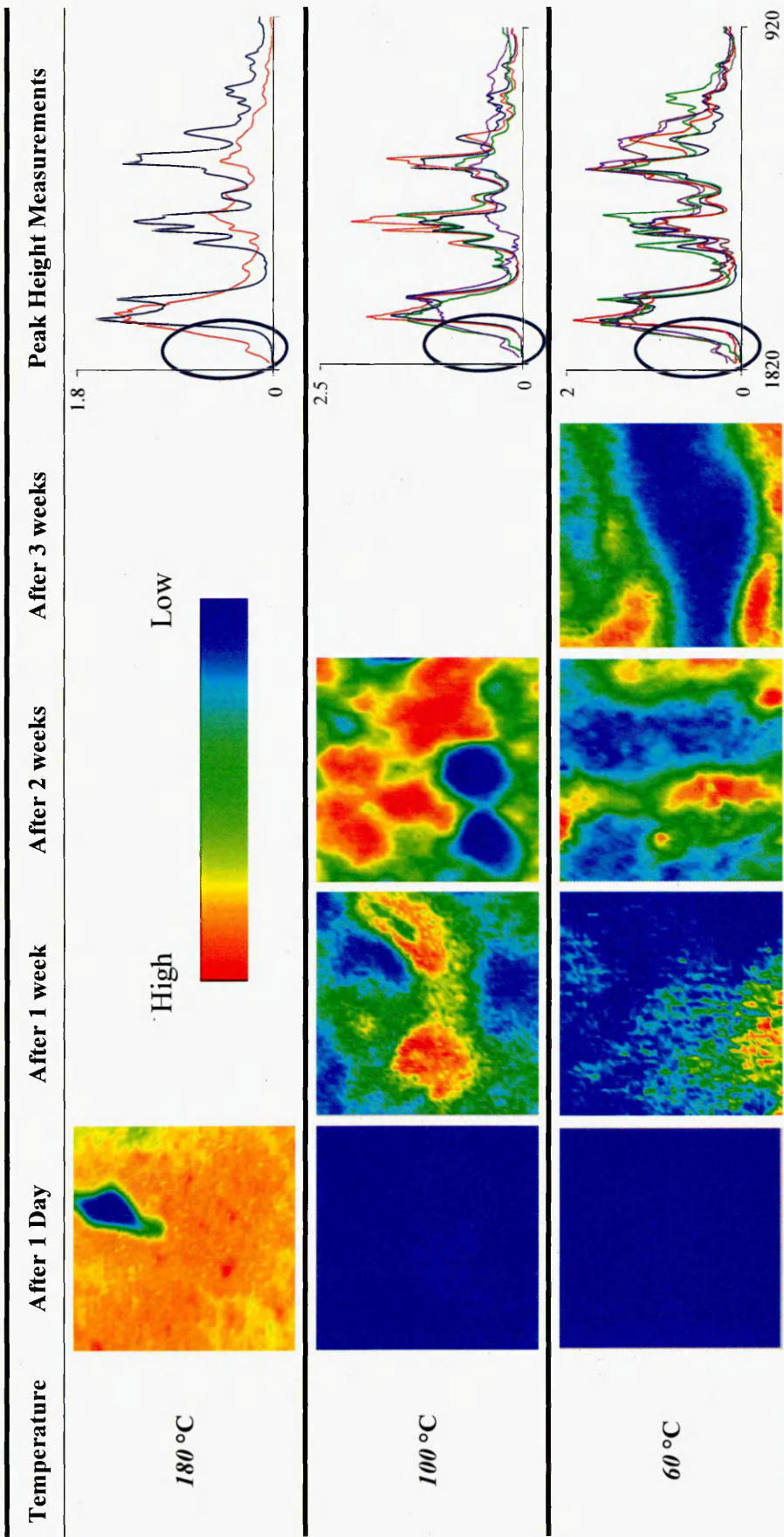
Figure 7.6. Thermal stability of solid dispersions
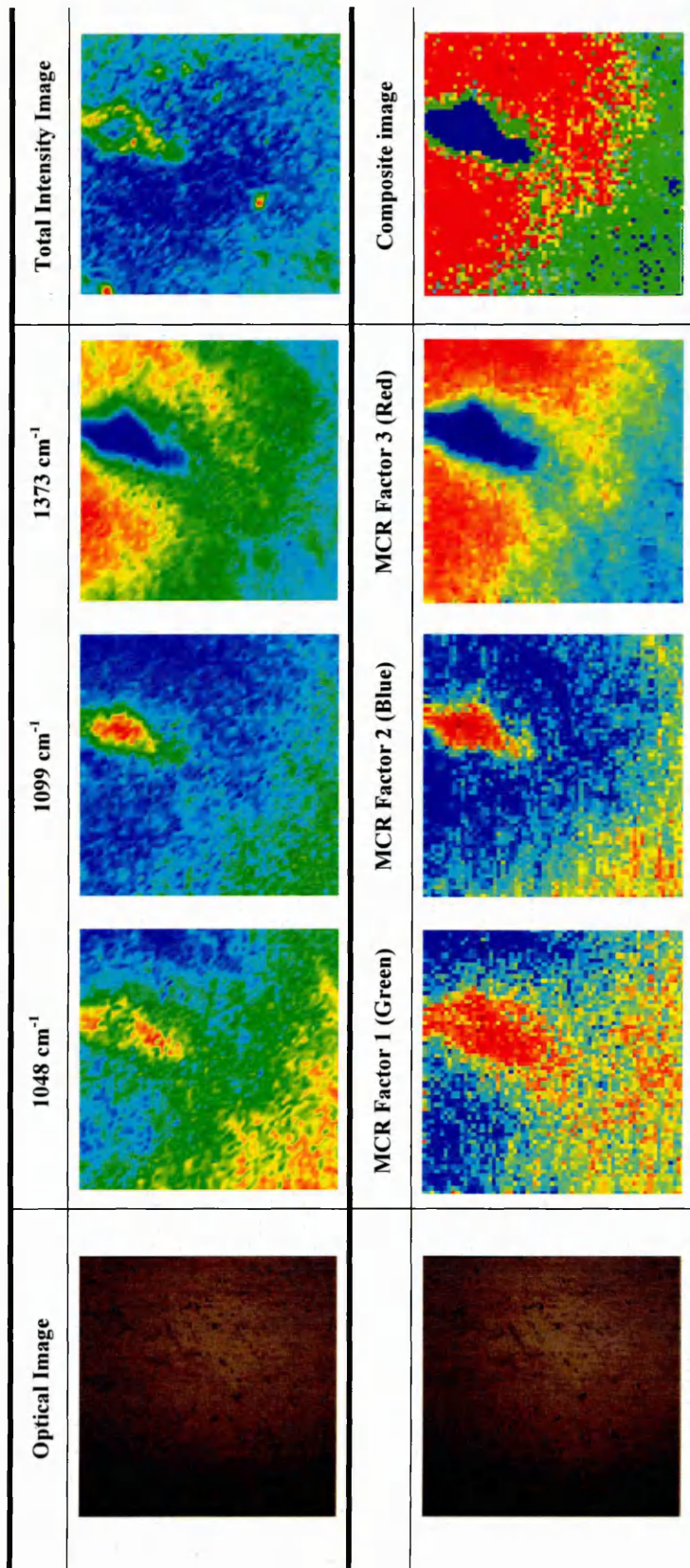
Figure 7.7. Solid dispersion stored at 180 °C -Univariate processed images (top) and MCR processed images (bottom)
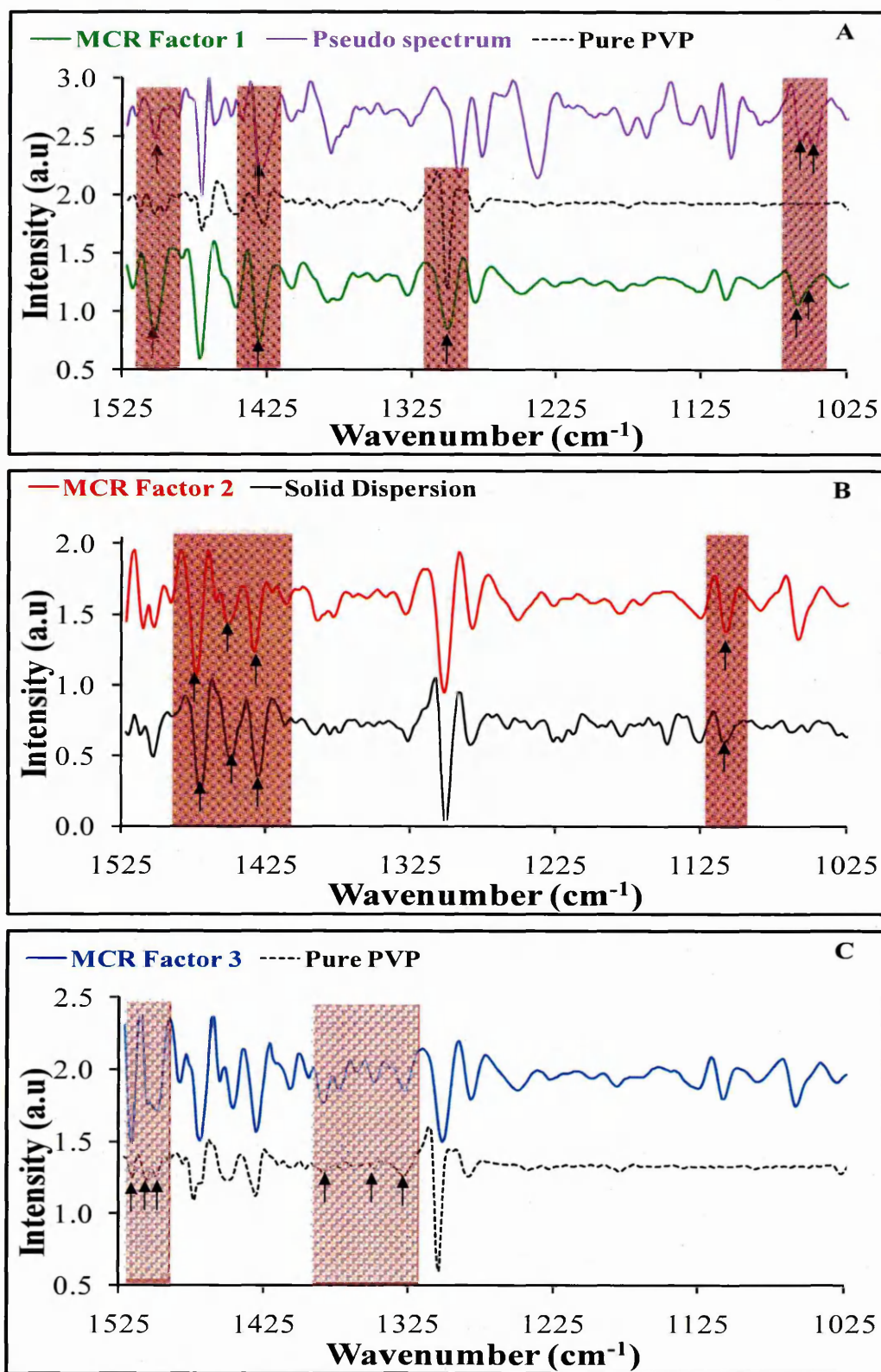
Figure 7.8 Second derivative "reference or pure" spectra and MCR factors of degradation products

CHAPTER 8.
SUMMARY AND CONCLUSIONS

8.1 Introduction

The aim of the present thesis was to provide working protocols to better characterise the morphology, distribution and formation of solid dispersions. The following problematic have driven this thesis

A) The application of vibrational spectroscopy to understand the dynamics involved in the formation of solid dispersions.

B) Evaluation and optimisation of experimental toolbox for analysing the acquired mid infrared chemical images.

C) Further work involving FTIR-Reflection Absorption imaging to better understand the potential scope and applications of these techniques in a wider context in determining phase separation, phase transition or phase transformation.

8.2 Bulk Spectroscopic Measurements

We have successfully developed a characterisation protocol wherein it is practically possible to monitor the formation of solid dispersions *in situ* using ATR-FTIR spectroscopy. To achieve our motivation we selected two different binary solvent mixtures (acetone/methanol, DCM/acetone), model drug-felodipine, model polymer-polyvinyl pyrrolidone, three different drug/polymer (20% w/w, 50% w/w and 80% w/w) ratios and different temperatures (30°C, 40°C and 50°C). Initially, changes in the peak positions and intensities were used to follow the kinetics of solvent evaporation and solid dispersion formation using t_{10} measurements. The t_{10} kinetic results were obtained using peak height measurements and chemometric (multivariate curve resolution) tools. There were significant differences only with the t_{10} methanol results. As a result, statistical analysis was carried out to better understand the kinetic results at a 95% confidence interval. We showed that MCR is a valuable tool to extract kinetic information from complex multi-component systems with overlapping spectral signatures.

Moreover, peak position changes, peak widths and intensities were simultaneously studied to provide insight into solvent-solvent, solvent solid and solid-solid molecular interactions. Finally, we studied the impact of solvent nature, temperature, polymer and drug loading on the final product characteristics like drug-polymer H-bond interactions,

drug-polymer miscibility, distribution and phase separation. Furthermore, interplay between t_{10}, molecular interactions and final production characteristics were studied.

The large scale application of solvent method is spray drying wherein the temperature is used as a secondary drying parameter. In this study, the temperature was used as a variable to study its impact on solvent evaporation rate/drying kinetics, molecular interactions and resultant final (solid dispersion) product characteristics. An increase in temperature increased the rate of evaporation of the solvents and did disrupt the solvent-solvent and solvent-solid interactions and ultimately the final product characteristics of PVP. However, the temperature was found to have no impact on the felodipine and 20% drug loaded felodipine/PVP solid dispersions. Higher drug loaded samples behave similarly to sample containing drug alone; hence interest was focussed in the low drug loaded solid dispersions only.

The selection of solvent or nature of the solvents was found to have a significant influence on the drying rate and molecular interactions. That is, acetone evaporated rapidly and was found not to interact with the solids in the acetone/methanol binary solvent mixture (BSM). However, we showed that methanol interacts with acetone, felodipine and PVP through the formation of hydrogen bonds. In order to confirm these findings a second binary solvent mixture comprising DCM/acetone was employed. Acetone was found to interact with felodipine (H-bond) but not with PVP (nonsolvent for PVP). However, DCM interacts with felodipine (H-bond interaction), with acetone and PVP (dipolar interactions). There were no significant differences observed in the bulk spectroscopic measurements. Interestingly, the results from spectroscopic imaging measurements showed that the distribution of various components within the solid dispersions was influenced. That is, when felodipine/PVP was cast from acetone/methanol the final product was homogeneously distributed, however there was phase separation when felodipine/PVP was cast from DCM/acetone. These results indicate that the nature of solvents play a vital role in the formation of solid dispersions.

The selection of solvents, temperature and drug loading, as mentioned, was found to influence the final product characteristics. The final product is brittle when cast from acetone/methanol at 30°C with a low drug loading of 20%. Conversely, PVP is globular when cast from DCM/acetone at 30°C with 0% drug loading. Felodipine final product characteristics were influenced by the solvent and polymer when compared to starting material. However there were no significant differences between two solvents (acetone/methanol or DCM/acetone) and various temperatures included in the study.

139

It was shown that the solvent nature and temperature played a crucial role in the kinetics of solvent evaporation. Whereas the solvent nature, temperature and solid loading protonation of solids, conformational changes in polymer etc.

8.3 Chemical Imaging Measurements

Chemical imaging or spectroscopic imaging systems and their potential applications in diverse fields became possible after the introduction of second generation focal plane array (FPA) detectors. However, pharmaceutical applications involving reflection-absorption FTIR imaging was scarce. The reasons were lack of basic understanding of the acquired hyperspectral data. In this context, we have developed a "bottom-up" approach to address the prospective applications of FTIR imaging measurements to study the pharmaceutical materials of interest. Firstly, we demonstrated the possible reasons for the introduction of optical non-linearities that can influence the acquired chemical images. Then data preprocessing steps were applied to remove the optical artefacts. In order to extract the distribution maps of various ingredients within the solid dispersions different data processing steps were applied. Finally, to understand the distribution maps clearly and effectively data visualisation/image enhancement tools were carried out.

To achieve our motivation, three different model systems of known composition were selected and studied. These model systems were used to demonstrate the efficiency of chemometric methods. Then data processing procedures like peak height measurements, compare correlation, principal component analysis and multivariate curve resolution were applied. The results indicated that model system I was phase separated, model system II was homogeneously distributed. The composition for model system I and model system II are fully known. Then these procedures were extended to model system III whose compositional distribution of components was unknown.

Peak Height Measurement is the simplest approach used to generate an intensity map. However, it is not straight forward if physical effects, optical artefacts and overlapping bands are present. Compare correlation requires library of pure components sometimes which is not possible. Principal component analysis identifies number of pure components present without supervision. However, obtained results cannot be directly compared to the pure spectra. In contrast, multivariate curve resolution extracts the identity and the distribution map of components that can be directly compared with the pure spectra. Moreover, it does not require any prior information about the sample and does not suffer from any interference. Finally, we showed that data visualisation

involving scatter plot provided better means to understand the complex data. Detailed analysis has shown that data pre-processing is vital in order to avoid misinterpretation.

Further work was carried out with the aim of understanding the scope of the mid infrared imaging techniques in a wider context. Firstly, we studied the solvent induced phase separation by casting felodipine/PVP solid dispersion from binary solvent mixtures of varying affinity to felodipine and PVP. In this study we showed that when interaction parameters between the solvent and two miscible components are different as with DCM/acetone, the solvent induces phase separation. This was successfully studied using FTIR imaging technique. Secondly we stored the felodipine/PVP spray coated solid dispersion from DCM/acetone in dessicator containing 95% moisture. After 12 hours the sample was studied using FTIR imaging and the acquired image was processed. The results indicated there is significant evidences for moisture induced phase transformation of felodipine from amorphous form to its crystalline form. Finally, felodipine/PVP solid dispersion was placed at different temperatures (60°C, 100°C and 180°C) to study the temperature induced phase separation and degradation. We showed that the mid infrared imaging was successful in extracting even minute quantities of degradation product.

The aforementioned studies show this thesis demonstrates the usefulness of mid infrared chemical imaging as a potentially useful tool to study the pharmaceutical materials based on the data mining procedures. However, the challenges still remaining with data extraction procedures (as shown by studying the degradation products) which will most probably continue to be one of the exciting areas of research.

8.4   Complementary techniques – TG-MS and TG-DTA

TG-MS was successfully used to understand the residual solvent to assist with the interpretation of t_{10} measurements, molecular interaction between drug and polymer, etc. With TG-MS measurements, it was found that the residual solvents within the studied systems (binary solvent mixture, 100% polymer and 100% drug loaded samples) were less than 10% which is accounted in our t_{10} measurements.

Moreover, TG-DTA was used to study and understand the degradation behaviour of drug alone, polymer alone, physical mixture of drug and polymer and finally solid dispersions. DTA results indicated that drug was in crystalline form in the starting material and physical mixture however in amorphous form when mixed with polymer as solid dispersion. TGA results revealed that drug, polymer and drug/polymer mixture did

not show any indication of degradation until 240°C when heated at 20°C/min, but the onset of degradation of drug in solid dispersion and physical mixture occurred at a higher temperature (~300°C) when compared to drug alone which ties well with, *in situ* studies.

CHAPTER 9.
FURTHER WORK

9.1 Kinetics of solvent evaporation and drying

The protocols presented here (Chapter 4 and Chapter 6) considered the model drug-felodipine which is a proton donor and a model polymer polyvinyl pyrrolidone. In order to gain a better insight on kinetics of drying and final product characteristics various aspects like model drug selection, model polymer selection, solvent selection and drug loading can be explored further.

For example, model drugs like griseofulvin (proton acceptor), Cinnarizine (dipole interactions), adamantane (neutral molecule) and other polymers like poly ethylene glycols, poly methacrylates, cellulose derivatives (hydroxyl propyl methyl cellulose, hydroxyl propyl cellulose), starch derivatives (cyclodextrins) etc. Moreover, drug loading selected here was to understand the amorphous product formation. In the pharmaceutical industry, the solid-solid compositional miscibility of drug in polymer is practically more relevant than the polymer in the drug. Also when the drug loading is higher than the miscibility composition, the prepared system tends to phase separate. The miscible drug loading of felodipine in PVP is 5-25% and its influence on the t_{10} measurements, molecular interactions with solvents and polymer can be studied in more detail. One other interesting area is to study the influence of solvent selection especially DCM/ethanol which is a widely used binary mixture solvent in preparing solid dispersions. When miscible solids interact with both solvents there are more chances that solvent will alter the phase behavior. Future work can also involve a systematic approach to calculate activation energy (E_a) and/or heats of vaporization which will be a useful approach to predict the rate of evaporation of solvents at any given temperature

9.2 Evaluation of image processing tools

In Chapter 5, three model systems of varying chemical composition were selected to optimize the data preprocessing, data processing and data post-processing procedures. The data pretreatment procedures comprised: selection of a narrow wavenumber region, Not-a-Number (NaN) masking, Savitsky-Golay second derivative and peak height normalization. The extraction of distribution maps was better explained using multivariate curve resolution or principal component analysis. Scatter plot was found to be very useful in visual interpretation of complex mixtures.

The optimized imaging analysis was successful in tracing the solvent induced phase separation and moisture induced phase transformation. However, the optimized methods were unsuccessful in extracting or tracing entire range of degraded products. With complementary characterizing techniques like TGA and *in situ* ATR-FTIR spectroscopy we showed that both carbonyl regions and CH regions were involved in degradation. Hence the future studies should involve alternative preprocessing steps like mean centre, standard normal variate or vector normalization etc. Also preprocessing different wavenumber regions (carbonyl, CH, ester etc) and design methodologies to combine the treated data to process the chemical images will be extremely useful to identify the degradation products.

9.3   Spectroscopic imaging to determine the final product characteristics

The distribution and association of the various components of solid dispersions may be critical to the product performance, for example physical stability, dissolution, bioavailability etc. In this perspective selection of different model drugs, solvent, model polymer etc. and their influence on the dissolution, stability, phase transformation or phase separation will be an attractive area of research. Moreover studies can involve by selecting a class of model drugs with varying strengths of intermolecular interactions with the selected model polymer and study their influence on distribution, storage stability, dissolution behavior etc.

In order to provide insight into the phase behavior, for example, moisture induced phase separation or phase transformation for the selected model systems, a range of relative humidities like 0%-95% at fixed temperature range can be studied. An investigation into the possibilities of imaging morphological features such as spherullite structure within the phase transformed samples will be an exciting area to understanding the scope of mid-infrared imaging techniques in a wider context.

9.4   Stability studies of solid dispersions

The thermal stability of solid dispersions is attributed to various intermolecular interactions like hydrogen bonding, Van der Waals interactions etc. The results from the degradation studies (cf. Chapter 7.5.2) showed that H-bonding interactions between felodipine and PVP inhibited the formation of imide like structures. Hence selection of interacting and non-interacting PVP/drug systems to understand the capability of mid infrared imaging in assessing the degradation products will be an interesting area of

144

research. A related area of interest is the investigation of degradation of solid dispersion systems by other types of stresses like Gamma or X-ray radiations and study the applicability of FTIR imaging in tracing the degradation products.

CHAPTER 10
BIBLIOGRAPHY

1. Rick NG Drugs-From Discovery to Approval, John Wiley and Sons Inc, Hoboken, NJ, 2004.

2. DiMasi JA, Hansen RW, Grabowski HG Journal of health economics 2003;22(2):151-185.

3. Aulton ME Pharmaceutics :the science of dosage form design. Edinburgh: Churchill Livingstone, 2002.

4. Bikiaris D, Papageorgiou GZ, Stergiou A, Thermochimica Acta 2005;439(1-2):58-67.

5. Janssens S, Van den Mooter G Journal of Pharmacy and Pharmacology 2009;61(12):1571-1586.

6. Sinha S, Baboota S, Ali M, Kumar A, Ali J Journal of Dispersion Science and Technology 2009;30(10):1458-1473.

7. Leuner C, Dressman J European Journal of Pharmaceutics and Biopharmaceutics 2000;50(1):47-60.

8. Betageri GV, Makarla KR International Journal of Pharmaceutics 1995;126(1-2):155-160.

9. Breitenbach J, Schrof W, Neumann J Pharmaceutical Research 1999;16(7):1109-1113.

10. Serajuddin ATM Journal of Pharmaceutical Sciences 1999;88(10):1058-1066.

11. Karavas E, Ktistis G, Xenakis A, Georgarakis E European Journal of Pharmaceutics and Biopharmaceutics 2006;63(2):103-114.

12. Chamarthy SP, Pinal R Colloids and Surfaces A: Physicochemical and Engineering Aspects 2008;331(1-2):68-75.

13. Craig DQM International Journal of Pharmaceutics 2002;231(2):131-144.

14. Hancock BC, Zograf G Journal of Pharmaceutical Sciences 1997;86(1):1-12.

15. Hancock BC, Shamblin SL, Zografi G Pharmaceutical Research 1995;12(6):799-806.

16. Hancock BC, Parks M Pharmaceutical Research 2000;17(4):397-404.

17. Murdande SB, Pikal MJ, Shanker RM, Bogner RH Journal of Pharmaceutical Sciences 2010;99(3):1254-1264.

18. Murdande S, Pikal M, Shanker R, Bogner R Pharmaceutical Research 2010;27(12):2704-2714.

19. Chiou WL Journal of Pharmaceutical Sciences 1977;66(7):989-991.

20. Chiou WL, Riegelman S Journal of Pharmaceutical Sciences 1971;60(9):1281-1302.

21. Corrigan OI Drug Development and Industrial Pharmacy 1985;11(2-3):697-724.

22. Karavas E, Georgarakis E, Sigalas MP, Avgoustakis K, Bikiaris D European Journal of Pharmaceutics and Biopharmaceutics 2007;66(3):334-347.

23. Craig DQM Drug Development and Industrial Pharmacy 1990;16(17):2501.

24. Sekiguchi K, Obi N Chemical & Pharmaceutical Bulletin 1961-11-25;9(11):866-872.

25. Goldberg AH, Gibaldi M, Kanig JL, Journal of Pharmaceutical Sciences, 1966, 55 (5), 482-487.

26. Goldberg AH, Gibaldi M, Kanig JL, Journal of Pharmaceutical Sciences, 1966, 55 (5), 487-492.

27. Kaushal AM, Chakraborti AK, Bansal AK Molecular Pharmaceutics 2008;5(6):937-945.

28. Vasconcelos T, Sarmento B, Costa P Drug Discovery Today 2007;12(23-24):1068-1075.

29. Arias MJ, Ginés JM, Moyano JR, Pérez-Martinez JI, Rabasco AM International Journal of Pharmaceutics 1995;123(1):25-31.

30. Van den Mooter G, Wuyts M, Blaton N, European Journal of Pharmaceutical Sciences 2001;12(3):261-269.

31. Zega A, Srcic S, Mavri J, Bester-Rogac M Journal of Molecular Structure 2008;875(1-3):354-363.

32. Muta H, Ishida K, Tamaki E, Satoh M Polymer 2002;43(1):103-110.

33. Chen Y, Wallace BA Biopolymers 1997;42(7):771-781.

34. Sagle LB, Zhang YJ, Litosh VA, Chen X, Cho Y, Cremer PS Journal of the American Chemical Society 2009;131(26):9304-9310.

35. Wohar MM, Seehra JK, Jagodzinski PW Spectrochimica Acta Part A: Molecular Spectroscopy 1988;44(10):999-1006.

36. Suzuki H, Miyamoto N, Masada T, Hayakawa E, Ito K Chemical & pharmaceutical bulletin 1996-02-15;44(2):364-371.

37. Kalinkova GN International Journal of Pharmaceutics 1999;187(1):1-15.

38. Rawlinson CF, Williams AC, Timmins P, Grimsey I International Journal of Pharmaceutics 2007;336(1):42-48.

39. Pignatello R, Ferro M, Puglisi G AAPS PharmSciTech 2002;3(2):35-45.

40. Kazarian SG, Martirosyan GG International Journal of Pharmaceutics 2002;232(1-2):81-90.

41. Ambike AA, Mahadik KR, Paradkar A International Journal of Pharmaceutics 2004;282(1-2):151-162.

42. Bansal SS, Kaushal AM, Bansal AK Molecular Pharmaceutics 2007;4:794-802.

43. Al-Obaidi H, Buckton G AAPS PharmSciTech 2009;10(4):1172-1177.

44. Bhugra C, Pikal MJ Journal of Pharmaceutical Sciences 2008;97(4):1329-1349.

45. Marsac PJ, Shamblin SL, Taylor LS Pharmaceutical Research 2006;23(10):2417-2426.

46. Van Eerdenbrugh B, Taylor LS Molecular Pharmaceutics 2010;7(4):1328-1337.

47. Gao P Molecular Pharmaceutics 2008;5(6):903-904.

48. Rumondor ACF, Marsac PJ, Stanford LA, Taylor LS Molecular Pharmaceutics 2009;6(5):1492-1505.

49. Ivanisevic I Journal of Pharmaceutical Sciences 2010;99(9):4005-4012.

50. Qi S, Belton P, Nollenberger K, Clayden N, Reading M, Craig DQM Pharmaceutical Research (Dordrecht) 2010;27(9):1869-1883.

51. Telang C, Mujumdar S, Mathew M Journal of pharmaceutical sciences 2009;98(6):2149-2159.

52. Janssens S, De Zeure A, Paudel A, Van Humbeeck J, Rombaut P, Van den Mooter G Pharmaceutical Research 2010;27(5):775-785.

53. Patel SK, Lavasanifar A, Choi P Biomacromolecules 2009;10(9):2584-2591.

54. Marsac PJ, Konno H, Taylor LS Pharmaceutical research 2006;23(10):2306-2316.

55. Pignatello R, Spadaro D, Vandelli MA, Forni F, Puglisi G Drug development and industrial pharmacy 2004;30(3):277-288.

56. Haaf F, Sanner A, Straub F Polymer Journal 1985;17(1):143-152.

57. Hassouna F, Therias S, Mailhot G, Gardette J Polymer Degradation and Stability 2009;94(12):2257-2266.

58. Bogatyrev VM, Borisenko NV, Pokrovskii VA Russian Journal of Applied Chemistry 2001;74(5):839-844.

59. Borodko Y, Lee HS, Joo SH, Zhang YW, Somorjai G Journal of Physical Chemistry C 2010;114(2):1117-1126.

60. Hillerstrom A, Andersson M, Pedersen JS, Journal of Applied Polymer Science 2009;114(3):1828-1839.

61. Sethia S, Squillante E International Journal of Pharmaceutics 2004;272(1-2):1-10.

62. Taylor LS, Zografi G Pharmaceutical Research 1997;14(12):1691-1698.

63. Valero M, Pérez-Revuelta BI, Rodríguez LJ International Journal of Pharmaceutics 2003;253(1-2):97-110.

64. Papageorgiou G, Bikiaris D, Karavas E, The AAPS Journal 2006;8(4):E623-E631.

65. Karavas E, Georgarakis E, Bikiaris D International Journal of Pharmaceutics 2006;313(1-2):189-197.

66. Kerc J, Srčič S, Mohar M, S mid-Korbar J International Journal of Pharmaceutics 1991;68(1-3):25-33.

67. Kerc J, Mohar M, Srcic S, Kofler B, Smid-Korbar J Acta Pharmaceutica Zagreb 1993;43(2):113-120.

68. Rollinger JM, Burger A Journal of Pharmaceutical Sciences 2001;90(7):949-959.

69. Srčič S, Kerč J, Urleb U, International Journal of Pharmaceutics 1992;87(1-3):1-10.

70. Fossheim R Journal of Medicinal Chemistry 1986;29(2):305-307.

71. Konno H, Taylor LS Journal of Pharmaceutical Sciences 2006;95(12):2692-2705.

72. Konno H, Handa T, Alonzo DE, Taylor LS European Journal of Pharmaceutics and Biopharmaceutics 2008;70(2):493-499.

73. Karavas E, Georgarakis E, Bikiaris D, Thomas T, Katsos V, Xenakis A Trends in Colloid and Interface Science Xv 2001;118:149-152.

74. Kerc J, Srcic S, Kofler B Drug Development and Industrial Pharmacy 1998;24(4):359-363.

75. Lou B, Bostroem D, Velaga SP Crystal Growth & Design 2009;9(3):1254-1257.

76. Lindfors L, Skantze P, Skantze U, Westergren J, Olsson U Langmuir 2007;23(19):9866-9874.

77. Won D, Kim M, Lee S, Park J, Hwang S International journal of pharmaceutics 2005;301(1-2):199-208.

78. Moneghini M, Bellich B, Baxa P, Princivalle F International Journal of Pharmaceutics 2008;361(1-2):125-130.

79. Bhugra C, Shmeis R, Krill S, Pikal M Pharmaceutical Research, 2006;23:2277-2290(14).

80. Bhugra C, Shmeis R, Krill SL, Pikal MJ Journal of Pharmaceutical Sciences 2008;97(1):455-472.

81. Matsumoto T, Zografi G Pharmaceutical Research 1999;16(11):1722-1728.

82. Aso Y, Yoshioka S Journal of Pharmaceutical Sciences 2006;95(2):318-325.

83. Karavas E, Georgarakis E, Bikiaris D European Journal of Pharmaceutics and Biopharmaceutics 2006;64(1):115-126.

84. Vasanthavada M, Tong W(, Joshi Y, Kislalioglu MS Pharmaceutical Research 2005;22(3):440-448.

85. Karavas E, Ktistis G, Xenakis A, Georgarakis E Drug Development and Industrial Pharmacy 2005;31(6):473-489.

86. Teberekidis VI, Sigalas MP Journal of Molecular Structure: THEOCHEM 2007;803(1-3):29-38.

87. Kestur US, Lee H, Santiago D, Rinaldi C, Won YY, Taylor LS Crystal Growth & Design 2010;10(8):3585-3595.

88. Marsac PJ, Rumondor ACF, Nivens DE, Kestur US, Stanciu L, Taylor LS Journal of Pharmaceutical Sciences 2010;99(1):169-185.

89. Marsac PJ, Li T, Taylor LS Pharmaceutical Research 2009;26(1):139-151.

90. Rumondor ACF, Stanford LA, Taylor LS Pharmaceutical Research 2009;26(12):2599-2606.

91. Rumondor ACF, Jackson MJ, Taylor LS Crystal Growth & Design 2010;10(2):747-753.

92. Baird JA, Van Eerdenbrugh B, Taylor LS Journal of Pharmaceutical Sciences 2010;99(9):3787-3806.

93. Van Eerdenbrugh B, Baird JA, Taylor LS Journal of Pharmaceutical Sciences 2010;99(9):3826-3838.

94. Alonzo DE, Zhang GGZ, Zhou D, Gao Y, Taylor LS Pharmaceutical Research 2010;27(4):608-618.

95. Karavas E, Georgarakis M, Docoslis A, Bikiaris D International journal of pharmaceutics 2007;340(1-2):76-83.

96. Barbara H. Stuart Infrared Spectrosocpy:Fundamentals and Applications. : John Wiley & Sons, LTD, 2008.

97. Wartewig S, Neubert RHH Advanced Drug Delivery Reviews 2005;57(8):1144-1170.

98. Burgula Y, Khali D, Kim S, Journal of Rapid Methods and Automation in Microbiology 2007;15(2):146-175.

99. Coates J Interpretation of Infrared Spectra, A Practical Approach. In: Meyer RA, editor. Encyclopedia of Analytical Chemistry. : JohnWiley & Sons Ltd, Chichester, 2000. pp. 10815-10837.

100. Pasquini C Journal of the Brazilian Chemical Society 2003;14(2):198-219.

101. Hollas JM Modern spectroscopy. : Wiley, 1992.

102. Griffiths PR, de Haseth JA Fourier Transform Infrared Spectrometry. United States of America: John Wiley & Sons, Inc, 1986.

103. Do TT, Celina M, Fredericks PM Polymer Degradation and Stability 2002;77(3):417-422.

104. Gendrin C, Roggo Y, Collet C Journal of Pharmaceutical and Biomedical Analysis 2008;48(3):533-553.

105. Salzer R, Siesler HW Infrared and Raman Spectroscopic Imaging. Weinheim: Wiley-VCH, 2009.

106. Clark D, Sasic S Cytometry Part A 2006;69A(8):815-824.

107. Koenig JL, Bobiak JP Macromolecular Materials and Engineering 2007;292(7):801-816.

108. Levin IW, Bhargava R Annual Review of Physical Chemistry 2005;56:429-474.

109. Bhargava R, Levin IW Analytical Chemistry 2001;73(21):5157-5167.

110. Colarusso P, Kidder LH, Levin IW, Fraser JC, Arens JF, Lewis EN Applied Spectroscopy 1998;52(3):106A-120A.

111. Gurny R, Maeder K European Journal of Pharmaceutics and Biopharmaceutics 2010;74(1):1-1.

112. Joseph E, Prati S, Sciutto G, Ioele M, Santopadre P, Mazzeo R Analytical and Bioanalytical Chemistry 2010;396(2):899-910.

113. Koenig JL, Wang SQ, Bhargava R Analytical Chemistry 2001;73(13):360A-369A.

114. Roggo Y, Chalus P, Maurer L, Lema-Martinez C, Edmond A, Jent N Journal of Pharmaceutical and Biomedical Analysis 2007;44(3):683-700.

115. Roggo Y, Edmond A, Chalus P, Ulmschneider M Analytica Chimica Acta 2005;535(1-2):79-87.

116. Garidel P, Boese M Microscopy Research and Technique 2007;70(4):336-349.

117. Koenig JL, Snively CM Spectroscopy 1998;13(11):22-28.

118. Snively CM, Koenig JL Macromolecules 1998;31(11):3753-3755.

119. Snively CM, Koenig JL Journal of Polymer Science Part B-Polymer Physics 1999;37(17):2353-2359.

120. Snively CM, Katzenberger S, Oskarsdottir G, Lauterbach J Optics Letters 1999;24(24):1841-1843.

121. Bobiak JP, Koenig JL Journal of Controlled Release 2005;106(3):329-338.

122. Gowen AA, O'Donnell CP, Cullen PJ, Downey G, Frias JM Trends in Food Science and Technology 2007;18(12):590-598.

123. Couts-Lendon C, Koenig JL Applied Spectroscopy 2005;59(6):717-723.

124. Bhargava R, Ribar T, Koenig JL Applied Spectroscopy 1999;53(11):1313-1322.

125. Bhargava R, Wang SQ, Koenig JL Applied Spectroscopy 2000;54(11):1690-1706.

126. Snively CM, Koenig JL Applied Spectroscopy 1999;53(2):170-177.

127. Giron D Journal of Thermal Analysis and Calorimetry 2002;68(2):335-357.

128. Dollimore D, Gamlen GA, Taylor TJ Thermochimica Acta 1984;75(1-2):59-69.

129. Materazzi S Applied Spectroscopy Reviews 1998;33(3):189-218.

130. Kamruddin M, Ajikumar PK, Dash S, Tyagi AK, Raj B Bulletin of Materials Science 2003;26(4):449-460.

131. Raemaekers KGH, Bart JCJ Thermochimica Acta 1997;295(1-2):1-58.

132. Pappa A, Kyriakou S, Mikedi K, Tzamtzis N, Statheropoulos M Journal of Thermal Analysis and Calorimetry 2004;78(2):415-426.

133. Statheropoulos M, Kyriakou S, Tzamtzis N Thermochimica Acta 1998;322(2):167-173.

134. Jovanovic N, Gerich A, Bouchard A, Jiskoot W Pharmaceutical research 2006;23(9):2002-2013.

135. Lavine BK Critical Reviews in Analytical Chemistry 2006;36(3):153.

136. Manuel Amigo J, Cruz J, Bautista M, Maspoch S, Coello J, Blanco M Trac-Trends in Analytical Chemistry 2008;27(8):696-713.

137. Shamsipur M, Hemmateenejad B, Akhond M, Javidnia K, Miri R Journal of pharmaceutical and biomedical analysis 2003;31(5):1013-1019.

138. de Juan A, Tauler R Critical Reviews in Analytical Chemistry 2006;36(3-4):163-176.

139. de Juan A, Maeder M, Hancewicz T, Tauler R Journal of Chemometrics 2008;22(5-6):291-298.

140. Pudney PDA, Hancewicz TM, Cunningham DG, Gray C Food Hydrocolloids 2003;17(3):345-353.

141. Rajko R, Nassab PR, Szabo-Revesz P Talanta 2009;79(2):268-274.

142. Rajko R Analytica Chimica Acta 2009;645(1-2):18-24.

143. Schoonover JR, Marx R, Zhang SLL Applied Spectroscopy 2003;57(5):154A-170A.

144. Jaumot J, Tauler R Chemometrics and Intelligent Laboratory Systems 2010;103(2):96-107.

145. Wei M, Shi S, Wang J, Li Y, Duan X Journal of Solid State Chemistry 2004;177(7):2534-2541.

146. Storey RF, Donnalley AB, Maggio TL Macromolecules 1998;31(5):1523-1526.

147. Cornel J, Mazzotti M Industrial & Engineering Chemistry Research 2009;48(23):10740-10745.

148. Brantley NH, Kazarian SG, Eckert CA Journal of Applied Polymer Science 2000;77(4):764-775.

149. Ping Z, Nauer GE, Neugebauer H, Theiner J, Neckel A Electrochimica Acta 1997;42(11):1693-1700.

150. Döppers L, Breen C, Sammon C Vibrational Spectroscopy 2004;35(1-2):27-32.

151. Sammon C, Li C, Armes SP, Lewis AL Polymer 2006;47(17):6123-6130.

152. Sammon C, Deng CS, Yarwood J Polymer 2003;44(9):2669-2677.

153. Sammon C, Bajwa G, Timmins P, Melia CD Polymer 2006;47(2):577-584.

154. Döppers L, Sammon C, Breen C, Yarwood J Polymer 2006;47(8):2714-2722.

155. Kassis A, Bhawtankar VM, Sowa Jr. JR Journal of pharmaceutical and biomedical analysis ;In Press, Corrected Proof.

156. Philippe LVS, Lyon SB, Sammon C, Yarwood J Corrosion Science 2008;50(3):887-896.

157. Banks SR, Sammon C, Melia CD, Timmins P Applied Spectroscopy 2005;59(4):452-459.

158. Philippe L, Sammon C, Lyon SB, Yarwood J Progress in Organic Coatings 2004;49(4):302-314.

159. Philippe L, Sammon C, Lyon SB, Yarwood J Progress in Organic Coatings 2004;49(4):315-323.

160. Philippe L, Lyon SB, Sammon C, Yarwood J Corrosion Engineering Science and Technology 2003;38(2):153-156.

161. Sammon C, Yarwood J, Everall N Polymer 2000;41(7):2521-2534.

162. Ali HRH, Edwards HGM, Scowen IJ Journal of Raman Spectroscopy 2009;40(8):887-892.

163. Walker GM, Bell SEJ, Greene K, Jones DS, Andrews GP Chemical Engineering Science 2009;64(1):91-98.

164. Aaltonen J, Heinänen P, Peltonen L, Journal of pharmaceutical sciences 2006;95(12):2730-2737.

165. Bhattacharyya R, Key B, Chen H, Best AS, Hollenkamp AF, Grey CP2010;9(6):504-510.

166. Jiang Z, Sun Y, Tang Y, The Journal of Physical Chemistry B 2010;114(18):6001-6005.

167. Zhao YF, Loo SCJ, Chen YZ, Boey FYC, Ma J Journal of Biomedical Materials Research Part A 2008;85A(4):1032-1042.

168. Zeng X, Ungar G, Spells SJ, King SM Macromolecules 2005;38(17):7201-7204.

169. Ungar G, Zeng XB, Spells SJ Polymer 2000;41(25):8775-8780.

170. Marcott C, Story GM, Dowrey AE, Applied.Spectroscopy. 2009;63(12):346A-354A.

171. Ping Z, Neugebauer H, Neckel A Electrochimica Acta 1996;41(5):767-772.

172. Cornel J, Mazzotti M Analytical Chemistry 2008;80(23):9240-9249.

173. Wray P, Chan KLA, Kimber J, Kazarian SG Journal of pharmaceutical sciences 2008;97(10):4269-4277.

174. Tang XLC, Pikal MJ, Taylor LS Pharmaceutical research 2002;19(4):477-483.

175. Tang XC, Pikal MJ, Taylor LS Pharmaceutical research 2002;19(4):484-490.

176. Bellamy LJ Advances in infrared group frequencies. : Chapman & Hall, 1968.

177. Chen H, Gan W, Lu R, Guo Y, Wang HF Journal of Physical Chemistry B 2005;109(16):8064-8075.

178. Andrew JJ, Hancewicz TM Applied Spectroscopy 1998;52(6):797-807.

179. Hancewicz TM, Andrew JJ Three-Dimensional and Multidimensional Microscopy: Image Acquisition and Processing V, Proceedings of 1998;3261:322-333.

180. Azzouz T, Tauler R Talanta 2008;74(5):1201-1210.

181. Saurina J, Leal C, Compañó R, Granados M, Prat MD, Tauler R Analytica Chimica Acta 2001;432(2):241-251.

182. Self R, Belton PS Extraction of Organic Analytes from Foods. : The Royal Society of Chemistry, 2005.

183. Max JJ, Chapados C The Journal of chemical physics 2005;122(1):14504.

184. Max JJ, Chapados C The Journal of chemical physics 2009;130(12):124513.

185. Castilho PCMF, Crampton MR, Yarwood J Vibrational Spectroscopy 1992;3(3):167-180.

186. Suzuki H, Miyamoto N, Masada T, Hayakawa E, Ito K Chemical & pharmaceutical bulletin 1996-02-15;44(2):372-377.

187. Soria V, Figueruelo JE, Abad C, Campos A Macromolecular Theory and Simulations 2004;13(5):441-452.

188. Max J, Chapados C Journal of Chemical Physics 2007;126(15):154511.

189. Lee D, Webb M Pharmaceutical analysis. Oxford: Blackwell, 2003.

190. Cabaço MI, Besnard M, Tassaing T, Danten Y Journal of Molecular Liquids 2006;125(2-3):100-106.

191. Painter PC, Pehlert GJ, Hu Y, Coleman MM Macromolecules 1999;32(6):2055-2057.

192. Boskey A, Camacho NP Biomaterials 2007;28(15):2465-2478.

193. Riccio M, Resca E, Bertoni L, Optics & Laser Technology 2011;43(2):317-322.

194. Krafft C, Sergo V Spectroscopy-an International Journal 2006;20(5-6):195-218.

195. Bird B, Miljkovic M, Diem M Journal of Biophotonics 2010;3(8-9):597-608.

196. Bird B, Bedrossian K, Laver N, Miljkovic M, Romeo MJ, Diem M Analyst 2009;134(6):1067-1076.

197. Ribar T, Koenig JL, Bhargava R Macromolecules 2001;34(23):8340-8346.

198. Bhargava R, Wang SQ, Koenig JL Liquid Chromatography Ftir Microspectroscopy Microwave Assisted Synthesis 2003;163:137-191.

199. Bhargava R, Wall BG, Koenig JL Applied Spectroscopy 2000;54(4):470-479.

200. Snively CM, Koenig JL Journal of Polymer Science Part B-Polymer Physics 1999;37(16):2261-2268.

201. Shin EM, Ribar T, Koenig JL, Wright N Applied Spectroscopy 2001;55(12):1573-1579.

202. Chalmers JM, Everall NJ, Schaeberle MD, Vibrational Spectroscopy 2002;30(1):43-52.

203. Chalmers JM, Everall NJ, Hewitson K, Analyst 1998;123(4):579-586.

204. Budevska BO, Sum ST, Jones TJ Applied Spectroscopy 2003;57(2):124-131.

205. Mills ENC, Parker ML, Wellner N, Toole G, Feeney K, Shewry PR Journal of cereal science 2005;41(2):193-201.

206. Prati S, Joseph E, Sciutto G, Mazzeo R Accounts of Chemical Research 2010;43(6):792-801.

207. Coutts-Lendon CA, Wright NA, Mieso EV, Koenig JL Journal of Controlled Release 2003;93(3):223-248.

208. Kazarian SG, Chan KLA Applied Spectroscopy 2010;64(5):135A-152A.

209. Palombo F, Danoux CB, Weinberg PD, Kazarian SG Journal of Biomedical Optics 2009;14(4):044008.

210. Chan KLA, Kazarian SG Polymeric Drug Delivery Ii: Polymeric Matrices and Drug Particle Engineering 2006;924:203-214.

211. Chan KLA, Kazarian SG Molecular Pharmaceutics 2004;1(4):331-335.

212. Lee J, Gazi E, Dwyer J, Analyst 2007;132(8):750-755.

213. Bassan P, Byrne HJ, Lee J, Analyst 2009;134(12):2484-2484.

214. Mohlenhoff B, Romeo M, Diem M, Wood BR Biophysical journal 2005;88(5):3635-3640.

215. Bassan P, Kohler A, Martens H, Journal of Biophotonics 2010;3(8-9):609-620.

216. Bassan P, Kohler A, Martens H, Analyst 2010;135(2):268-277.

217. Amigo JM Analytical and Bioanalytical Chemistry 2010;398(1):93-109.

218. Hough D Computer 1981;14(3):70-74.

219. Bassan P, Byrne HJ, Bonnier F, Lee J, Dumas P, Gardner P Analyst 2009;134(8):1586-1593.

220. Broderick G, Paris J, Valade JL Chemometrics and Intelligent Laboratory Systems 1995;29(1):19-28.

221. de Juan A, Maeder M, Martinez M, Tauler R Chemometrics and Intelligent Laboratory Systems 2000;54(2):123-141.

222. Dahlberg C, Millqvist-Fureby A, Schuleit M, Furó I European Journal of Pharmaceutical Sciences 2010;39(1-3):125-133.

223. Isys5.0. Chemical Imaging Analysis Software, User's Manual, Malvern Instruments Limited, United Kingdom.

224. Vosough M, Mason C, Tauler R, Jalali-Heravi M, Maeder M Journal of Chemometrics 2006;20(6-7):302-310.

225. Tauler R, Smilde A, Kowalski B Journal of Chemometrics 1995;9(1):31-58.

226. Budevska BO Vibrational Spectroscopy 2000;24(1):37-45.

227. Wu K, Li J, Wang W, Winstead DA Journal of pharmaceutical sciences 2009;98(7):2422-2431.

228. Corrigan DO, Healy AM, Corrigan OI International journal of pharmaceutics 2003;262(1-2):125-137.

229. Ambike AA, Mahadik KR, Paradkar A Pharmaceutical research 2005;22(6):990-998.

230. Wulsten E, Kiekens F, van Dycke F, Voorspoels J, Lee G International journal of pharmaceutics 2009;378(1-2):116-121.

231. Dayal P, Kyu T Journal of Applied Physics 2006;100(4).

232. Shirota H, Ushiyama H The Journal of Physical Chemistry B 2008;112(43):13542-13551.

233. Shirota H, Castner EW Journal of Chemical Physics 2006;125(3).

234. Hao C, Zhao Y, Zhou Y, Journal of Polymer Science Part B: Polymer Physics 2007;45(13):1589-1598.

235. Gokhale A, Khusid B, Dave RN, Pfeffer R The Journal of Supercritical Fluids 2007;43(2):341-356.

236. Celebioglu A, Uyar T Materials Letters 2011;65(14):2291-2294.

237. Zafarani-Moattar MT, Khoshsima Z The Journal of Chemical Thermodynamics 2008;40(11):1569-1574.

238. Guettari M, Gharbi A Journal of Macromolecular Science Part B-Physics 2010;49(3):592-601.

239. Konno H, Taylor LS Pharmaceutical research 2008;25(4):969-978.

240. Blagden N, de Matas M, Gavan PT, York P Advanced Drug Delivery Reviews 2007;59:617-630.

241. Takeno H, Kobayashi M, Aikawa T Macromolecules 2006;39(6):2183-2190.

242. Li X, Wang Y, Lu X, Xiao C Journal of Membrane Science 2008;320(1-2):477-482.

243. Kirci B, Guner A European Polymer Journal 2001;37(2):361-365.

244. Soh YS, Kim JH, Gryte CC Polymer 1995;36(19):3711-3717.

245. Hellmann EH, Hellmann GP, Rennie AR Colloid and Polymer Science 1991;269(4):343-352.

246. Bercea M, Eckelt J, Morariu S, Wolf BA Macromolecules 2009;42(10):3620-3626.

247. Mandal TK, Woo EM Macromolecular Chemistry and Physics 1999;200(5):1143-1149.

248. Borodko Y, Humphrey SM, Tilley TD, Frei H, Somorjai GA The Journal of Physical Chemistry C 2007;111(17):6288-6295.

249. Borodko Y, Habas SE, Koebel M, Yang P, Frei H, Somorjai GA The Journal of Physical Chemistry B 2006;110(46):23052-23059.

250. Marciniec B, Ogrodowczyk M Acta Poloniae Pharmaceutica 2006;63(6):477-484.

251. Marciniec B, Jaroszkiewicz E, Ogrodowczyk M International journal of pharmaceutics 2002;233(1-2):207-215.

252. Marciniec B, Kozak M, Ogrodowczyk M Journal of Thermal Analysis and Calorimetry 2004;77(2):581-596.

253. Burger J, Geladi P Analyst 2006;131(10):1152-1160.

254. Li GY, Koenig JL Polymer Degradation and Stability 2003;81(3):377-385.

255. Li GY, Koenig JL Applied Spectroscopy 2002;56(11):1390-1396.

256. Trojak A, Kocevar K, Musevic I, Srcic S International journal of pharmaceutics 2001;218(1-2):145-151.